UNIVERSITY OF CAPE TOWN

IYUNIVESITHI YASEKAPA • UNIVERSITEIT VAN KAAPSTAD

THE FACULTY OF ENGINEERING AND THE BUILT ENVIRONMENT

The Department of Civil Engineering

The Influence of Fly Ash and Ground Granulated Blastfurnace Slag on Restrained Shrinkage Cracking of Bonded Overlays

Prepared By: Chizya Chibulu

Supervisor: A/Prof. Hans Beushausen

Date of Submission: 23rd May, 2016.

A dissertation submitted to the Department of Civil Engineering, University of Cape Town in partial fulfilment of the requirements for the degree of Master of Science in Civil Engineering.

The author wish to acknowledge with gratitude the financial assistance from the Concrete Materials and Structural Integrity Research Integrity (CoMSIRU) towards this research. Opinions expressed and conclusions arrived at, are those of the author and are not necessarily to be attributed to CoMSIRU.

Declaration

I, Chizya Chibulu, hereby declare that this Dissertation is my own, unaided work. I know the meaning of plagiarism and declare that all the work in this document, save for that which is properly acknowledged, is my own. It is being submitted for the degree of Master of Science in Engineering in the University of Cape Town. It has not been submitted before for any degree or examination in any other University.

Signed by candidate

Chizya Chibulu

Student Number: CHBCHI004

Date: 23rd May 2016

Acknowledgements

The author wishes to acknowledge and express sincere gratitude to the following persons, institutions, and companies who provided valuable support towards the completion of this dissertation.

- The supervisor, Associate Professor Hans Beushausen, for his patient guidance, enthusiastic encouragement, and useful critiques of this research work.
- The directors of the Concrete Materials and Structural Integrity Research Unit (CoMSIRU), Professor Mark Alexander and Professor Pilate Moyo, for giving constructive criticisms and useful insight during research seminars and presentations.
- The administrative staff of CoMSIRU, Mr Werner Van Der Ross, and formally Ms. Elly Yelverton, for their assistance on administrative issues concerning this research.
- The Department of Civil Engineering at the University of Cape Town for providing resources and assisting with administrative matters.
- Mr. Steve Crosswell on behalf of Portland Pretoria Cement Ltd (PPC), for their donation of the cement used in this research.
- Mr Nooredien Hassen, the Civil Engineering Concrete Laboratory Manager, and his deputy Tahir Mukaddam for their diligence in ensuring all laboratory administrative issues concerning this research were promptly executed.
- The Civil Engineering Concrete Laboratory staff, Mr Charles May, Mr Leonard Adams, Mr Elvino Witbooi, and most especially Mr Hector Mafungwa, for assisting with the experimental work.
- The Postgraduate Students of CoMSIRU, for providing useful peer evaluation towards this research.
- Family and friends for their continuous support and encouragement throughout this study.

The author also wishes to specially thank CoMSIRU for providing financial support throughout the duration of this dissertation.

Summary

The concrete repair industry is driven by deterioration of, damage to, and defects in concrete structures. The impact of deterioration or damage is a reduction in the service life of the concrete structure. One of the common methods used to repair and rehabilitate damaged concrete structures is the bonded overlay technique. However, bonded overlays are prone to restrained shrinkage cracking which impairs their performance. The mechanism leading to restrained shrinkage cracking of bonded concrete overlays is complex and depends on material properties, such as shrinkage, tensile strength, elastic modulus, and tensile relaxation. In order to reduce the risk of cracking in bonded concrete overlays, one or a combination of the following is required: lower shrinkage strains, higher tensile strength, lower elastic modulus, and increased stress relaxation. The development of these material properties depends on the degree of hydration of the binder material. Fly ash (FA) and slag (GGBS) are known to influence the hydration reaction when added to the binder material. This change in hydration reactions affects the development of the mechanical properties of the concrete, which ultimately affects the outcome of restrained shrinkage. An increase in age at cracking with the use of fly ash and slag in bonded concrete overlays was hypothesised. The research aimed at investigating the influence of fly ash and slag on the performance of bonded concrete overlays with regards to restrained shrinkage cracking. The research also aimed at using the influence of fly ash and slag on the specific material properties governing restrained shrinkage to analyse and predict the performance of the overlay materials

Preliminary modelling of tensile stress and tensile strength development in FA and GGBS concrete was carried out so as to inform the ensuing experimental investigation and reinforce the findings from the literature review. The results obtained from the preliminary investigation suggested that the age at cracking of bonded overlays could at least be increased with the use of GGBS. The FA results indicated otherwise. Experimental tests were then conducted to determine the influence of FA and GGBS on restrained shrinkage cracking. The tests included compressive and tensile strength, tensile relaxation, elastic modulus, free shrinkage, and ring tests. Analytical modelling of material properties was also carried out in order to predict the age at cracking. Ten different laboratory-made mortar mixes were considered for experimentation. These mixes were composed of cement mixes blended with FA (0%, 30% and 50%) or GGBS (0%, 50% and 70%). Two water-binder ratios of 0.45 and 0.65 were considered, by means of fixed water content. One curing method (saturated hessian sheets) was selected and only a minor component of the research focused on the effects of curing duration on the blended cement mixes.

It was generally observed that the replacement of cement with FA or GGBS resulted in lower tensile strength values, at both w/b ratios investigated. Furthermore, the tensile strength decreased with an increase in fly ash or slag content. Overall, the elastic modulus decreased with the use of FA or GGBS as was expected. At the lower replacement levels of both FA and GGBS, the elastic modulus of the concrete did not show significant increases between 7 and 28 days for both w/b ratios. In addition, increasing the percentage replacement level of both FA and GGBS by 20% did not drastically affect the 28-day elastic modulus. Tensile relaxation increased with increasing FA or GGBS content. The effect of GGBS on tensile relaxation was

slightly less prominent in comparison to FA at low w/b ratio, but at higher w/b ratio the 70% GGBS specimens had the largest relaxation values. At lower replacement levels, the tensile relaxation of the FA or GGBS specimens was almost equivalent to the reference specimens. The results also indicated that the specimens had higher relaxation capacity at early ages. At 28 days, the tensile relaxation capacity decreased in all specimens. The reduction of tensile relaxation in the reference specimens was more distinct than in FA and GGBS specimens. The partial replacement of Portland cement with FA or GGBS resulted in a decrease in the magnitude of free shrinkage strain. This observation was more apparent in the higher w/b ratio specimens.

The net age at cracking of the FA and GGBS specimens was generally higher than that of the reference specimens. The net age at cracking increased with increasing fly ash and slag content with the exception of the 50% slag mix which had the lowest age at cracking at both w/b ratios. Crack areas were also decreased with increase in FA content at both w/b ratios, with reference specimens showing the largest crack areas. Similar observations were made in the GGBS ring tests, with the exception of the 50% GGBS specimens at w/b 0.45 which showed the largest crack area. The crack areas measured on air cured specimens were varyingly lower than the crack area of the wet cloth cured specimens. The wet cloth cured specimens may have experienced greater shrinkage than the air cured specimens. The predicted age at cracking from the analytical modelling was consistent with the ring test results, an increase in age at cracking with increase in FA or GGBS replacement levels was observed. The analytical modelling did not give the exact age at cracking, but did however give an identical order of cracking when comparing the different materials. This suggests that the ring test is sufficient for the assessment of relative susceptibility to cracking of FA and GGBS bonded overlays. Additionally, a correlation existed between the net age at cracking and the crack area, specimens with higher net age at cracking exhibited the smallest cracks. It was also noted that on average, the ring test results were 62 ± 7% that of the analytical modelling result for w/b ratio 0.45. At w/b ratio 0.65, the age at cracking from the analytical modelling was on average 66 ± 7% that of the ring test results.

Table of Contents

List of Figures

List of Tables

Abbreviations

AAEM	Age Adjusted Effective Modulus
ACI	American Concrete Institute
Al_2O_3	Aluminium Oxide (Alumina)
ASTM	American Society for Testing and Materials
BCO	Bonded Concrete Overlay
C_2S	Dicalcium Silicate
CaO	Calcium Oxide (Lime)
$Ca(OH)_2$	Calcium Hydroxide
C-S-H	Calcium Silicate Hydrate
CoV	Coefficient of Variation
FA	Fly Ash
Fe_2O_3	Ferric Oxide
GGBS	Ground Granulated Blastfurnace Slag
HVFA	High Volume Fly Ash
ITZ	Interfacial Transition Zone
JCI	Japan Concrete Institute
MgO	Magnesia
NIST	National Institute of Standards and Technology
OFA	Original Fly Ash
OPC	Ordinary Portland Cement
PC	Portland cement
RH	Relative Humidity
SANS	South African National Standard
SCA	Slag Cement Association
SiO_2	Silicon Dioxide (Silica)
UTM	Universal Testing Machine
w/b	Water-Binder Ratio
w/c	Water-Cement Ratio
wt %	Weight percent

List of Variables

A, B	Tensile strength regression coefficients (unitless)
C, D	Tensile relaxation regression coefficients (unitless)
E, F	Elastic modulus regression coefficients (unitless)
G, H	Free shrinkage strain regression coefficients (unitless)
D_i	Inner diameter of mortar annulus (mm)
D_o	Outer diameter of mortar annulus (mm)
E_{cm}	Mean elastic modulus at 28 days (GPa)
E_t	Tensile Elastic Modulus (GPa)
$E_{t,i}$	Mean elastic modulus in the interval from t_{i-1} to t_i, (GPa)
f_{ck}	Characteristic cylinder strength (MPa)
$f_{ck,cube}$	Characteristic cube strength (MPa)
f_{cm}	Mean compressive strength at 28 days (MPa)
f_t	Tensile strength (MPa)
$f_{t,i}$	Tensile strength at time t (MPa)
h	Height of steel ring (mm)
t	Arbitrary point in time (any unit of time)
t_i	Time i (days)
t_0	Initial point in time (any unit of time)
t_{IS}	Thickness of inner steel ring (mm)
t_{OS}	Thickness of outer steel ring (mm)
$t_{overlay}$	Thickness of overlay (mm)
α	Degree of restraint (unitless)
β	Mean tensile relaxation in the interval from t_{i-1} to t_i (%)
ε_{FSS}	Free shrinkage strain ($\times 10^{-6}$)
$\Delta\varepsilon_{FSS}$	Change in fee shrinkage strain in the interval from t_{i-1} to t_i, ($\times 10^{-6}$)
ψ	Tensile relaxation factor (unitless)
ψ_i	Mean tensile relaxation factor from interval t_{i-1} to t_I (unitless)
$\sigma_{t,i}$	Tensile stress at time t_i (MPa)
$\sigma_{t,i-1}$	Tensile stress at time t_{i-1} (MPa)

CHAPTER ONE

1 Introduction

1.1 Background and scope of research

The concrete repair, protection and strengthening industry is driven by deterioration of, damage to, and defects in concrete structures. Even with its superior physical properties, concrete is not a perfect material. Concrete has low ductility and low tensile strength. It is permeable and thus can allow ingress of harmful substances such as chlorides, making it susceptible to chemical attack. Deterioration is often quickened through the use of materials of poor quality, substandard designs, and accelerated construction processes. Like any other manmade product, concrete also experiences time-dependent deterioration under weathering or harsh working environments. The impact of deterioration or damage is a reduction in the service life of the concrete structure. Fortunately, repairing the concrete can restore the structural function, protect the underlying reinforcement from aggressive environments, or restore any lost performance requirements (Shiu & Goodwin, 2014; Strategic Development Council, 2006). Achieving durable and reliable repair of existing structures is one of the biggest challenges in the civil engineering industry at present. Majority of concrete structures constructed in the 1960 and 1970s have already surpassed their designed service life, further emphasizing the need for repair and rehabilitation. (Lukovic, et al., n.d.).

Concrete repair is however, a complex process that possess unique challenges different from those associated with new concrete construction. The process involves the formation of a composite system that must integrate old materials with new materials. This system must be able to endure exposure to service loads, environment, and time (Vaysburd & Emmons, 2006). One of the common methods used to repair and rehabilitate damaged concrete structures is the bonded overlay technique. The technique involves replacement of the damaged concrete with a new concrete or mortar layer. This method can be used for both structural and non-structural repairs and is particularly suitable for the repair, lining, and retrofitting of concrete structures, roads and pavements (Beushausen & Alexander, 2006). However, the effects of surface cracking due to restrained thermal and hygral deformations impair the performance of the overlays (Beushausen & Chilwesa, 2013).

The mechanisms that lead to restrained shrinkage cracking are complex and depend predominantly on material parameters, environmental conditions, and the degree to which the overlay is restrained in the composite system (Beushausen & Alexander, 2007). The restraint of the overlay volume changes leads to a locked-in strain energy which causes tensile stresses to develop within the overlay, and shear stresses at the interface. These stresses depend on the magnitude of the restrained deformation and elastic properties. The induced stresses often surpass the tensile strength of the overlay, causing cracking (Beushausen & Alexander, 2006). In most cases, early-age cracking does not reduce the structural capacity of the construction element (Pigeon, et al., 2000). However, cracks affect the appearance of concrete as well as impair durability by increasing the permeability of concrete, allowing the ingress of deleterious substances (Beushausen & Alexander, 2006; Pigeon, et al., 2000; Li & Li, 2009).

Tensile strength, tensile relaxation, elastic modulus, and shrinkage have been identified as key material parameters influencing the overlay's susceptibility to cracking (Emmons & Vaysburd, 1996; Pane & Hansen, 2008; Darquennes, et al., 2012; Beushausen & Chilwesa, 2013). These properties are dependent on the age and degree of hydration (Pane & Hansen, 2002) among other things. Hydration represents the conversion of different phases in the cement paste to form a rigid load-bearing solid element. This process is linked to the development of the microstructure of concrete and ultimately relates to important physical properties such as strength and elastic modulus (Pane & Hansen, 2005; Bentz, 2008). Literature shows that in-depth knowledge of these mechanical properties of the overlay material is essential for the prediction of stress development (Pane & Hansen, 2002; Scrivener & Nonat, 2011; Bentz, 2008; Mounanga, et al., 2006). This knowledge can be used to carefully select the constituents of a concrete mixture so as to improve the performance of the overlays. Cement extenders such as ground granulated blast furnace slag (GGBS) or fly ash (FA) present a viable solution to improving the performance of the overlay with respect to cracking. According to Schneider, et al. (2011), cements containing several main constituents offer a large potential in terms of durability. In addition, they tend to exhibit slower hydration, which relates to lower levels of heat release, and thus less internal tension in the concrete elements.

1.2 Research Aim

The research aims at investigating the influence of fly ash and ground granulated blastfurnace slag on the performance of bonded concrete overlays with regards to restrained shrinkage cracking. The research also aims at using the influence of FA and GGBS on the specific material properties governing restrained shrinkage to analyse and predict the performance of the overlay materials.

1.3 Research significance

Effects of FA and GGBS have long been recognized primarily for long-term concrete performance. However, their effects on stress development in hydrating concrete and on the material properties of bonded overlays still need to be investigated. The long-term performance of concrete is strongly influenced by its short term behaviour; the concrete has to withstand the early-age problems in order to guarantee good long term behaviour (Pane & Hansen, 2008). Thus looking at the short-term behaviour is of importance to fully understand what would constitute a durable repair material. Using FA and GGBS introduces several components of varying reactivity and composition into the concrete. In order to correctly utilise such materials, a good understanding of the mechanisms underlying their performance is required (Zajac & Haha, 2014).

This investigation makes a relevant input towards continued development in understanding and improving the prediction of bonded concrete overlay performance with regards to restrained shrinkage. The use of fly ash and slag for the improvement in performance of overlay materials as well as the ability to use existing analytical modelling to predict this

improvement would add great value to this field of research. Considering the present day volume of damaged and deteriorated structures, advancements that increase the reliability of concrete repair are of great significance to engineering and economics. Ensuring the durability of these composite systems requires a systematic approach that incorporates various aspects such as condition evaluation, design objectives, material selection, and research (Vaysburd & Emmons, 2006). This dissertation is therefore a contribution towards that goal and is written in the interest of both education and practice.

1.4 Thesis objectives and research strategy

The objectives of this research are to:

1. Identify key material parameters that affect the cracking potential of bonded concrete overlays,
2. Describe the mechanism of the cracking phenomenon, showing the interaction of each of the main material parameters,
3. Identify the main factors affecting each of the material parameters identified in (1),
4. Describe the effect of the cement extenders on the materials parameters identified in (1) and identify from literature which material parameters are most affected by the inclusion of the cement extenders,
5. Numerically model the development of stresses in order to project the overall effect of using cement extenders in concrete overlays, and
6. Carry out experimental investigation to determine the actual performance of the concrete overlays in respect to restrained shrinkage cracking.

An extensive literature review, numerical modelling and experimental investigation form the basis of this research. According to Scrivener & Kirkpatrick (2008), there is a need to reduce extensive empirical testing of each individual material. Numerical modelling will also assist in determining the important variables necessary for the experimental investigation. This would reduce the number of tests required.

Figure 1.1 shows the schematic of the strategy to be adopted in this research.

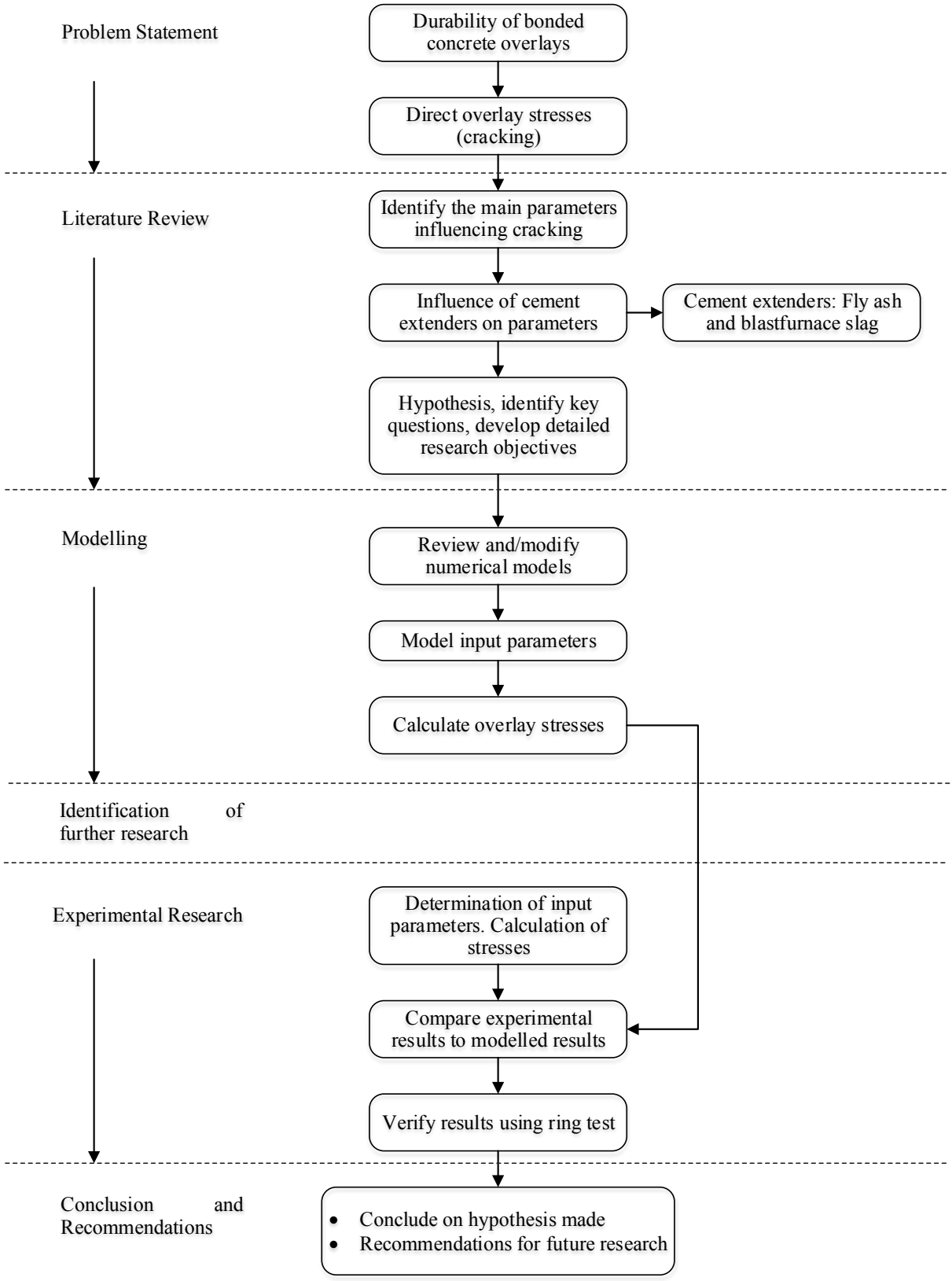

Figure 1.1: Thesis structure and research strategy

Following the above, recommendations for the design of bonded overlays using fly ash and GGBS will be given. Areas in need of further research will also be highlighted.

1.5 Outline of thesis document

The thesis document is divided into six chapters. Chapter one presents an overall introduction to the study. It specifies the scope of the research as well as its objectives.

Chapter two provides a critical discussion from literature on restrained shrinkage cracking of bonded concrete overlays. The chapter elaborates on the fundamental mechanisms behind the cracking phenomena in the overlay material. The chapter begins by giving a brief overview on bonded concrete overlays, this is followed by a review of the use of fly ash and slag in concrete, focussing only on the relevant aspects to this research. Restrained shrinkage and the key material properties influencing the cracking potential are then discussed. The emphasis is on shrinkage, strength development, elastic modulus and, tensile relaxation. This information is then extrapolated to the influence cement extenders have on the individual parameters and ultimately on the behaviour of the concrete overlay. Following the synthesis of the literature, a hypothesis is made on the possible use of fly ash and slag to reduce cracking in concrete overlays. This chapter also identifies the gaps in knowledge and draws out key questions from the literature. Based on the above, the need for research is identified. The chapter is concluded by reiterating the main research objectives, taking into account the findings from the literature.

Chapter three discusses the preliminary modelling approach used in this research. The chapter reviews a selected model used in previous studies, and applies the model to the current research question. Through this preliminary modelling, the relevant variables were identified and used to streamline the experimental investigation.

Chapter four gives a comprehensive description of the experimental procedures that were carried out during the study. It highlights the main parameters considered and the important variables investigated in this study. The chapter provides an overview on the experimental approach and also includes a brief description on the analysis methods used in the investigation.

Chapter five presents and discusses the results obtained from the experimental investigation and analytical modelling of material properties. An attempt is made to relate the obtained results to the literature in order to improve understanding.

Chapter six provides the conclusions drawn from the experimental results, as well as recommendations for future research.

CHAPTER TWO

2 Literature Review

2.1 Introduction

This chapter provides a detailed review of the literature concerning the performance of bonded concrete overlays, specifically with respect to restrained shrinkage cracking of non-load-bearing bonded overlays. The chapter begins by giving an overview on the definition, factors affecting, and materials properties of bonded concrete overlays in Section 2.2. Building on the description of overlay material types and properties, a brief review on properties of fly ash and slag, (potential overlay materials) is provided in Section 2.3. The properties of fly ash and slag concretes are well documented and as such, only the relevant information pertaining to their influence on the material properties identified will be reviewed. Section 2.3 is intended to provide an understanding of the fundamental properties of fly ash and slag that govern their behaviour. This is then followed by a detailed review on restrained shrinkage cracking, discussing the mechanisms and driving forces behind the phenomenon, and the factors that affect it (Section 2.4). The focus is drawn onto the material properties and how they are affected by the partial replacement of cement with fly ash or slag. This is in an attempt to develop a hypothesis on the influence of fly ash and slag on restrained shrinkage cracking to justify the research topic. Finally, a summary of the gathered information is provided in Section 2.5. Key questions based on the findings from the literature review are raised, and the detailed research objectives are outlined to tackle the questions.

2.2 Overview on bonded overlays

2.2.1 Definition of bonded overlays

Yun & Suh (1999), describe two classifications of concrete overlays: the type used in concrete pavements, and the type used for interface treatments. Concrete overlays of the pavement type included jointed plain concrete overlays, jointed reinforced concrete overlay, and continuously reinforced overlays. Bonded concrete overlays (BCO) were said to belong to the second type of overlays, those used for interface treatments. The BCO method was described as one in which the substrate and overlay are bonded together and act monolithically. The deteriorated surface of the substrate concrete is removed, and a relatively thin layer (50 – 120 mm) of concrete is overlain to produce a monolithic structure. An anatomy of the BCO repair is shown in **Figure 2.1**.

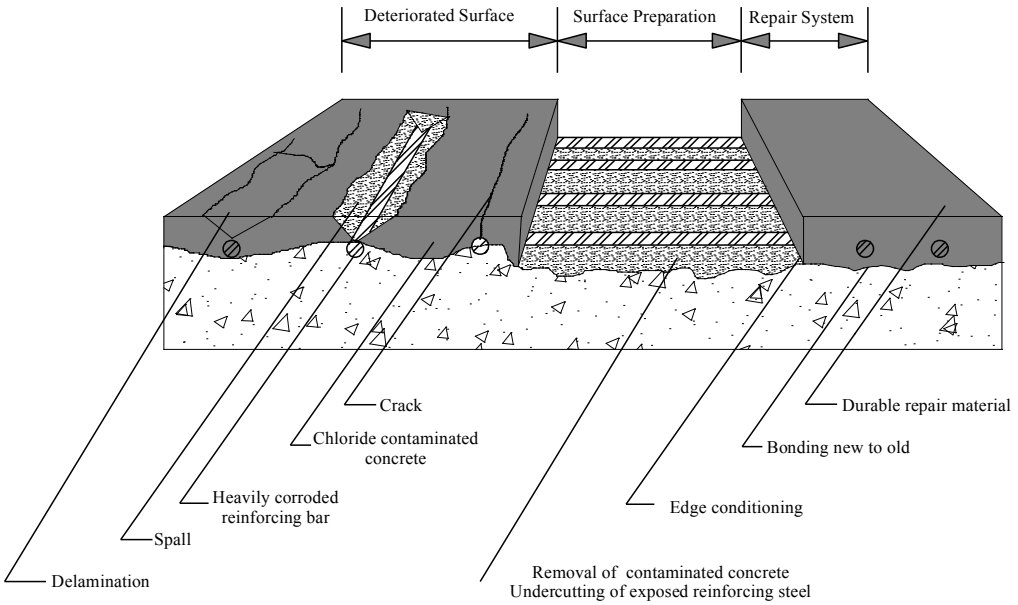

Figure 2.1: Anatomy of concrete repair using the bonded overlay technique (Adapted from Emmons & Vaysburd (1996)).

This repaired concrete structure is considered a composite system of composite materials that are exposed to exterior and interior environments and their reactions. The systems can be characterised as a three phase system, comprising of the existing substrate, the repair material, and the transition zone between them (Vaysburd & Emmons, 2006) as illustrated in **Figure 2.2**.

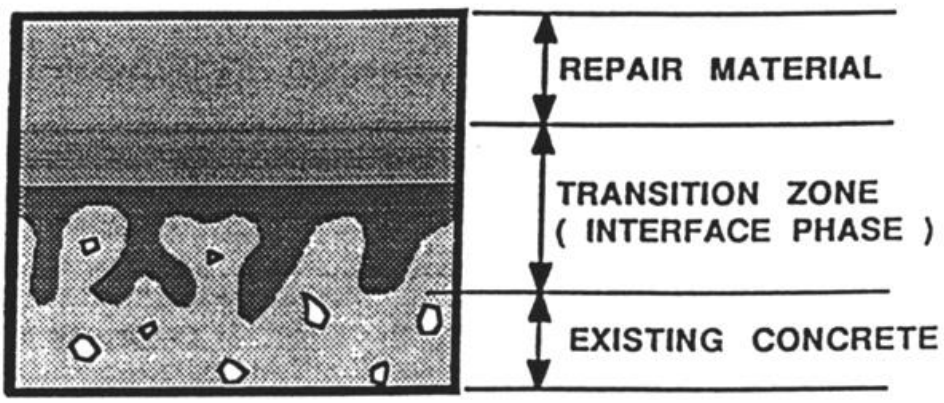

Figure 2.2: Idealized model of a surface repair system (Vaysburd, et al., 2000).

Bonded concrete overlays have been in existence since 1909. The primary purpose of the overlay is to help extend the service life of structural elements such as concrete slabs, pavements, or bridge decks (Fowler & Trevino, 2011). Concrete bridge decks are one of the bridge elements that are most severely exposed to harsh environmental loads and as such, experience frequent damages. This is particularly true for concrete bridge decks built in the 1960's at a time when there was little knowledge on concrete durability. Other elements such

as edge beams, parapets, supports, slopes and embankment ends also show frequent damages. Bonded concrete overlays are often the best repair alternative to repair this type of deteriorated concrete (Silfwerbrand & Beushausen, 2006).

2.2.2 Overlay material types and properties

Growth in the development of repair materials considered to be "durable materials" such as low slump dense concrete, resin-based repair mortar/concrete, and polymer modified mortar/concrete has been experienced in recent years. However, the current concrete repair experiences reveal a mixed review of repair performance. Almost half of all concrete repairs have been estimated to fail in the field. Concrete repairs are perceived to lack early age performance as well as long-term durability. This makes developing effective and durable repair systems of great research significance. Durable repair systems should be able to protect the repaired concrete structure from aggressive environments and address the underlying concrete deterioration problems (Tayeh, et al., 2012). A number of decisions are involved with the use of bonded concrete overlays, i.e. availability of resources, type of rehabilitation, type of overlay, and suitability of a bonded concrete overlay. Following the decision to use a bonded concrete overlay, the design must ensure that the overlay achieves the desired service life (Trevino & Fowler, 2004).

To understand how the performance of a composite repair system is affected by various factors, the notion of 'compatibility' must be introduced. Compatibility in this case refers to a balance of physical, chemical, electrochemical, and deformation properties between the substrate and the repair system. Achieving this balance ensures that the system as a whole is able to withstand shrinkage-induced tensile stresses, as well as chemical or electrochemical effects without premature failure. Dimensional compatibility of the repair material with the existing substrate is one of the most important compatibility components. This includes factors such as drying shrinkage of the repair material, thermal expansion/contraction differences, elastic modulus, and creep properties (Emmons & Vaysburd, 1996; Morgan, 1996; Hassan, et al., 2001). An ideal repair material would thus be volumetrically stable, that is, it would neither shrink nor expand, and would display similar elastic modulus and thermal expansion characteristic as the substrate concrete. Unfortunately, such a product does not appear to exist despite the efforts of product formulators. As it is, the best type of repair material that can be hoped for is one with suitable modulus of elasticity, and sufficiently low volume change capacity (Morgan, 1996).

The types of repair material can be grouped under three generic categories, resinous materials, polymer modified cementitious materials, and plain cementitious materials. The mechanical properties of resin mortars are vastly different from those of plain cementitious mortars, while the mechanical properties of polymer modified cementitious mortars tend to be intermediate between the two. Cementitious mortar are thus more likely to have mechanical properties closest to most substrate concretes and could be argued to be the most appropriate repair material in attaining compatibility. Though this view may hold in certain types of repairs, it may not be the best remedial solution for others. For example, when the original concrete has deteriorated as a result of aggressive exposure conditions. It goes to show that there is no such thing as the ideal repair material. The application, exposure conditions, and physical and

chemical compatibility of the repair material dictate the type of repair material to be used (Morgan, 1996). Fly ash and slag are materials well known to improve the durability of concrete and influence the development of mechanical properties. These materials present a viable alternative for use in BCO. Using fly ash or slag introduces several components of varying reactivity and composition into the concrete. In order to correctly utilise such materials, a good understanding of the mechanisms underlying their performance is required (Zajac & Haha, 2014). The following section is therefore intended at providing information on the fundamental properties of fly ash and slag.

2.3 Review of fly ash and ground granulated blastfurnace slag in concrete

Fly ash (FA) and ground granulated blastfurnace slag (GGBS) are now routinely used in concrete construction. These materials are able to improve the microstructure of the cement pastes as well as the engineering properties and durability of the concrete if used judiciously (Ballim & Graham, 2009). Fly ash and slag are both industrial by-products. Fly ash is a by-product of coal combustion. Finely ground coal dust is injected into a furnace. The non-combustible material of the coal dust melts while in suspension, and cools rapidly as it exists the furnace. The rapid cooling results in the formation of spherical particles with glassy and crystalline phases known as fly ash which is a pozzolanic material that in itself does not possess cementitious characteristics (Mukheibir, 1990). Blastfurnace slag is a by-product of the iron manufacturing industry. Iron ore, coke and limestone are placed in a furnace resulting in molten slag floating above the molten iron. Once the molten iron is removed, the remaining molten slag which contains mostly siliceous and aluminous residues, is water-quenched rapidly. This forms glassy granulate which is then dried and ground to form what is known as ground granulated blastfurnace slag (Leung & Wong, 2011). The glassy slag particles formed, in contrast to fly ash, are reactive in their own right (Young, et al., 1998).

2.3.1 Chemical composition

The composition of fly ash depends largely on the type of coal used. The three main constituents of fly ash are SiO_2, Al_2O_3, and Fe_2O_3. Fly ash is mostly composed of non-crystalline glassy phases and the chemical reactivity is essentially dependent on the nature and amount of the phase present in the material (Mukheibir, 1990; Krüger, 2003). In general, there are two classes of fly ash: ‘low-lime fly ash’ with truly pozzolanic characteristics, and ‘high-lime fly ash’ which show some cementitious properties in addition to the pozzolanic activity. Low-lime fly ashes are classified as type-F, while high-lime fly ashes are classified as type-C. All South African fly ashes comply with the definition of type-F fly ash (Gogol, 1994). Blastfurnace slag comprises mainly of CaO, MgO, Al_2O_3, and SiO_2, similar to Portland cement. There is very little change in composition of slag provided the sources of iron ore, coke, and flux are consistent (Leung & Wong, 2011). **Table 2.1** provides the chemical analysis of South African fly ash and slag.

Table 2.1: Chemical analysis of South African FA and GGBS (Mantel, 1992).

	Portland cement	South African FA	South African Slag
SiO_2	22.9	56.1	36.6
Al_2O_3	4.2	31.6	13.2
Fe_2O_3	3.8	3.4	0.6
Mn_20_3	0.4	-	1.2
TiO_2	-	1.6	1.9
CaO	65.0	4.1	33.0
MgO	3.3	1.0	10.7
P_2O_2	-	0.4	-
SO3	0.2	0.1	2.5
Na_2O	0.1	0.4	0.2
K_2O	0.6	0.6	0.9
CaO/SiO_2	2.84	0.07	0.9

Figure 2.3 summarises the above information and shows relative concentrations of the three main constituents of fly ash and slag, in comparison to that in ordinary Portland cement. Reactivity of the cementitious material is a function of the lime content, and generally increases with increase in lime content (Grieve, 2009) (i.e., increases towards the bottom left corner of the triangle shown).

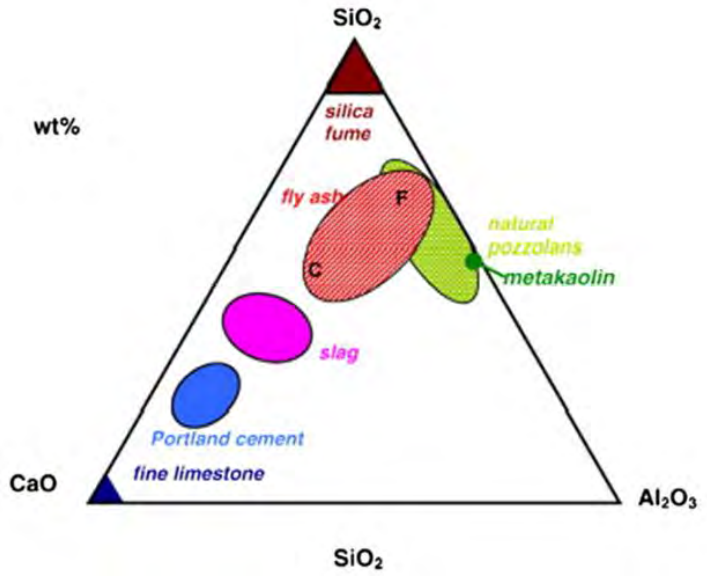

Figure 2.3: $CaO–Al_2O_3–SiO_2$ ternary diagram of cementitious materials (Scrivener & Nonat, 2011).

2.3.2 Physical properties

The fresh and hardened properties of fly ash concrete are influenced by the fineness, particle size distribution, shape, and physical composition of the fly ash particle used. The pozzolanic activity is governed by the fineness and particle distribution of the fly ash particles; the finer the fly ash, the greater the surface area and the better the pozzolanic activity. Fly ash particles

are generally spherically shaped (see **Figure 2.4**), which is strikingly different from the angular shape of Portland cement particles. The spherical shape of the fly ash particles results in improved workability of the concrete (Mukheibir, 1990). The specific surface area of South African fly ash marketed as cement extender is 350 – 400 m^2/kg, an accurate value is difficult to determine. This is due to the trouble in accurately determining the density of fly ash which is required to calculate the specific surface. This is because the hollow fly ash particles have entrapped air in them. The specific surface area is also significantly increased with increase in carbon content of the fly ash (Krüger, 2003).

The fineness of slag particles is normally in the range of 350 – 380 m^2/kg (Blaine). Slag particles are said to show conchoidal faces which is a characteristic typical of glassy materials (Addis, 1987).

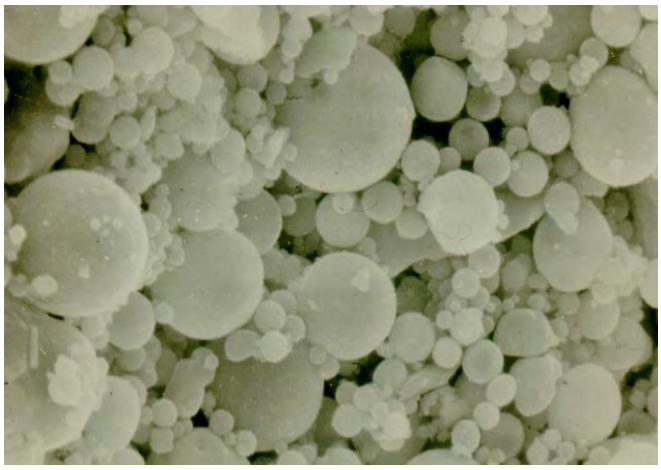

Figure 2.4: An electron micrograph of a typical South African FA. Magnification: 2 000 (Krüger, 2003).

2.3.3 Hydration and microstructure of FA and GGBS concretes

2.3.3.1 Effect of FA and GGBS on degree of hydration

The reaction of cement is a complex process that involves interactions between water and anhydrous solid compounds. During the reaction, water is consumed and the anhydrous compounds continuously disappear in the paste to form solid products. This process is called hydration. Just like any typical chemical process, the hydration reaction involves phase transformations, substance redistribution, energy changes, and physical changes. The final product of this reaction is a solid, porous material that possesses engineering properties and contains different phases such as anhydrous reactant, hydration products, air voids, and pore solution (Chen, 2006). Knowledge on the basic kinetic mechanisms of hydration is necessary in providing informed decisions on the proportioning and selection of mineral admixtures. Understanding the hydration process provides a foundation for understanding the interactions leading to the development of the microstructure of the cement paste (Bullard, et al., 2011). It was therefore essential to briefly review the hydration reactions of fly ash and slag concretes in order to fully understand their effects on the development of the material properties discussed in Section 2.4.

There are four main phases in Portland cement, all of which can react with water to produce different types of hydration products. These are: tricalcium silicate (C_3S), dicalcium silicate (C_2S), tricalcium aluminate (C_3A), and tetracalcium aluminoferrite (C_4AF). The chief strength-producing compounds in hydrating cement are the calcium silicates. These tend to make up about 75 – 80% of the cement. Their hydration reactions are very similar and can be expressed as shown in Equation 2.1.

$$\begin{aligned} 2C_3S + 7H &\rightarrow C_3S_2H_8 + 3CH;\ \Delta H = -500\ J \cdot g^{-1} \\ 2C_2S + 5H &\rightarrow C_3S_2H_8 + CH;\ \Delta H = -250\ J \cdot g^{-1} \end{aligned} \qquad [2.1]$$

The negative enthalpy values indicate that the reactions are exothermic. Overall, the reactions can be written as:

$$\text{Calcium silicates } \left(C_3S + C_2S\right) + \text{ water} \rightarrow \text{ Calcium silicates hydrate + calcium hydroxide} \qquad [2.2]$$

The amount of calcium hydroxide (CH) produced depends on the relative proportions of the silicates in the cement (Young, et al., 1998).

Fly ash is a pozzolanic material composed primarily of siliceous and aluminous phases, and does not possess cementing properties. However, in the presence of moisture, fly ash reacts with calcium hydroxide to form cementitious compounds. Calcium hydroxide thus plays a critical role for the pozzolanic reaction of fly ash. The calcium hydroxide consumed by the pozzolanic reaction is produced from the cement hydration (see Equation 2.1 & 2.2), therefore the hydration rate of the pozzolanic reaction is dependent on the amount of calcium hydroxide that can be liberated (Young, et al., 1998; Zajac & Haha, 2014).

The reaction can be expressed as:

$$2S + 3CH + 7H \rightarrow C_3S_2H_8 \qquad [2.3]$$

It is therefore expected that at higher replacements of Portland cement with fly ash, less calcium hydroxide is available for the pozzolanic reaction, resulting in more retardation of the hydration reaction. The calcium silicate hydrate produced is similar to that formed from the hydration of C_3S and C_2S in Portland cement (Young, et al., 1998; Krüger, 2003. The pozzolanic reaction results in lower quantities of heat generated, and the reaction is generally slower than the hydration reaction of ordinary Portland cement, with appreciable reactions only occurring after 28 days (Young, et al., 1998; Zajac & Haha, 2014).

More slag can be used than fly ash because of its cementitious character. Only 25 wt % of pozzolan, by weight of cement will react with the calcium hydroxide formed by the hydration of Portland cement and the excess remains as an unreactive dilutant (Young, et al., 1998). The hydration reaction of slag-blended concrete is however more complex than that of Portland cement because the simultaneous hydration of the two constituents interfere with each other. Slag is activated by the calcium hydroxide produced by the Portland cement hydration, while

also consuming large amounts of calcium hydroxide. The hydration of slag-blended cement can be compared to that of C_2S in Portland cement paste. This however differs greatly from one slag to another due to the different reactivity of slag. **Figure 2.5** shows typical curves for the degree of hydration reaction of slag-blended concretes as a function of hydration time for different slag proportions. The degree of hydration is retarded by the presence of large amounts of slag. However, the slag hydration continues at later stages due to the large amount of anhydrous slag in the cement (Chen, 2006).

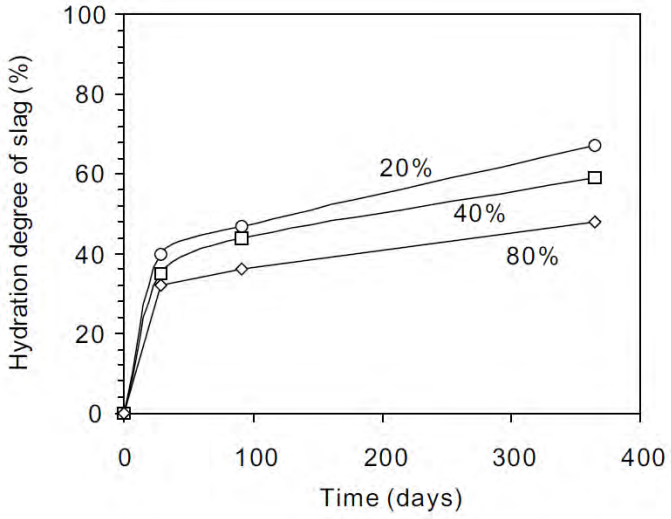

Figure 2.5: Hydration degree of slag in blended cement paste with different slag proportions in cement, w/c = 0.5, T = 20°C, determined with the EDTA method, after Schäfer (2004) (Chen, 2006).

2.3.3.2 Effect of FA and GGBS on pore structure of cement paste

Attention needs to be given to the pore structure that develops during the hydration process as it is of great significance in determining the resultant properties of the concrete (Young, et al., 1998).

Hwang, et al. (2004), reported on the influence of fly ash on the pore size distribution. At 28 days, partial replacement of cement with fly ash resulted in higher total pore volume than in the plain Portland cement concrete. The pore volume was also observed to increase with increasing fly ash content. At 6 months, the total pore volume of both fly ash and reference concrete was lower than at 28 days. Li & Zhao (2003), used Scanning Electron Microscopy (SEM) to make observation on high-volume fly ash (HVFA) specimens at the age of 7 and 360 days. The image characteristics of the concretes at 7 days showed that there are still numerous un-hydrated FA particles present in the concrete (**Figure 2.6**).

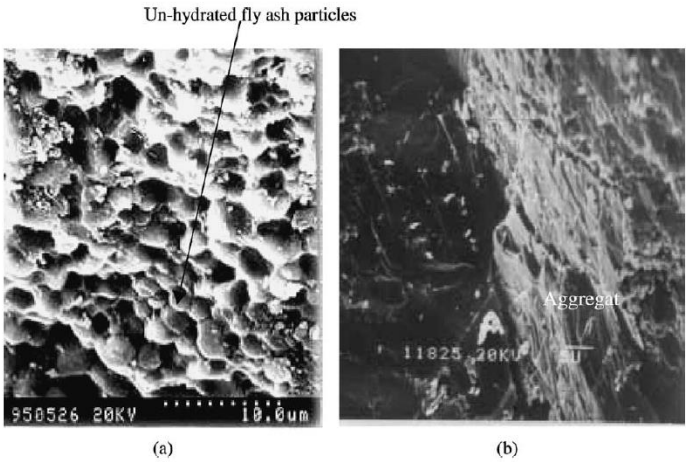

Figure 2.6: SEM micrograph of HVFA concrete: (a) 7 days, (b) 360 days (Li & Zhao, 2003).

A similar observation was also made by Kourounis, et al. (2007), on slag concretes using SEM. It was noticed that with cement substitution of 30% and 45 %, there were still partially hydrated slag particles present in the hardened paste (**Figure 2.7**). Energy Dispersive Analysis (EDAX) was also used to show unreacted slag grains present in the hardened cement paste.

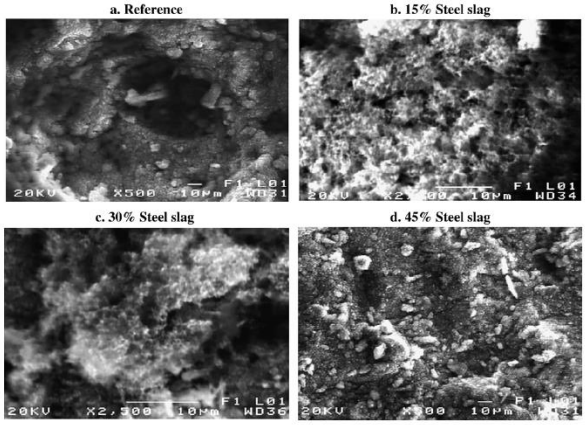

Figure 2.7: SEM photos of blended cements, hydrated at 28 days (Kourounis, et al., 2007).

Zhou, et al. (2006), investigated the effects of slag content on the pore structure of cement pastes at 1 and 3 days. The cumulative volume of the pore structure was seen to increase with increase in slag content. This was attributed to the decrease in the overall degree of hydration and the corresponding reduction of the amount of hydration products. The influence of slag on the pore size distribution was also investigated. At 1 day, the pore structure is mostly made up of larger capillary pores. As the hydration reactions proceed, the pore structure becomes finer. Up to 3 days, the amount and size of the capillary pores decreased, while the amount of gel pores increased. Capillary pores are the empty or water-filled spaces between the hydration products while gel pores formed within the hydration products. Slag had the effect of decreasing both the capillary pore diameter and gel pore diameter with increasing content (Zhou, et al., 2006).

Similar observations were made by Bijen (1996), concrete with slag of fly ash was found to have a substantially finer pore size distribution. Bijen (1996), measured the pore size distribution for a Portland cement paste with and without fly ash or slag using mercury porosimetry. The initial pore size distribution of the fly ash concrete was coarse, but this was reversed at a later stage. The slag concrete exhibited a finer pore distribution from the very beginning.

2.3.3.3 Effect of FA and GGBS on heat of hydration

The hydration of cement is an exothermic reaction, meaning heat is released as the reaction progresses. The total amount of heat generated and the rate of heat generation from the hydration of the individual compounds can be used as an index of the reactivity of the binder material. The heat of hydration can also be used to characterise the setting and hardening behaviour of the binder material (Mheta & Monteiro, 2001).

The partial replacement of Portland cement with fly ash reduces the peak heat rate. A similar effect is observed in the slag concrete. Peak heat rate reduces with increase in fly ash or slag content in the binder. Adiabatic calorimeter results obtained from fly ash-blended cements and slag-blended cements are shown in **Figure 2.8**. The figures shows the heat rate curves.

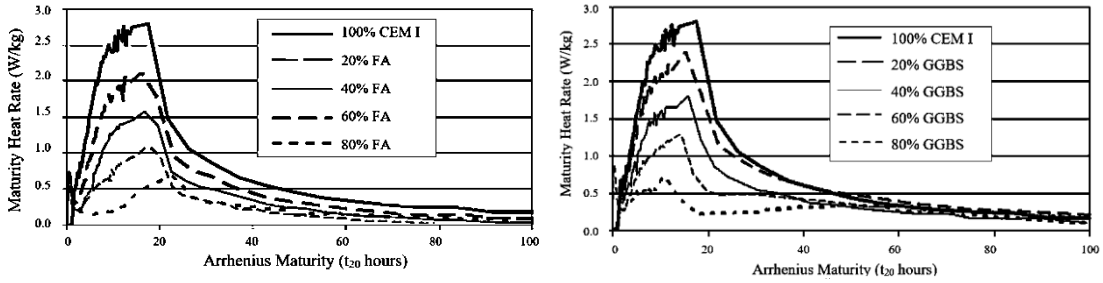

Figure 2.8: Heat rate profiles for FA and GGBS concretes (Ballim & Graham, 2009).

The peak heat rate decreases with increase in fly ash or slag content. The addition of fly ash or slag to the binder delays the start of active hydration, there is significant retardation of the hydration reaction in comparison to plain Portland cement concrete. This is more pronounced at higher levels of fly ash or slag replacement (Ballim & Graham, 2009). Krüger (2003), states that as a rule, for every 10% by mass of Portland cement replaced with fly ash, a 5-6% reduction in the heat of hydration can be expected.

The use of fly ash and slag results in the reduction of heat of hydration of the mixture. **Figure 2.9** gives the changes in heat of hydration that result when slag is used in concrete. The test were carried out under adiabatic conditions (Grieve, 1987). The slag concrete releases less heat because of the low reactivity of slag at the early age (Zhou, et al., 2006). **Figure 2.10** gives information on the heat generated when fly ash is incorporated into the mixture. The heat of solution method was used to obtain the results (Grieve, 1987).

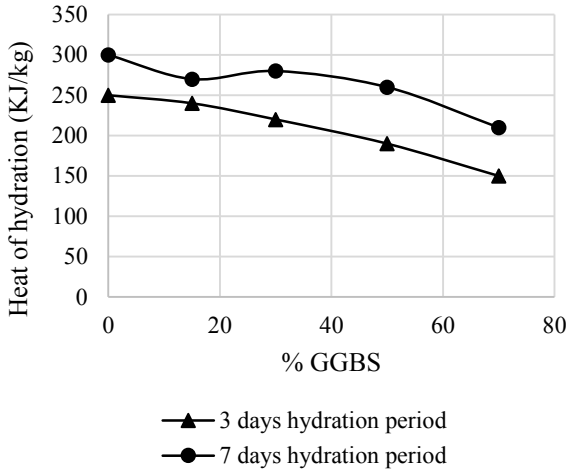

Figure 2.9: Heat of hydration of pastes of ordinary Portland cement and slag mixtures (using adiabatic heat of hydration) (Grieve, 2009).

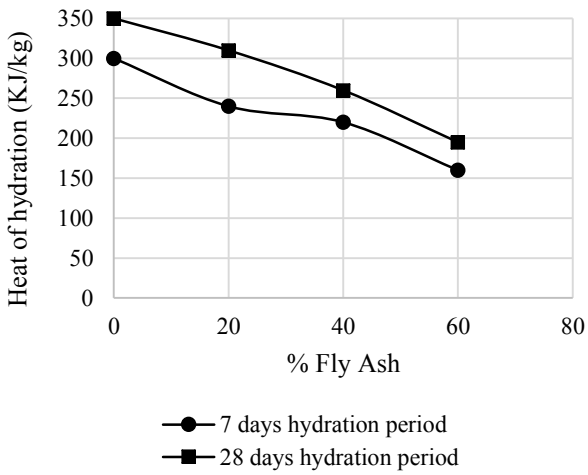

Figure 2.10: Heat of hydration of pastes of ordinary Portland cement and slag mixtures (using heat of solution method) (Grieve, 1987).

Kolani, et al. (2012), carried out experiments in which the heat of hydration of different binders containing slag (30%, 50% and 70%) and pure clinker were compared for a duration of 120 hours. The results showed that incorporating slag into the binder material lowers the heat of hydration. This is because the hydration kinetics of slag is lower than that of clinker and requires the presence of alkali coming from the clinker dissolution. This leads to an overall reduction in the heat of hydration, with larger reductions observed at higher substitutions. The results of the experiments are shown in **Figure 2.11** and **Figure 2.12**.

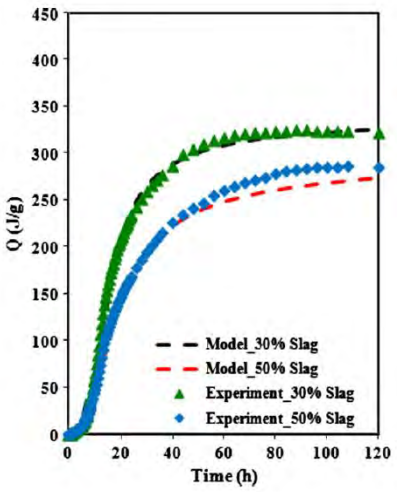

Figure 2.11: Prediction of heat of hydration of blended cements with 30% and 50% slag (Kolani, et al., 2012).

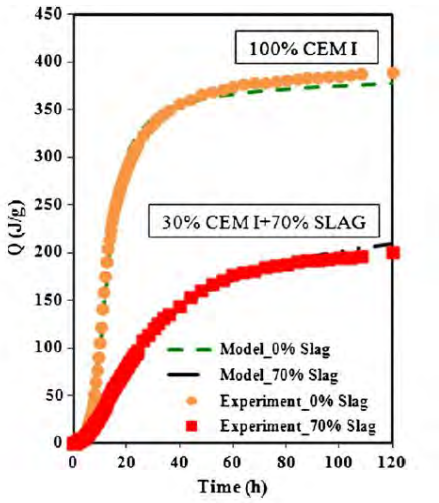

Figure 2.12: Calibration of heat of hydration of pure Portland cement and blended cement with 70% slag (Kolani, et al., 2012).

2.3.3.4 Summary

The development of the mechanical properties of the hardened cement paste are influenced by the degree of hydration (Maia, et al., 2012). The change in mechanism of the hydration reaction

due to the presence of fly ash or slag can thus be expected to affect the development of mechanical properties of the concrete. Thermal stresses in the concrete can be reduced by simply lowering the maximum rate of heat evolution. The same approach could perhaps be used to ensure the maximum shrinkage-induced tensile stresses occur at a time when the concrete has developed sufficient strength, thereby prolonging the onset of cracking. This can perhaps be achieved by delaying occurrence of the maximum peak heat rate (Greensmith, 2005). The above literature shows that the basic nature (physical and chemical composition) of fly ash and slag, tends to cause retardation of the hydration reaction and reduction in the heat of hydration. Section 2.4 discusses the key mechanical properties of concrete influencing restrained shrinkage cracking. The influence of fly ash and slag on these mechanical properties owing to the modification of the hydration reaction is also discussed in order to understand the overall effect on restrained shrinkage.

2.4 Restrained shrinkage cracking of bonded overlays

The cement-based overlay material and the substrate material constitute a composite structural system. The structural behaviour of this composite system is determined by the interaction of these two materials with each other and with external boundary conditions. Governing the structural behaviour are one or a combination of the following actions: differential deformations of the two layers due to autogenous shrinkage, thermo-mechanical effects caused by cement hydration and/or external environmental influences, and drying shrinkage. These actions result in the development of stresses which are dependent on the relative stiffness between the two layers. The build-up of stresses may eventually lead to failure in the form of crack propagation, de-bonding, or both (Denarie & Silfwerbrand, 2004). As mentioned earlier, for the purpose of this research, only the tensile stresses that cause cracking were investigated. The failure modes of bonded overlays (de-bonding and crack formation) are illustrated in **Figure 2.13**.

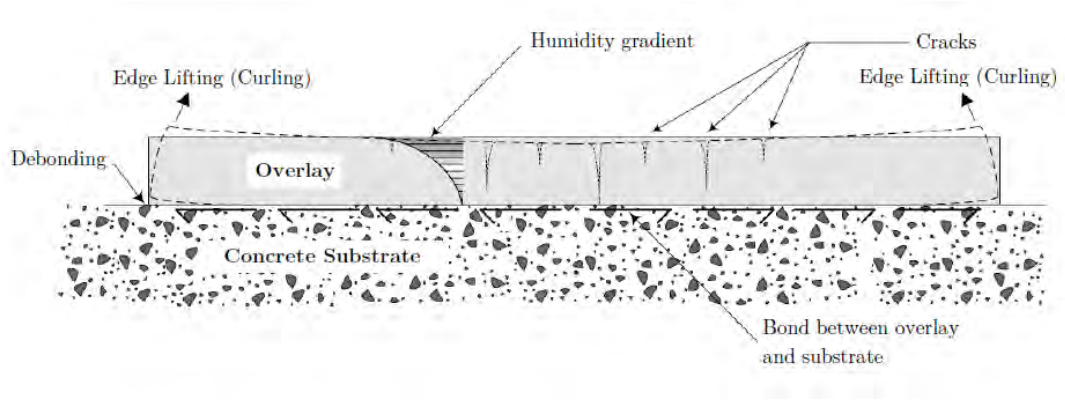

Figure 2.13: Failure modes of bonded overlays (adapted from Cärlsward, 2006) (Bester, 2015).

Stresses generated due to restrained movements can principally be calculated by the product of three factors according to the equation below. Each factor is considered equally important.

$$stress = stifness \times free\ strain \times degree\ of\ restraint \qquad [2.4]$$

The stiffness is dependent on both the elastic modulus and the creep/relaxation. The free strain is the strain developed in a member that is completely unrestrained. This strain may be due to thermal or moisture changes, shrinkage, or any other internal or external cause initiating volumetric change of the member material. The degree of restraint α can be defined as the ratio between the real stress σ_{real}, taking into account the effective stiffness of the composite structure, and the stress occurring in a completely restrained composite structure σ_{full}.

$$\alpha = \frac{\sigma_{real}}{\sigma_{full}} \qquad [2.5]$$

It must be noted that a complete bond between substrate and overlay does not necessarily result in complete restraint in the overlay. This is because the substrate material does not possess infinite stiffness. The volumetric deformation of the overlay material is thus only partially restrained by the substrate material. Due to the absence of complete restraint, it follows that there is a substantial reduction in stresses generated. Combined with stress relaxation, the maximum tensile stresses can possibly be kept below the tensile strength of the overlay, delaying the onset of cracking (Denarie & Silfwerbrand, 2004). Previous research (Beushausen & Alexander, 2006; Beushausen & Alexander, 2007; Beushausen & Chilwesa, 2013) showed that for common substrate and overlay dimensions, 60% of the free overlay shrinkage strain was restrained by the substrate concrete. A value of 0.6 will thus be used as the degree of restraint in this research. This value will remain constant for all model calculations and will only acts as a scale factor for overlay stresses.

Restrained shrinkage cracking of the repair material can be reduced by one, or a combination of the following factors: low shrinkage of the repair material, high relaxation capacity, low elastic modulus, and high tensile strength of the repair material (Vaysburd & Emmons, 2000). The mechanisms, and influence of fly ash and slag on these factors are discussed in the sections that follow.

2.4.1 Autogenous shrinkage

The Japan Concrete Institute (JCI) Committee defined autogenous shrinkage as “the microscopic volume reduction of cementitious materials when cement hydrates after initial setting”. Autogenous shrinkage was also defined not to include the volume changes caused by loss or ingress of substances, variation in temperature, or the application of an external force or restraint. From an engineering point of view, it was often thought that autogenous shrinkage could be overlooked because it is much less than drying shrinkage. However, it has been proven that autogenous shrinkage can be large enough to cause cracking, more especially in high-strength concrete structures. As a result, more and more studies have been carried out on autogenous shrinkage (Tazawa, et al., 2000).

Autogenous shrinkage occurs as a result of chemical shrinkage, the absolute volume of the hydration products is less than that of the total volume of the reactants. The negative volumetric balance, known as Le Chetelier contraction or chemical shrinkage, is in the order of 10% of the volume of the hydration products. On formation of the solid skeleton, chemical shrinkage results in the formation of pores in the hydrating paste structure. In the absence of

an external source of water, the hydration reaction proceeds through the consumption of the capillary water. The continuous emptying of the pore structure is essentially a self-desiccation process. According to the kelvin equation, there is a gradual increase in the tensile stress in the pore water due to the formation of menisci. The build-up of capillary tension results in contraction of the hardening concrete (Ji, 2008; Gagne, et al., 1999).

In summary, before the setting of samples under sealed conditions, there is only external autogenous shrinkage, which is proportional to the amount of reacted cement. External autogenous shrinkage is caused by the simultaneous effects of chemical shrinkage and physical action of the meniscus in the capillary pore network. After setting, both external and internal autogenous shrinkage occur. Internal autogenous shrinkage is the total volume of the gas-filled spaces created in the capillary pore network. The sum of the internal and external shrinkage is the total autogenous shrinkage (Gagne, et al., 1999). Determination of the autogenous shrinkage is difficult to perform due to the complex fluid-solid transition that occurs at the time of setting. This makes it challenging to compare shrinkage results directly because autogenous shrinkage is zeroed at different times. In fact, autogenous shrinkage strongly depends on the start time of the measurement because the process of self-desiccation begins as soon as hydration begins. To obtain the maximum potential autogenous shrinkage, measurements must therefore begin before initial setting time (Lee, et al., 2006).

It should be pointed out, that there is a difference between autogenous and chemical shrinkage. This is illustrated in **Figure 2.14**. In the plastic state, the autogenous and chemical shrinkage are essentially the same. However, when the hydration products percolate to form a structural skeleton, the restraint of autogenous shrinkage by the skeleton results in deviation from the theoretical chemical shrinkage (Li, 2011).

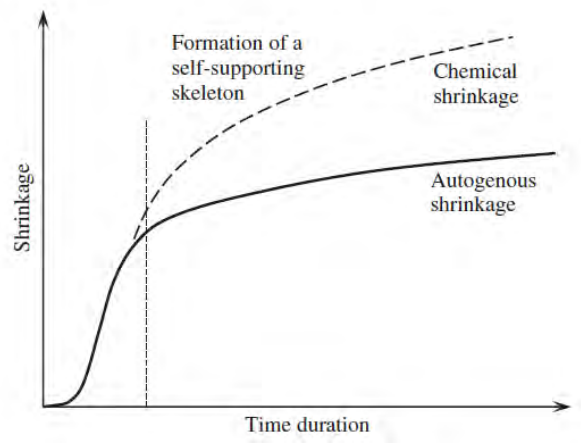

Figure 2.14: Relationship between autogenous shrinkage and chemical shrinkage (Li, 2011).

2.4.1.1 Effect of w/b on autogenous shrinkage

Autogenous shrinkage is dependent mainly on the w/b ratio and the mineral composition of the binder. The effects of w/b on autogenous shrinkage are very clear, autogenous shrinkage increases with decreasing w/b ratio. At w/b ratio greater than 0.45, the autogenous shrinkage of concrete remains less than 100 μm/m, but increases rather rapidly when the w/b ratio is below 0.40. This is simply an effect of pore size, there is an inverse relationship between the

tensile stresses in the liquid phase and the pore size at the interface with the gaseous phase. High strength concretes with low w/b ratio are thus more prone to significant autogenous shrinkage (Ji, 2008). Li (2011), also notes that although autogenous shrinkage was considered a factor contributing to the total shrinkage in the 1930s, it was later discovered that autogenous shrinkage only occurred at very low w/b ratios.

This theory is supported by experimental works. For example, Tazawa, et al. (2000), observed an increase in autogenous shrinkage with decreasing water-binder ratio. **Figure 2.15** shows the autogenous shrinkage of cement pastes with different water-binder ratio. It was also noted that the autogenous shrinkage of cement pastes with low water-binder ratio increased at a faster rate than for cement pastes with higher water-binder ratio.

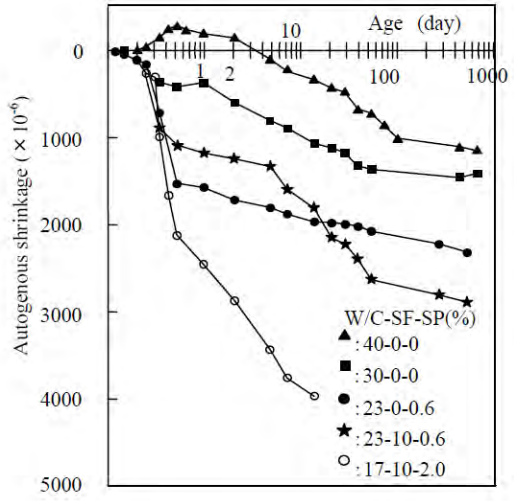

Figure 2.15: Effect of water-binder ratio on autogenous shrinkage of cement paste (Tazawa, et al., 2000).

2.4.1.2 Effect of FA and GGBS on autogenous shrinkage

According to research carried out by Zhou, et al. (2006), the autogenous shrinkage of portland cement blended with blastfurnace slag is higher than that of plain Portland cement concrete. A Mini-TSTM developed at Delft University of Technology was used to measure the autogenous deformation of cement pastes. Linear deformations of autogenous deformation were performed at a room temperature of 20±3°C, and the results continuously collected by computer. Investigations on the heat evolution and microstructure of the cement pastes were also carried out using isothermal condition calorimetry, mercury intrusion porosimetry, and scanning electron microscopy. The increase in autogenous shrinkage in blastfurnace slag concrete was attributed to greater chemical shrinkage, finer pore structure, and higher contents of Alumina-rich C-S-H gel and AFm phases in slag pastes. The autogenous shrinkage of slag blended pastes was investigated at 0%, 50% and 70% replacement levels. The development of autogenous shrinkage was divided into four stages and is shown in **Figure 2.16**. In the early stages (stage I and II), the slag pastes deformed slower than the plain Portland cement paste. After being activated by the calcium hydroxide from the hydration of the Portland cement, the slag reaction leads to larger chemical shrinkage and finer pore structure.

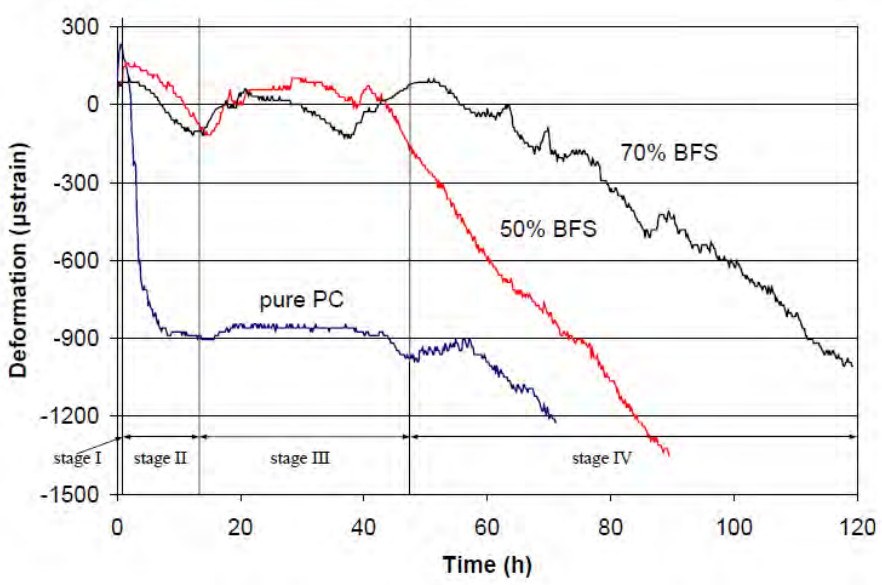

Figure 2.16: Autogenous shrinkage of Portland cement pastes blended with 0%, 50% and 70% slag (Zhou, et al., 2006).

In stage III, the deformation of the plain Portland cement paste is more stable than that with slag, and the duration of this stage is influenced by the slag content. In the last stage, the paste with slag shows a larger autogenous shrinkage owing to the finer pore structure of the slag paste. At this stage, the stiffness of the paste is more developed, meaning that restrained autogenous deformations would lead to higher stresses in the slag cement paste in comparison to the plain Portland cement paste.

Tazawa, et al. (2000), found that the effect of slag on autogenous shrinkage was influenced by the fineness of the slag. The authors observed a reduction in autogenous shrinkage when low Blaine fineness blastfurnace slag was added to the cement paste. In contrast, the addition of blastfurnace slag with high Blaine fineness led to increased autogenous shrinkage, especially at large replacement ratios. The effect of blastfurnace slag on autogenous shrinkage of cement paste is illustrated in **Figure 2.17**. Similarly for fly ash concretes, Termkhajornkita, et al. (2005), observed an increase in autogeneous shrinkage with an increase in Blaine surface area. The degree of hydration increases with an increase in Blaine surface area, resulting in corresponding autogenous shrinkage.

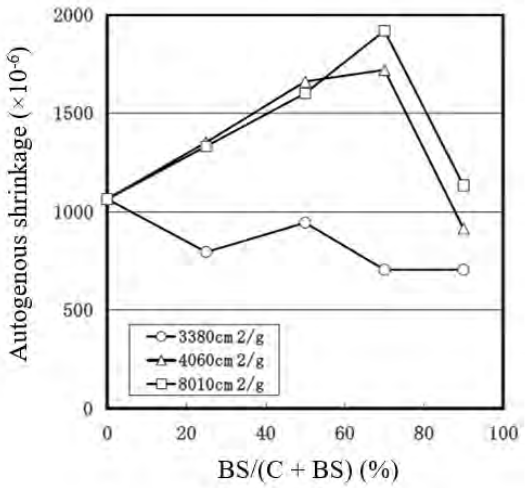

Figure 2.17: Effect of blastfurnace slag on autogenous shrinkage of cement paste (W/(C+GGBS) = 0.40) (Tazawa, et al., 2000).

Zhang, et al. (2000), found similar results. Cement paste containing superfine GGBS exhibited higher autogenous shrinkage than paste with only Portland cement type I (PC.I). At seven days, the autogenous shrinkage of specimens with a fineness of 740 m^2/kg and 500 m^2/kg increased by 60% and 17% respectively. Thus it was concluded that the higher the fineness of GGBS, the more the autogenous shrinkage. **Figure 2.18** shows these results.

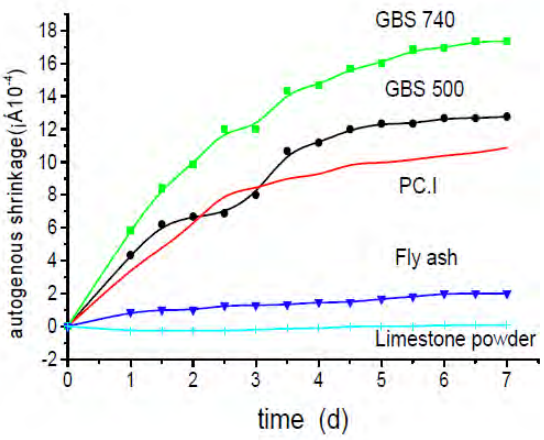

Figure 2.18: Autogenous shrinkage of cement paste containing different mineral additives (Zhang, et al., 2000).

Fly ash on the other hand was found to reduce autogenous shrinkage. This was attributed to the spherical nature of the fly ash particles which are assumed to retain less water than irregular cement or GGBS particles. As a result, a higher free water content exists in the fly ash mixture than in the mixtures without fly ash prepared with the same water-binder ratio. The large free water content leads to less autogenous shrinkage. Schieβl, et al. (2000), add that lower content of mesopores are formed during the pozzolanic reaction which favours the reduction of autogenous shrinkage in fly ash cement paste. The autogenous shrinkage strain results that were obtained after replacing cement with various amounts of fly ash are shown in **Figure 2.19**

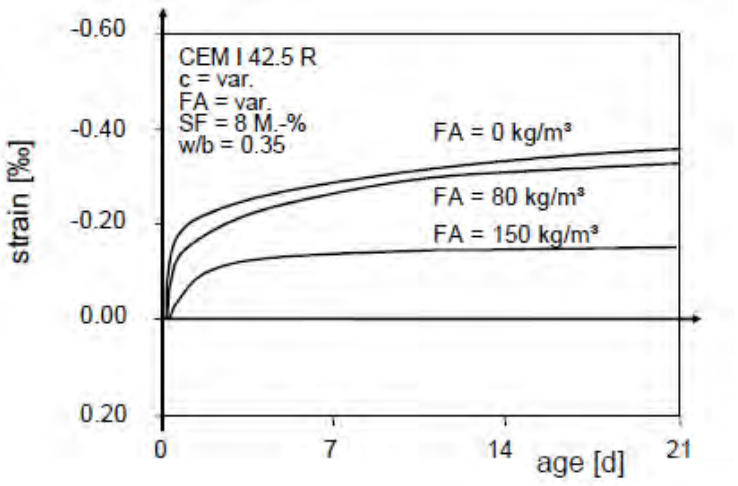

Figure 2.19: Effect of fly ash content on free autogenous shrinkage (Schieβl, et al., 2000).

The autogenous shrinkage was seen to decrease with increasing cement replacement. The autogenous shrinkage for the concretes with 0 and 80 kg/m^3 fly ash contents showed similar results, however at a higher replacement of 150 kg/m^3, the autogenous shrinkage strain was reduced by more than half after 21 days of testing.

Termkhajornkita, et al. (2005) reported conflicting reuslts, showing that fly ash increases the autogenous shrinkage of concrete. The authors pointed towards the works carried out by several researchers that have reported on autogenous shrinkage of high-belite Portland cement mixtures being higher than that of ordinary Portland cement. One explanation for this is that high-belite Portland cement has lower amounts of C_3A or lower reactive Al_2O_3. It was theorised that the same phenomenon occurs in fly ash-cement mixes. Approximately 2 to 5 hours after mixing, the amount of ettringite in fly ash concrete mixes is higher than in the plain Portland cement mixes. The chemical reaction of Al_2O_3 in fly ash that produces ettringite consumes large amounts of water, which may cause the pores to empty, thereby increasing the autogenous shrinkage. Termkhajornkita, et al. (2005), also investigated the relationship between autogenous shrinkage and the degree of hydration of fly ash concrete. Autogenous shrinkage was found to increase as the degree of hydration increased. A relationship was observed between the autogenous shrinkage of 50% fly ash concrete and the degree of hydration, however there was no distinct relation in the 25% fly ash concrete. It was concluded that at low fly ash content, the autogenous shrinkage was primarily affected by the hydration of the Portland cement. At early ages, there was no relation between the autogenous shrinkage and the degree of hydration, regardless of the kind of fly ash. The authors established that it is insufficient to explain the mechanism of autogenous shrinkage using only the degree of hydration.

2.4.2 Drying shrinkage

Drying shrinkage is a time-dependent volume decrease that is caused by the migration and transfer of moisture to the environment. Without the actions of external loads, drying shrinkage contributes the largest part of the volume change (Theiner & Hofstetter, 2012). Along with low tensile strength, drying shrinkage is likely the most disadvantageous property of Portland cement concrete. Drying shrinkage generally leads to cracking which ultimately results in

durability issues. This is particularly true in the case of concrete overlays where shrinkage is hindered by external and internal restraints and drying occurs from only one face of the concrete element. The bond between the repair layer and the substrate concrete causes the external restraint. The internal restraint is as a result of the humidity gradient that exists in concrete prior to the attainment of the hygrometric equilibrium with the surroundings. Local shrinkage is directly linked to pore humidity, therefore a gradient of shrinkage deformation exists during the course of drying. This induces tensile stresses in the repair layer which may ultimately overcome the tensile strength and cause the overlay to crack (Bissonnette, et al., 1999).

Drying shrinkage of cementitious material is mainly caused by the contraction of the C-S-H gel in the hardened cement paste when the moisture of the gel is decreased. The saturated cement paste does not maintain dimensional stability when exposed to ambient humidity that is below saturation. This is mainly because of the shrinkage strains caused by the loss of physically absorbed water from the C-S-H (Asad, et al., 1997). The paste of the concrete is thus the source of shrinkage. Two factors that affect paste deformation is the ability of the C-S-H particles to slip and move relative to each other due to the nature of the bonding, and the capillary porosity. Changes in C-S-H that cause changes in these two factors are related to the degree of hydration (Young, et al., 1998).

2.4.2.1 Influence of w/b on drying shrinkage

Hardened cement paste can be thought as comprising of layers of solid gel particles, with very small gel pores formed between the spaces of the solid gel layers, and larger capillary pores formed from any excess water. The structure is affected by the w/b ratio and the degree of hydration. At lower w/b ratios, the degree of hydration is higher and the volume of hydration products formed is greater thereby increasing the ratio of gel pore to capillary pore volume. Water is held in the paste at different bonding energies, interlayer and gel pore water is more tightly bound than free capillary water. As a result, the paste first loses capillary water when it begins to dry, followed by gel-pore water, and then interlayer water. Loss of free water in the capillaries leads to small shrinkage strains as opposed to removal of tightly bound water which causes larger shrinkage strains. **Figure 2.20** shows the effects of w/b ratio on shrinkage of pastes. The lower the w/b ratio, the lower the ultimate shrinkage, which is reached at more quickly. Early ages of drying represent the loss of free water at which the shrinkage is similar for all the pastes considering only capillary water is lost (Alexander & Beushausen, 2009).

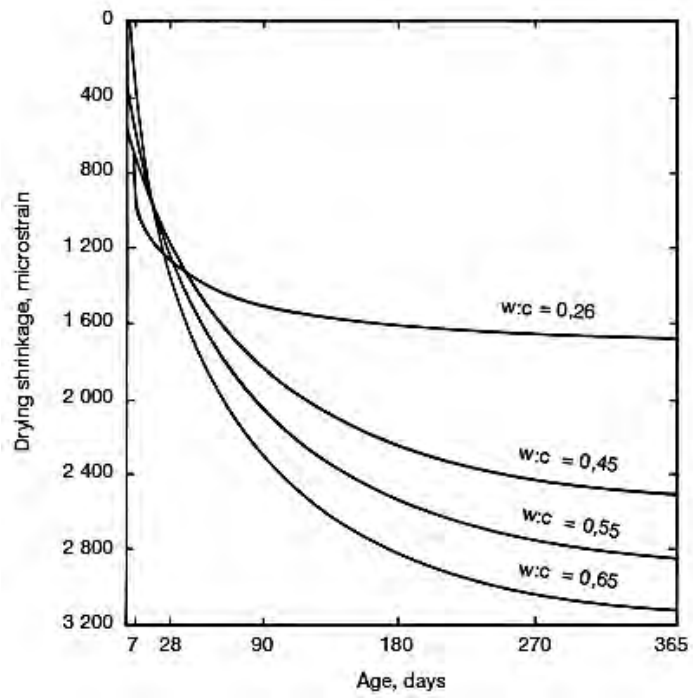

Figure 2.20: Effect of water-binder ratio on shrinkage of cement paste (Alexander & Beushausen, 2009).

Although high w/b pastes lose more water than low w/b pastes, the shrinkages are not very different. Gel water begins to be removed once the free capillary water has been lost, subjecting the paste to contraction forces. Though low w/b ratio pastes have a greater gel volume, they are also stiffer and hence experience less contraction strain than weaker pastes (higher w/b ratio). Low w/b ratio pastes are also less permeable, obstructing the free movement of moisture from the paste microstructure. In the normal range of w/b ratios ($0,40 < w/b < 0,70$), the influence of w/b ratio is less pronounced than illustrated in the figure due to presence of large volumes of aggregates that mask the paste behaviour (Alexander & Beushausen, 2009).

2.4.2.2 Influence of FA and GGBS on drying shrinkage

Previous research (Kumar, et al., 2007) shows that fly-ash-blended concretes exhibited less drying shrinkage in comparison to plain Portland cement concretes. The drying shrinkage decreased with increasing amounts of fly ash, and decreasing w/b ratio. This is illustrated in **Figure 2.21**. The mixture containing the highest volume of fly ash, and lowest w/b ratio value showed the least shrinkage. The decrease in drying shrinkage with increasing fly ash content and decreasing w/b ratio was attributed to the reduction in paste volume. Since the fundamental cause of drying shrinkage is loss of gel-pore water, any reductions in cement paste is expected to lower the drying shrinkage of the concrete (Kumar, et al., 2007). A similar result was obtained by Atis (2003) in high volume fly ash concrete (HVFA). High volumes of fly ash in the concrete significantly lowered the drying shrinkage in comparison to the control mix at all ages. The lower shrinkage values were said to be as a result of lower water content used in the HVFA concrete as well as a reduction in paste volume in the HVFA concrete.

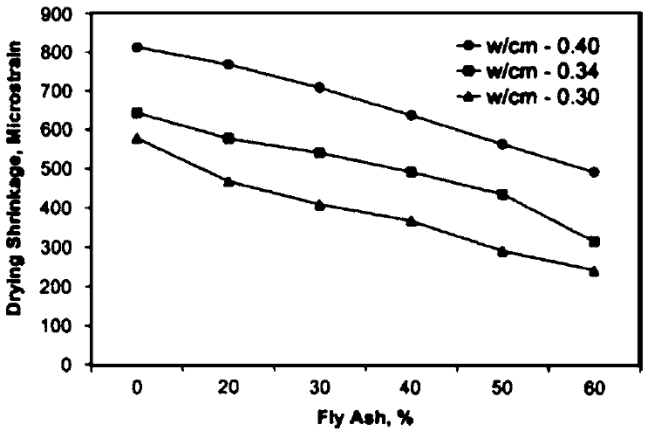

Figure 2.21: Variation of drying shrinkage of concrete with fly-ash content (Kumar, et al., 2007).

Chindaprasirta, et al. (2004), investigated the influence of the fineness of fly ash on the properties of the hardened mortar. A fly ash dosage of 40% by weight of binder was used throughout the experiment. From the tests, it was found that the incorporation of all fly ashes significantly reduced the drying shrinkage when compared to the mortar without fly ash. **Table 2.2** shows the results obtained. OFA (the original fly ash complying with ASTM C618, Class F) and the fine grades of fly ash all showed a significant reduction in drying shrinkage.

Table 2.2: Drying shrinkage of fly ash mortars of varying fineness (adopted from Chindaprasirta, et al. (2004))

Material Properties					**Drying shrinkage, 10^{-6} mm/mm**						
Materials	Symbol	Specific gravity	Blain fineness (cm^2/g)	% by weight of the OFA	1 day	4 days	7 days	18 days	25 days	60 days	90 days
Ordinary Portland cement	OPC	3.12	3500	N/A	182	345	588	732	816	909	987
Original fly ash	OFA	1.99	3000	100	90	270	484	605	669	704	721
Fly ash passed sieve no. 200	F200	2.22	3900	50	103	333	566	633	702	729	768
Fly ash passed sieve no. 325	F325	2.36	4800	35	133	338	554	653	689	730	756
Fly ash – fine	FF	2.44	9300	10	86	291	537	628	665	688	709
Fly ash – medium	FM	2.11	4900	25	95	296	493	573	643	670	696
Fly ash – coarse	FC	1.88	1800	65	141	342	567	693	773	802	852

No definite trend on the effect of the fineness of the fly ash on the drying shrinkage was observed except that the OFA and all the fine fly ash reduced the drying shrinkage. This was attributed to the reduction in water content of the mixes and hence lower water/binder ratio. The fine fly ash required less water due to the spherical shape and smooth surface. The coarse fly ash also reduced the drying shrinkage but to a lesser extent. The use of the coarse fly ash increased the water requirement significantly therefore causing an increase in drying shrinkage. Unlike the OFA, the coarse fly ash lacked both medium and fine portions and had a rougher surface thereby leading to an increase in water demand. In summary, the water-binder ratio

was found to be the prime factor with the mortars with low water-binder ratio exhibiting lower shrinkage. Darquennes, et al. (2012), evaluated the shrinkage of concrete with high contents of fly ash and slag in both free and restrained conditions. The investigation resulted in the conclusion that addition of fly ash and slag modifies the kinetics and long term value of drying shrinkage. At a replacement level of 50% or less, the evolution rate and amplitude at long term of drying shrinkage is lower than that of the plain Portland cement. At replacement levels greater than 50%, the total shrinkage of the fly ash and slag concrete was similar to that of the plain Portland cement concrete. The difference in behaviour was said to be mainly due to the porous structure of the cementitious materials.

Krüger (2003), stated that comparisons of drying shrinkage results obtained by various researchers serves little purpose because of the different concrete mixes investigated and different methods of determination used. However, in general, partial replacement of Portland cement with South African fly ashes results in either drying shrinkage of similar magnitude or slightly lower to that of ordinary Portland cement.

Research on South African blastfurnace slags has shown that at normal replacement levels (50%), slag has the effect of possibly increasing the shrinkage at early ages by up to 20% in small exposed laboratory specimens. However, this effect is normally reversed at later ages (Alexander & Beushausen, 2009). In contrast, experimental results obtained by Yuan, et al. (2015), showed that at constant paste content, the partial replacement of Portland cement with slag decreased the free shrinkage of the mixtures and that the greatest reductions were generally observed at early ages. The reductions in shrinkage were also observed to increase with increasing replacement level of cement with slag. Lee & Yoon (2014), observed increases in both autogenous and drying shrinkage with the incorporation of slag in High-Strength Concrete (HSC). However, according to a literature survey carried out by the Slag Cement Association (SCA) (2013), the free drying shrinkage of slag-blended concrete is slightly higher than that of ordinary Portland cement concrete. However, the difference was considered to be insignificant. Quantitatively, the average increase in shrinkage was only 2.9%, and 1.5% when corrected for paste volume. In addition, there was not perceivable influence of increasing slag content on the relative drying shrinkage.

Aly & Sanjayan (2008), found that during a 7-day moist curing period, all slag concrete mixes expanded 2.5 to 3 times more than the 0% slag reference mix. The results obtained are shown in **Figure 2.22**.

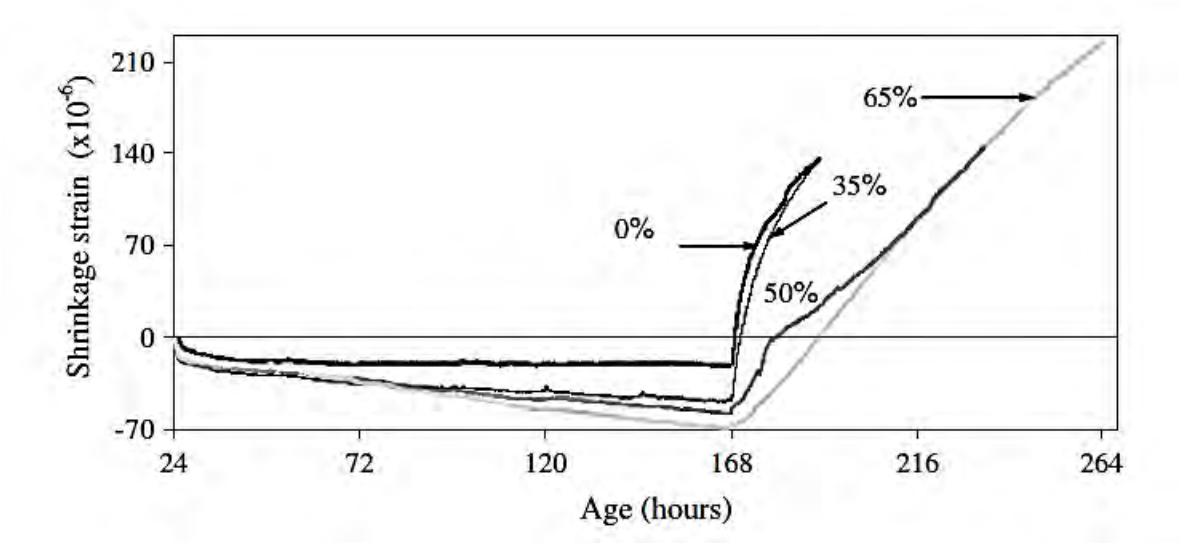

Figure 2.22: Free expansion and shrinkage of slag-blended concrete mixes (Aly & Sanjayan, 2008).

The expansions were said to be due to higher ettringite formation with different morphology due to low $Ca(OH)_2$ content in slag concretes as well as higher amounts of gypsum in the slag-blended cement. The hydroxyl ion concentration in pore solution has an effect on the size of ettringite formation. Ettringite formed in the absence of lime is said to be about 6 times longer than and twice as thick as that formed in the presence of lime after 24 hours. In slag-blended mixes, increasing slag amounts results in lower amounts of calcium hydroxide. The ettringite formed would thus be longer and thicker than in the 0% slag mixes thereby resulting in higher expansions. This initial swelling had a positive effect in avoiding crack formation. The swelling induced compressive restraining forces, delaying the onset of tensile restraining forces.

2.4.3 Tensile strength

In principle, cracking in bonded concrete overlays occurs when the shrinkage-induced tensile stresses exceed the tensile strength of the material. It is therefore extremely important to measure the tensile properties of the overlay material. Although cracks are initiated as soon as the tensile stresses reach the tensile strength limit, crack growth can only occur if the energy required to break the material is supplied. Cracking can thus be treated using the energy theory of fracture mechanics (Dao, et al., 2009). Tensile strength of concrete is much lower than its compressive strength. This is due to stress concentration generated by the defects in the concrete. Concrete is a porous material which contains microcracks even before loads are applied. The stress-raising flaws can be minute surface or interior cracks, internal pores, or grain corners at the surface or within the interior of the material. Flaws are significant when considering the tensile strength of the concrete as failure tends to be initiated at flaws. The severity of this effect is governed by the size of the flaw and orientation of the flaw relative to the direction of loading (Shah, 1997; Perrie, 2009; Li, 2011). Stress concentration can be explained with the help of an elliptical hole representing the defect as shown in **Figure 2.23**. Under tensile loading, the stress distribution in the cross-section through the centre of the ellipse is non-uniform. The edges of the ellipse experience the highest stresses (Li, 2011).

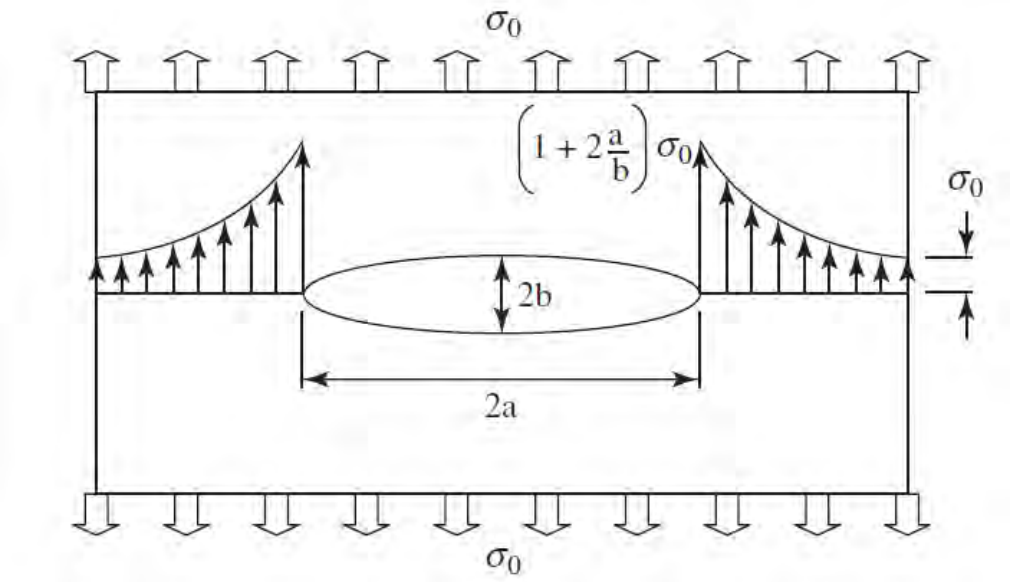

Figure 2.23: Sketch of stress concentration (Li, 2011).

It must be noted that there is no direct proportionality between compressive strength and tensile strength. The tensile strength increases as the compressive strength increases, but at a decreasing rate. This implies that the tensile/compressive strength ratio depends on the level of compressive strength. The higher the compressive strength, the lower the ratio. The relationship between the compressive strength and tensile strength/compressive strength ratio depends on various effects of both the hardened cement paste matrix and the transition zone. This is affected by not only curing, but also on the characteristics of the concrete mixture (Li, 2011).

2.4.3.1 Influence of w/b on strength of concrete

Hardened cement paste consists of gel pores and capillary pores. The compressive strength of concrete is related to the gel-space ratio. Since this relationship is based on the overall volume of gel, only capillary pores are relevant. Capillary porosity is a function of the w/b ratio and degree of hydration of the cement. Intuitively, the strength of concrete is largely influenced by the w/b ratio and degree of hydration (Perrie, 2009). The degree of hydration determines the extent to which void spaces among cement grains are filled by hydration products. The impact of water content on porosity of the hardened cement paste is one of the well-known trends in literature, an increase in w/b ratio increases the porosity and thus decreases the compressive strength (Hover, 2011). **Figure 2.24** shows the effect of capillary porosity on compressive strength of hardened cement paste. As the capillary porosity increases to the right, the compressive strength decreases.

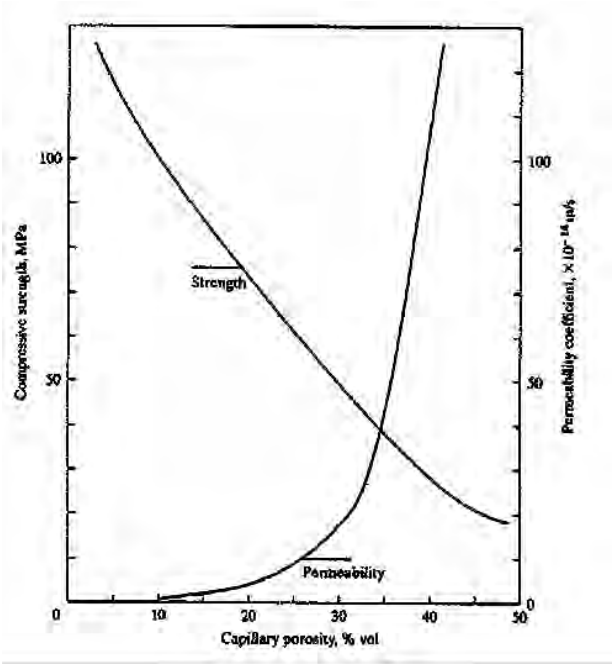

Figure 2.24: Effect of capillary porosity on compressive strength and permeability of hardened cement paste (Young, et al., 1998).

Although most discussions surrounding w/b ratio involve compressive strength, tensile strength also increases with a decrease in w/b ratio (Mindess, et al., 2003). The following discussion will comprise both compressive and tensile strength results obtained by various researchers.

2.4.3.2 Influence of FA and GGBS on strength of concrete

The partial replacement of Portland cement with fly ash or slag concretes, is generally expected to retard the early age compressive strength and tensile strength development. As highlighted in Section 2.3.3, the slag and pozzolanic reactions of fly ash are slower than that of ordinary Portland cement. The significance of this is that it results in lower rates of heat liberated and accordingly, slower strength development. In general, fly-ash-blended concretes are somewhat slower than slag-blended concretes in developing strength (Mheta & Monteiro, 2001).

Research carried out by Siddique (2004) on concrete mixtures with 0%, 40%, 45%, and 50% fly ash replacements yielded results (**Figure 2.25**) in agreement with the literature. At 28 days, the fly ash concretes had 28%, 34%, and 38% reductions in compressive strength. However, beyond 90 days, significant improvements in strength were observed. The increase in strength was due to the continued cement hydration, but more significantly due to the pozzolanic reaction of fly ash. Splitting tensile strength of concrete was determined on the concrete mixtures. Results (**Figure 2.26**) show that the variation in splitting tensile strength with fly ash content was similar to that observed in compressive strength specimens. The tensile strength decreased with increasing fly ash content. Similar early age and long-term strength developments were observed by several other researchers (Mukheibir, 1990; Gogol, 1994; Hwang, et al., 2004; Kumar, et al., 2007).

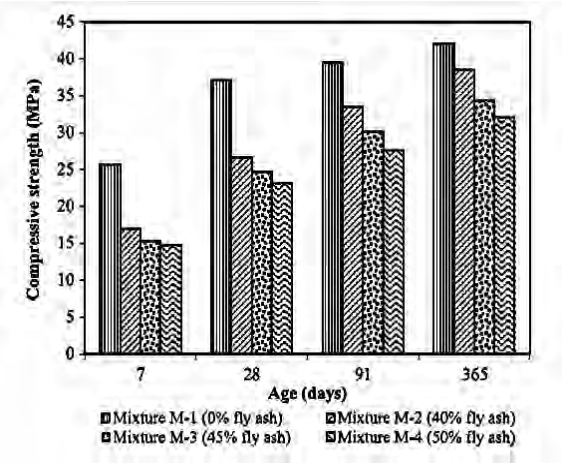

Figure 2.25: Compressive strength versus age (Siddique, 2004).

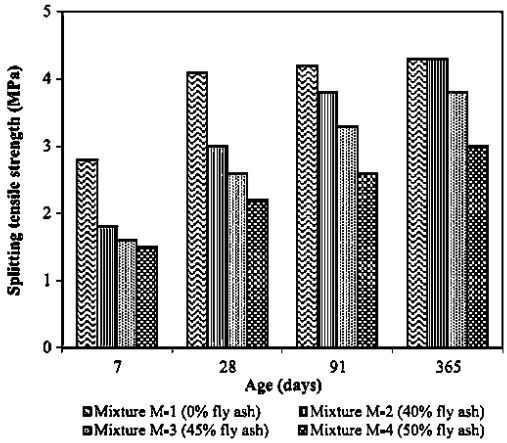

Figure 2.26: Splitting tensile strength versus age (Siddique, 2004).

The use of fly ash and slag has the effect of improving the long-term pore structure by densifying the paste-aggregate transition zone, which in turn affects the fracture characteristics. This is because fracture energy of concrete increases with increasing strength of the concrete. Consequently, in addition to the reduction in both splitting tensile strength and flexural strength due to high fly ash and slag additions, there is also a reduction in fracture toughness. This may be due to the presence of large amounts of unhydrated fly ash or slag particles that act as flaws that cause failure to be initiated earlier than ordinary Portland cement concrete (Bharatkumar, et al., 2005).

The partial replacement of Portland cement with slag causes decreased compressive strength in comparison to plain Portland cement concrete. However, the ultimate strength can increase with slag as shown in **Figure 2.27**. Strength development of slag-blended concrete is also more sensitive to the curing temperature than ordinary Portland cement concrete. Low curing temperature can result in remarkably slow strength gain (Chen, 2006). Aly & Sanjayan (2008), carried out splitting tensile strength tests on slag-blended concretes. All slag mixes exhibited lower splitting tensile strength development compared with plain Portland cement concrete.

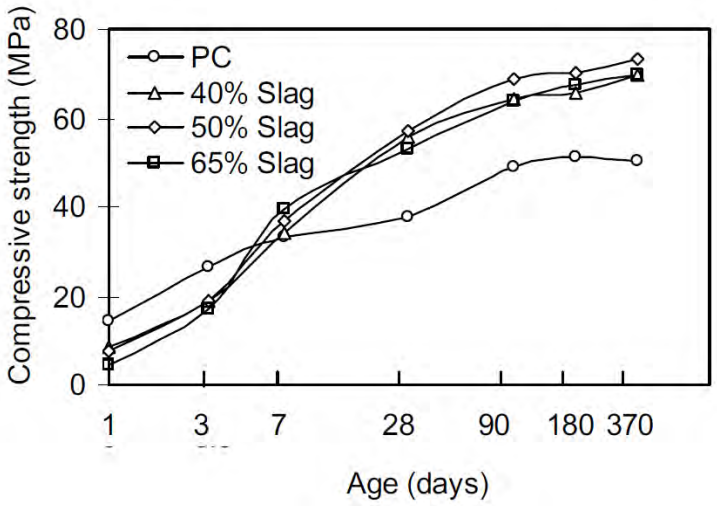

Figure 2.27: Compressive strength development of mortar cube samples containing various amounts of slags (Dubovoy et al., 1986) (Chen, 2006).

Beushausen, et al. (2012), observed low compressive strengths at early ages in slag mortars. This was owed to the longer setting time and lower early heat development of the slag mortars in comparison to the plain Portland cement mortars. The 1-day compressive strengths were also found to closely relate to the slag replacment levels, higher replacments levels resulted in lower strengths as expected (**Figure 2.28**). For the range of w/b ratios and replacement levels investigated, the relationship between strength reduction and replacment levels was near linear.

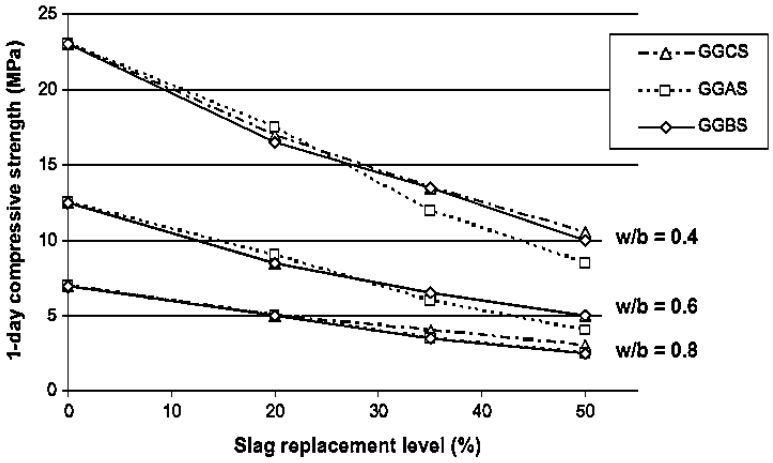

Figure 2.28: 1-day compressive strength of slag concrete mixes (Beushausen, et al., 2012).

2.4.4 Elastic Modulus

The elastic modulus is important for the analysis of shrinkage-induced stresses because it is directly related to stress development. Knowledge on the evolution of the elastic modulus is therefore essential for accurate stress predictions and the corresponding risk of cracking (Maia, et al., 2012). The elastic modulus of concrete is defined as the ratio of uniaxial stress to the resultant strain. It is a representation of the level of stiffness of the concrete material to an opposed load. The stress-strain relationship for concrete does not obey Hooke's law, although this is not an implicit requirement in the definition of elasticity. This non-linearity is largely

due to the non-linear stress-strain responses of the hardened cement paste and ITZ, and also due to microcracking in the cement paste matrix. The major factors affecting the elastic modulus of the concrete is the strength (and hence the stiffness of the paste), the stiffness of the embedded aggregates, and the nature of the ITZ between the paste and aggregates. Higher elastic moduli are achieved by higher stiffness of these individual phases. The stiffness of the aggregates normally determines the elastic modulus since it is usually the stiffest phase in the concrete and has the highest volume concentration. For a given volume of aggregate, the elastic modulus increases with increasing stiffness of the paste which is determined by its porosity (Alexander & Beushausen, 2009).

The evolution of the elastic modulus of cement-based materials is linked to the growth of solid volume and the degree of connectivity of the solids. The development of the elastic modulus is thus normally described as a function of the degree of hydration, and is said to develop at a faster rate than the strength of concrete at early ages. **Figure 2.29** shows the elastic modulus as a function of the degree of hydration. The degree of hydration was determined by dividing the measured chemical shrinkage by the estimated total chemical shrinkage. From this figure it is observed that there is a nearly linear relationship between the elastic modulus and the degree of hydration. At higher degrees of hydration, non-linearity is observed (Maia, et al., 2012).

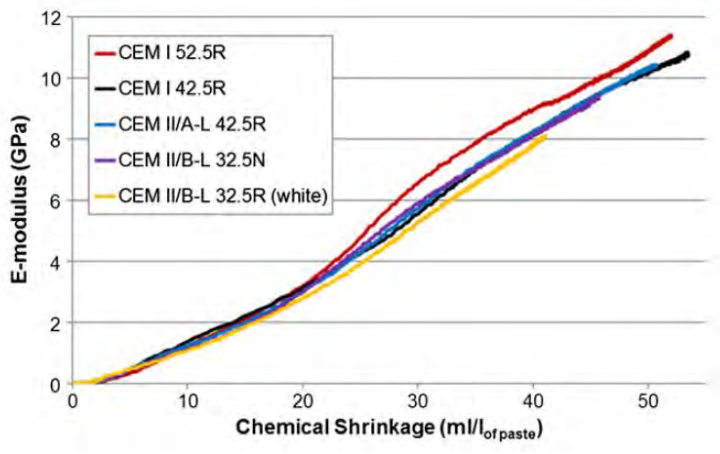

Figure 2.29: Elastic modulus evolution vs chemical shrinkage evolution (per volume unit) (Maia, et al., 2012).

2.4.4.1 Influence of w/b on elastic modulus

Maia, et al. (2011), observed a strong and clear influence of w/b ratio on the elastic modulus development of the hardened cement paste. At lower w/b ratios, the elastic modulus was seen to increase faster and reached a higher value than in pastes with higher w/b ratio. The explanation was related to the initial porosity of the pastes (Maia, et al., 2012). This is illustrated in **Figure 2.30** for w/b ratios ranging between 0.30 and 0.50. When the elastic modulus at a certain age was related to the w/b of the mix, this trend became better defined through parabolic curve fitting as shown in **Figure 2.31**.

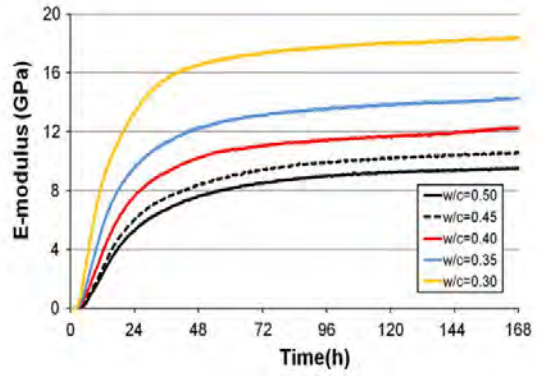

Figure 2.30: Influence of w/b ratio on the evolution of the elastic modulus of hardened cement paste (Maia, et al., 2011).

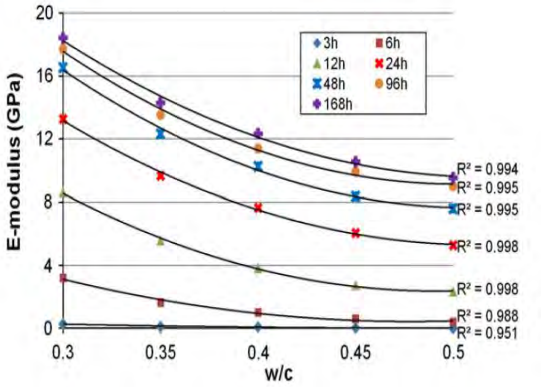

Figure 2.31: Elastic modulus of cement paste vs w/b ratio at different ages (parabolic fitting) (Maia, et al., 2011).

2.4.4.2 Influence of FA and GGBS on elastic modulus

The modulus of rupture usually determines the deformation behaviour when concrete elements are in tension. Schubert (1991) investigated the modulus of rupture of mass concrete with a high fly ash – cement ratio of 0.67. The concrete containing fly ash produced lower values for the modulus of elasticity, particularly in the young concrete. This was attributed to a slower rate of hydration in the fly ash concrete. At later ages, the elastic modulus of the fly ash concrete was found to be comparable to that of the concrete without fly ash.

Pane & Hansen (2002), investigated the key properties that influence early-age stress development in concrete and the effect of blended cements. The properties investigated were tensile creep, elastic modulus, tensile strength and autogenous shrinkage. Strength and Young's modulus data were considered very important for the analysis of early-age stresses in concrete. According to the authors, knowledge of these mechanical properties is imperative for the assessment of cracking tendency. The concrete properties were determined experimentally on concretes with 25% fly ash, 25% slag and 10% silica fume by weight of cement. Two water-binder ratios were chosen to represent two typical w/b ratios used for pavement concrete (w/b = 0.45) and high strength concrete (w/b = 0.35). The results of the investigation are shown in **Figure 2.32**. Fly ash was seen to reduce the early stiffness of the concrete while the slag had very little effect at early ages. Pane & Hansen (2002), state that the development of these material properties with time gives an indication on the rate of the hydration reaction. This is affected by the reactivity of each additive included in the concrete mixture.

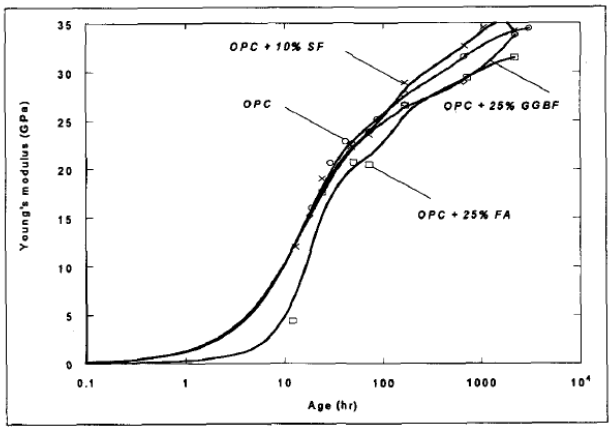

Figure 2.32: Young's modulus development with time (Pane & Hansen, 2002).

Siddique (2004) investigated the modulus of elasticity using the secant modulus for 33% of the maximum stress at ages 28, 91 and 365 days. In this study, one control mix M-1 designed to have 28-day compressive strength of 37.2 MPa was used. Three other concrete mixtures were made by replacing cement with 40%, 45%, and 50% of Class F fly ash by mass. The water-binder ratio was kept almost constant so as to investigate the effects of cement replacement with high volumes of Class F fly ash, keeping all other parameters constant. The test samples were kept in a water-curing room until the time of the test. The results (**Figure 2.33**) show that the use of large proportions of fly ash reduces the elastic modulus of the concrete in comparison to the reference mixture. At 28 days, the reference mixture achieved an elastic modulus of 29.9 GPa, whereas that of 40%, 45%, and 50% fly ash achieved an elastic modulus of 20.9 GPa, 19.8 GPa, and 19 GPa respectively. Similar observations were recorded by Maia, et al. (2011). In this study the elastic modulus of cement paste was measured using the Elasticity Modulus Monitoring through Ambient Response Method (EMM-ARM). The water-binder ratio was kept constant at 0.45, with fly ash/cement ratios equal to 0.20, 0.40, and 0.60. Samples were kept moulded in a climatic chamber at 20°C until the onset of testing. Higher replacement levels of fly ash resulted in a significant delay in the elastic modulus evolution at early ages (**Figure 2.34**). Strong decreases in elastic modulus were observed even at later ages for very high substitutions.

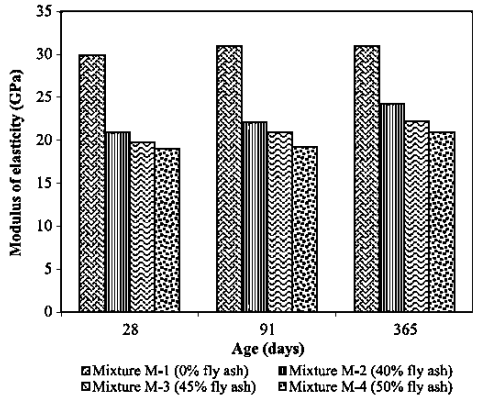

Figure 2.33: Modulus of elasticity versus age (Siddique, 2004).

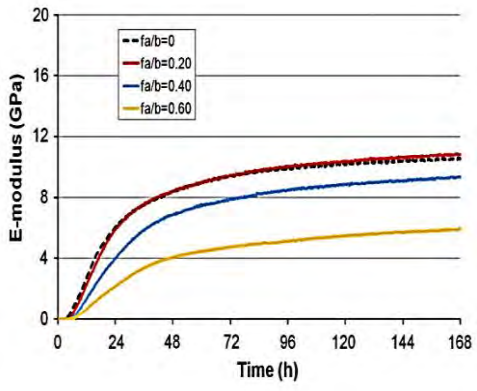

Figure 2.34: Influence of fly ash content on paste elastic modulus evolution (w/b=0.45) (Maia, et al., 2011).

According to research carried out by Aly & Sanjayan (2008), concretes containing 35%, 50%, and 65% slag replacements showed lower tensile elastic modulus than plain Portland cement concrete. The reduction was considered significant in reducing stress development and the potential of cracking. The positive effect of the reduced elastic modulus was reported to more than compensate the negative effect of the reduced tensile strength.

2.4.5 Tensile relaxation

Tensile relaxation is an important parameter for the prediction of tensile stress development in bonded concrete overlays. It has been recognised as one of the main stress relief mechanisms for bonded overlays subjected to restrained shrinkage. The shrinkage-induced tensile stresses can be decreased by as much as 60% owing to tensile relaxation (Beushausen & Chilwesa, 2013). Tensile relaxation imparts stress relief to the overlay material, prolonging the onset of cracking (Chilwesa, 2012) as shown in **Figure 2.35**.

.

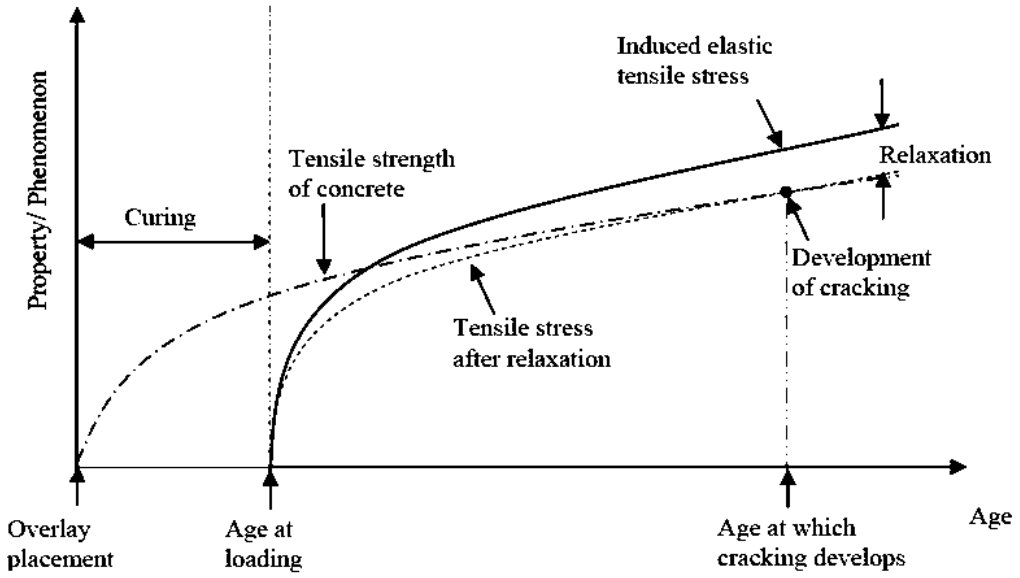

Figure 2.35: Schematic of simplified approach for modelling overlay stress relaxation (Chilwesa, 2012).

Concrete deforms in the direction of applied strain when subjected to a tensile strain. If the strain is sustained over a period of time, as is the case in bonded overlays, the stress experienced by the concrete begins to decay with time and asymptotically reaches a relaxed stress value (Bester, 2015). This is shown in **Figure 2.36**.

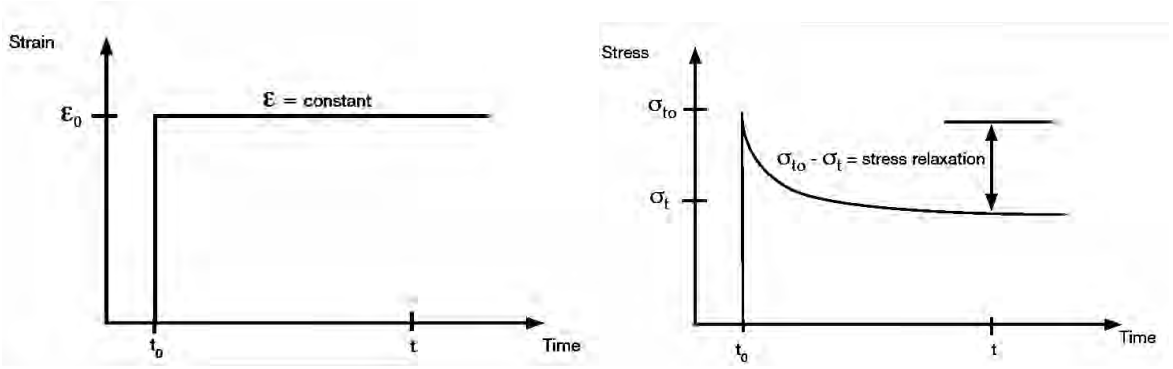

Figure 2.36: Characteristics of relaxation: time-dependent decrease in stress under constant imposed strain (Alexander & Beushausen, 2009).

Experimental results have indicated that the largest amount of tensile relaxation occurs at early ages. During a certain time period, relaxation at the beginning of that time period develops faster in comparison to the build-up of additional stresses. In modelling tensile stress, relaxation can thus be assumed to occur simultaneously with stress initiation for the sake of practical analysis. Induced shrinkage strains can then be adjusted by using the time-dependent overlay relaxation factor (Beushausen & Alexander, 2006).

The mechanism by which tensile relaxation occurs are not wholly understood. Tensile relaxation is often attributed to various mechanisms. The two main mechanisms used to explain tensile relaxation are viscous shear theory, and microcracking theory (Bester, 2015). According to the viscous shear theory, tensile relaxation is caused by the sliding of cement gel particles, and that the sliding rate is increased by the instability in the cement paste microstructure caused by macroscopic flux of water through the concrete (Bazant & Chern, 1985). According to the microcracking theory, tensile relaxation is caused by the formation of microcracks. As the solid particles migrate out of the loaded regions into more stable parts of the microstructure, the loading on them is relaxed (Bazant, 1982).

2.4.5.1 Influence of w/b on tensile relaxation

Beushausen, et al. (2012), determined the influence of w/b ratio on relaxation values by comparing the 72-hour relaxation results of specimens with w/b ratio 0.45 and 0.60. The relaxation values of specimens with w/b ratio 0.60 were 30%, 22%, and 14% higher than that of the 0.45 w/b ratio specimens at ages 2, 7, and 28 days (**Figure 2.37**). The higher relaxation values in specimens with higher w/b ratio were said to be due to the less dense microstructure, similar to the effect of w/b ratio on creep characteristics. The results also showed that the influence of w/b ratio decreased with increasing specimen age.

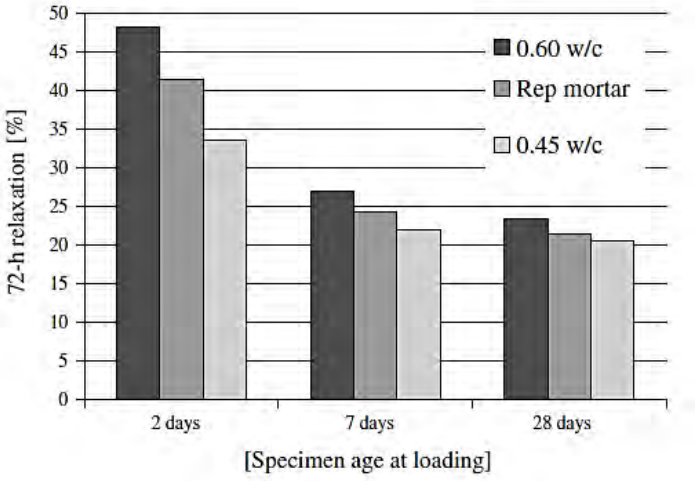

Figure 2.37: 72-hour tensile relaxation values of specimens at ages 2, 7, and 28 days (Beushausen, et al., 2012).

The w/b ratio influences the tensile relaxation by influencing the stiffness of the hardened cement paste, stiffer pastes result in decreased tensile relaxation. Since lowering the w/b ratio increases the elastic modulus of the paste, it follows that lowering the w/b ratio decreases the tensile relaxation capacity (Bester, 2015).

2.4.5.2 Influence of FA and GGBS on tensile relaxation

There is a lack of knowledge in literature concerning the effects of fly ash and slag on tensile relaxation of concrete. Pane & Hansen (2008), however, developed a procedue for calculating the early-age stress development in concrete that incorporated the aging visco-elastic effects of blended cements. The procedure included elements of tensile creep and heat of hydration. To validate the stress prediction, experiments were carried out to measure the stress development in the blended concrete mixes. The use of slag and fly ash were observed to be beneficial in reducing the risk of early age cracking. This is because the use of fly ash and slag was observed to significantly influence the relaxation of the concrete. Darquennes, et al. (2012), reported a similar result on slag concretes. Concretes with blastfurnace slag were characterised by a large relaxation capacity.

2.5 Summary and justification of research

The mechanism leading to restrained shrinkage cracking of bonded concrete overlays is complex and depends on material properties, environmental conditions, and the degree of restraint. The overlay material properties that govern restrained shrinkage cracking were discussed in Section 2.4. The material properties discussed included shrinkage, tensile strength, elastic modulus, and tensile relaxation. It was determined that the development of these material properties depends on the degree of hydration of the binder material. Fly ash and slag are known to influence the hydration reaction when added to the binder material. The change in hydration reactions affects the development of these mechanical properties of the concrete.

It was revealed form literature that the in order to reduce the risk of cracking in bonded concrete overlays, one or a combination of the following is required: lower shrinkage strains,

higher tensile strength, lower elastic modulus, and increased stress relaxation. With this in mind, the effects of fly ash and slag on the identified material properties was discussed by drawing from the results of previous studies. It was discovered that fly ash and slag have a range of influences on these material properties. A summary of these findings is provided in **Table 2.3**.

Table 2.3: Simplified summary of factors influencing restrained shrinkage cracking.

	Required effect to reduce risk of cracking	Effect of increasing w/b	Effect of increasing fly ash content	Effect of increasing slag content
Autogenous shrinkage	↓	✓ ↓	↑↓	↑↓
Drying shrinkage	↓	× ↑	↑↓	↑↓
Tensile strength	↑	× ↓	× ↓	× ↓
Elastic modulus	↓	✓ ↓	✓ ↓	✓ ↓
Tensile relaxation	↑	✓ ↑	✓ ↑	✓ ↑

↑: Increase ↓: Decrease ↑↓: Increase or decrease ✓: Positive influence ×: negative influence

From the table it can be seen that fly ash and slag affect the elastic modulus and tensile relaxation in a favourable manner for the prevention of restrained shrinkage cracking. However, fly ash and slag also negatively affect the tensile strength which may be detrimental to the behaviour of the overlay. The influence of fly ash and slag on autogenous and drying shrinkage showed conflicting results from literature and could not be confidently deduced. Based on the findings from literature, a hypothesis on the influence of fly ash and slag on restrained shrinkage cracking was made. It is understood that the disparities in the literature are a cause for pause in framing a strong hypothesis due to the absence of clear experimental evidence. However, the formulation of the hypothesis was considered beneficial in providing a foundation for the experimental investigation.

2.5.1 Hypothesis

The research proposes that the partial replacement of Portland cement with fly ash or ground granulated blastfurnace slag has a positive influence on the age at which restrained shrinkage causes cracking. It is proposed that the combined effects of increased stress relaxation, and decreased stiffness are sufficient in overcoming the reduction in tensile strength to ultimately lower the stress development and increase the age at which restrained shrinkage cracking occurs.

2.5.2 Key research questions

The following are the key questions raised from the literature survey:

1. Does the partial replacement of fly ash or slag increase or decrease the free shrinkage of concrete?
2. Is the combined effect of decreased elastic modulus and increases tensile relaxation sufficient enough to counteract the lower tensile strength and delay the onset of cracking in fly ash or slag overlays?

3. Taking into account the above, are fly ash and slag appropriate materials for use in bonded concrete overlays?

2.5.3 Detailed research objectives

Based on the foregoing literature survey and discussion, the following are the detailed research objectives:

1. Carry out restrained shrinkage cracking tests to determine the influence of FA and GGBS. This would assess the overall performance and determine their suitability for the overlay application.
2. Carry out free shrinkage, tensile strength, elastic modulus, and tensile relaxation tests to determine the magnitude of the influence of FA and GGBS on these properties. This would help to answer the question of whether the reduced tensile strength can be overcome by the reduction of stiffness and increased stress relaxation.
3. Analytically model the development of tensile stresses against tensile strength in order to predict age at cracking and to establish if this method is adequate in predicting restrained shrinkage cracking in FA and GGBS overlays by comparing the modelled results to the experimental results obtained. The analytical model to be used has successfully been used by Chilwesa (2012) to predict the age at cracking of different repair mortars. This however did not include FA or GGBS bonded overlays.

The first step in achieving these objectives was to carry out preliminary stress modelling prior to carrying out any experimental investigation. This was done in an attempt to forecast the expected results and therefore reinforce the research hypothesis. This is explained in detail in Chapter 3.

CHAPTER 3

3 Preliminary modelling of tensile stresses

3.1 Introduction

This chapter presents the modelling method that was used to provide preliminary results prior to the onset of the experimental investigation. This initial modelling was done so as to inform the ensuing experimental investigation as well as reinforce the findings from the literature review. A combination of analytical and numerical modelling was carried out to predict the age at cracking of bonded concrete overlays made with fly ash or slag.

The chapter begins by explaining the theory and underlying principle behind the modelling approach. This is followed by the assumptions and simplifications made in obtaining the various parameters and variables. The results of the modelling are then presented and conclusions are summarised.

3.2 Modelling approach

The modelling approach used in this chapter is based on the 'Level 1 Model' defined by the National Institute of Standards and Technology (NIST) (Vaysburd, et al., 2000). A 'Level 1 Model' was classified to be a modelling approach that evaluates the susceptibility to cracking of a particular material under standardised conditions. The model should be able to give an estimation of the increase in restraint-induced tensile stresses as a function of time and compare that with the developing tensile strength. The strength-to-stress ratio is then used to determine the likelihood of cracking. A ratio significantly greater than 1 would indicate low possibility of cracking, while a value significantly less than 1 would point towards a high possibility of cracking. This type of model was said to be a viable tool for screening the performance of alternative materials and as such was adopted for this research. To implement a 'Level 1 Model', the following information about the repair material is required:

- The development of tensile strength,
- The development of the elastic modulus,
- The development of shrinkage, and
- Stress relaxation properties under tensile loading.

A challenge associated with this type of model is in representing the uncertainty in the results (Vaysburd, et al., 2000). However, since this is simply a preliminary investigation aimed at building onto the literature review, this was not of much concern. There are several numerical methods available that can be used to predict shrinkage cracking. The 'Level 1 Model' and modelling approach used in this investigation is adopted from research of a similar kind, carried out by Beushausen (2015). This is a simplistic model that has proven to yield reasonably accurate results (Masuku, 2009; Chilwesa, 2012, Dittmer, 2013). The general numerical model and the assumptions made in implementing it are described in Sections 3.2.1.

3.2.1 General numerical model

The numerical model is based on the notion that restrained shrinkage is proportional to the free shrinkage strains. Free shrinkage strains can thus be measured and converted into restrained shrinkage strains to predict the induced tensile stresses. The shrinkage-induced tensile stresses are proportional to the elastic modulus of the overlay, but are however lowered due to tensile relaxation of the overlay. To implement the model, the individual material properties of the overlay are measured and input into an equation that relates the above information. The calculated tensile stresses are then compared to the measured tensile strength of the overlay to predict the onset of cracking. In this preliminary investigation, the individual material properties of the overlay were estimated using a combination of material models, and measured data from previous research (see Section 3.3). The general numerical model is expressed as shown in Equation 3.1.

$$\sigma_t = (1-\psi)\cdot\alpha\cdot\varepsilon_{FSS}E_t \qquad [3.1]$$

Where: σ_t is the tensile stress; ψ is the relaxation coefficient; α is the coefficient accounting for the magnitude of shrinkage restraint; ε_{FSS} is the free shrinkage strain; and E_t is the tensile elastic modulus. In order to estimate the time-development of the tensile stress based on Equation 3.1, a step-by-step method was used. The stresses were calculated in one-day increments based on the principle of superposition which states that "the stress produced by a strain increment applied at any time is not affected by any strain applied either earlier or later" (Gilbert, 1988). This was done by estimating the change in free shrinkage in that time interval, and estimating the mean elastic modulus and mean tensile relaxation at the middle of that time interval. Equation 3.1 could therefore be expressed as:

$$\sigma_{t,i} = \sigma_{t,i-1} + \alpha\cdot\Delta\varepsilon_{FSS}\cdot E_{t,i}\cdot\psi_i \qquad [3.2]$$

Where: $\sigma_{t,i}$ = induced tensile stress at time t_i,
$\sigma_{t,i-1}$ = induced tensile stress at time t_{i-1},
α = is the average degree of restraint,
$\Delta\varepsilon_{FSS}$ = change in free shrinkage strain in the interval from t_{i-1} to t_i,
$E_{t,i}$ = mean elastic modulus in the interval from t_{i-1} to t_i, and
ψ_i = mean relaxation factor from interval t_{i-1} to t_i, defined as,

$$\psi_i = 1-\frac{\beta_i}{100}$$

Where β_i is the tensile relaxation in the interval from t_{i-1} to t_i.

The development of the shrinkage-induced tensile stresses were estimated at each time interval and plotted on the same graph as the tensile strength development of the concrete. The intersection of the two curves represents a strength/stress ratio of 1. This indicates the time at which cracking would occur.

3.2.1.1 Model assumptions

Due to the complex nature of the material properties governing restrained shrinkage cracking, there is a need for simplifying assumptions so as to avoid complicated modelling procedures.

The following three assumptions were made in order to accomplish the analytical modelling with simplicity (Chilwesa, 2012):

1. **Tensile relaxation is instantaneous**

Previous research shows that the majority of tensile relaxation occurs at early ages of loading (Beushausen & Alexander, 2006). Chilwesa (2012) therefore suggested that in order to simplify analytical modelling of overlay stresses, it is reasonable to model tensile relaxation as occurring instantaneously with the incremental loading from shrinkage (**Figure 3.1**). The stress increment at a particular time, t, could then simply be multiplied as shown in Equation 3.2. This assumption is supported by work done by Masuku (2009) on tensile relaxation of bonded overlays.

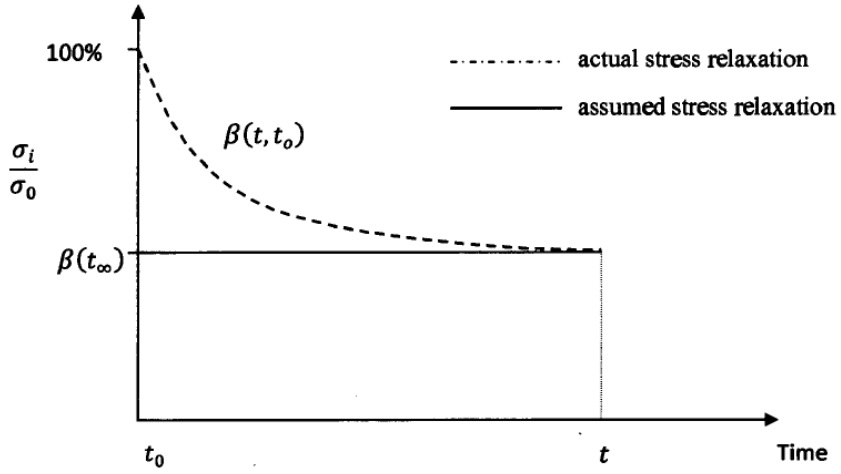

Figure 3.1: Simplified instantaneous ultimate relaxation used for analytical modelling (Chilwesa, 2012).

From **Figure 3.1** the relaxation function may be taken as a constant value after time, *t*. In this investigation, a 24-hour relaxation value was taken as the ultimate relaxation. .

2. Restrained shrinkage is proportional to free shrinkage

Previous research has shown that restrained shrinkage in bonded overlays is approximately 60% of the free overlay shrinkage (Beushausen, 2005). The coefficient α (degree of restraint) was thus taken as 0.6 to estimate the change in restrained shrinkage strains. The following conversion equation was therefore applied:

$$\Delta\varepsilon_i = \alpha \cdot \Delta\varepsilon_{FSS,i} = 0.6 \cdot \Delta\varepsilon_{FSS,i} \qquad [3.3]$$

Where $\Delta\varepsilon_i$ is the change in restrained shrinkage in the interval t_{i-1} and t_i; and $\Delta\varepsilon_{FSS,i}$ is the change in free shrinkage strain in the interval t_{i-1} and t_i.

3. **No drying shrinkage during curing**

During curing, it is assumed that no drying shrinkage occurs. The only shrinkage that occurs is autogenous shrinkage.

Effective curing is known to mitigate and delay drying shrinkage by preventing loss of moisture from the concrete to the environment. However, autogenous shrinkage is independent of the environmental conditions and could thus still occur during the curing process (Alexander & Beushausen, 2009).

3.2.2 Modelling strategy

The strategy employed by Beushausen (2015) was to vary several parameters that are known to affect the material properties that influence restrained shrinkage cracking. The parameters varied include strength class of concrete, overlay thickness, relative humidity, and curing duration. The effect of varying the said parameters is described in the sub-sections that follow. The results of the study were used to feed into the current preliminary investigation. However, for this investigation it was not necessary to carry out such a comprehensive study. It was therefore decided that only one combination of parameters would be used to perform this initial investigation. It was opted to select the worst case scenario, that is, a combination of parameters with the worst effect on the age at cracking. This was done in an attempt to ensure that any positive results obtained are as a result of the partial replacement of Portland cement with FA or GGBS.

3.2.2.1 Strength class

Beushausen (2015) investigated the effects of different grades of concrete strength classes on cracking of bonded overlays. The range of concrete strength classes were that relevant for common overlay applications ($f_{ck}/f_{ck,cube}$ 12/15 to 50/60). The strength class had an influence on the tensile strength, elastic modulus, and tensile relaxation of the concrete. The increase in strength class had the effect of significantly increasing the tensile strength, and decreasing the stress relaxation. The influence of strength class on relaxation however showed less difference with increasing age. This is because the creep factor decreases at a decreasing rate as the strength class increases. The overall effect of compressive strength class on overlay age at cracking is shown in **Figure 3.2**.

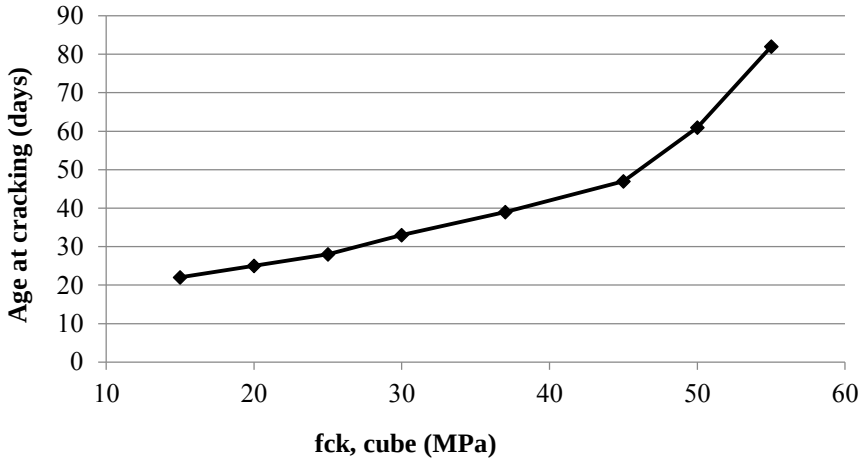

Figure 3.2: Influence of strength class on overlay age at cracking ($t_{overlay}$ = 60 mm, 70% RH, 7 days curing) (Beushausen, 2015).

The figure shows that there's a relatively linear increase in age at cracking with increasing strength class. The strength classes used in the current investigation were limited to FA and GGBS strength data available form previous research. The strength classes selected for this study were thus C20/25 and C40/50 for the FA modelling, and C20/25 and C30/37 for the GGBS modelling. This corresponded to replacement levels of 50% in both cases.

3.2.2.2 Overlay thickness

Overlay thickness ($t_{overlay}$) affects the drying shrinkage and relaxation of the concrete. Increased thickness results in lower drying shrinkage and lower tensile relaxation. The influence of overlay thickness on age at cracking obtained by Beushausen (2015) is shown in **Figure 3.2**. The age at cracking was significantly increased with increasing thickness. The author did however indicate that these effects are not as pronounced in practice.

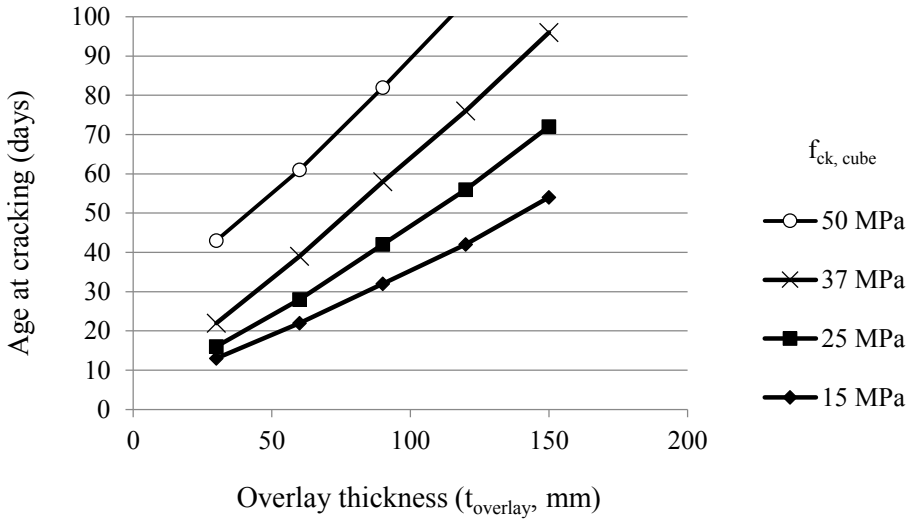

Figure 3.3: Influence of overlay thickness on age at cracking (various compressive strengths, 70% RH, 7 days curing) (Beushausen, 2015).

The influence of overlay thickness was not of interest for the current preliminary investigation. Therefore an overlay thickness of 40 mm was selected as it resulted in the lowest values of age at cracking. This was so as to ensure that the positive effects of a large overlay thickness does not mask the influence of FA or GGBS on the age at cracking.

3.2.2.3 Ambient relative humidity

Changes in relative humidity (RH) also affect the drying shrinkage and tensile relaxation of the overlay. An increase in RH lowers the drying shrinkage and reduces the relaxation capacity. The influence of relative humidity on age at cracking obtained by Beushausen (2015) is shown in **Figure 3.4**.

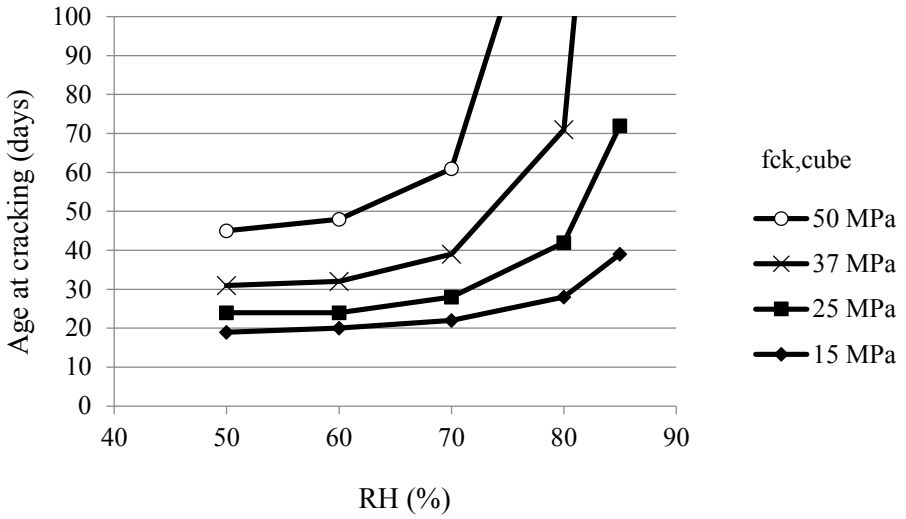

Figure 3.4: Influence of relative humidity on overlay age at cracking (for various compressive strengths, $t_{overlay}$ = 60 mm, 7 days curing) (Beushausen, 2015).

Increasing the RH resulted in an overall positive effect on the net age at cracking of the overlay. The influence of RH was not of interest for the current preliminary investigation. Therefore a relative humidity of 50% was selected as it resulted in the lowest values of age at cracking. This was so as to ensure that the positive effects of high relative humidity do not mask the influence of FA or GGBS on the age at cracking. A relative humidity of 50% was also used in the experimental investigation as discussed in Chapter 4.

3.2.2.4 Curing duration

Adequate curing is considered one of the most important factors for the prevention of shrinkage cracking in bonded overlays. This is based on the idea that longer curing delays the onset of drying shrinkage development, thereby delaying the stress development to a later time when sufficient tensile strength has developed. However, Beushausen (2015) argues that the influence of curing duration on cracking is more complicated than this. The influence of curing duration on age at cracking obtained by Beushausen (2015) is shown in **Figure 3.5**.

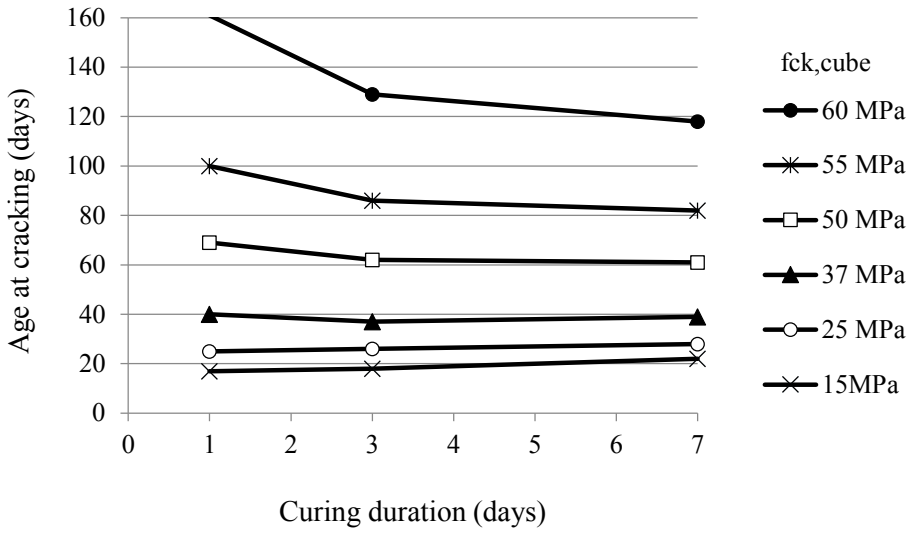

Figure 3.5: Influence of curing duration on overlay age at cracking ($t_{overlay}$ = 60 mm, RH 70%) (Beushausen, 2015).

Increasing the duration of curing had a slight positive effect on age at cracking of lower strength concretes, but resulted in earlier cracking in higher strength concretes. This was attributed to higher rate of stress development in concretes cured for longer. It was argued that the magnitude of shrinkage is not influenced by curing, and that a later onset of drying does not reduce the shrinkage strain development. In fact, increased curing merely delays the shrinkage strain development to a time when the relaxation coefficient is smaller and the elastic modulus is higher resulting in higher stresses. The influence of curing duration was not of interest for the current preliminary investigation. Therefore a curing duration of 7 days was selected as it resulted in the overall lowest values of age at cracking. This was so as to ensure that the positive effect of low curing duration does not mask the influence of FA or GGBS on the age at cracking. Curing duration of 7 days was also used in the experimental investigation as discussed in Chapter 4.

3.3 Modelling of material parameters

In the study carried out by Beushausen (2015), the material properties were not experimentally measured but were modelled according to the provisions in BS EN 1992-1-1:2004. The code provides simplified material models that were used for the prediction of tensile strength, elastic modulus, creep, and shrinkage. These material properties are modelled based on the concrete's mean compressive strength. However, the partial replacement of cement with high volumes of cement extenders is not taken into account in these models. As such, information from previous research was used in combination with the material models provided by the code to roughly estimate the effects of fly ash and slag on cracking potential. In order to obtain relevant results, the compressive strength data was taken from research carried out on South African fly ashes and blastfurnace slags. The fly ash compressive strength data was taken from research carried out by Mukheibir (1990), on Lethabo fly ash while the slag compressive strength data was taken from research carried out by Beushausen, et al. (2012).

3.3.1 Compressive and tensile strength

In the BS EN 1992-1-1:2004 code, tensile strength is modelled as a function of the characteristic compressive strength. The time-development of tensile strength is predicted using an exponential function. The code's equation for a mean temperature of 20°C and class N cement was used by Beushausen (2015) to model the tensile strength development. The same equation was used in this investigation to model the tensile strength development. Owing to the code's lack of provisions for concretes with high replacement levels of FA and GGBS as discussed earlier, the compressive and tensile strength were modelled based on data retrieved from previous research (Mukheibir, 1990; Beushausen, et al., 2012). The 28-day compressive strength of fly ash and slag obtained from previous research was taken as the mean compressive strength and used to model the fly ash and slag strength developments according to the equations provided by the code (Equation 3.4). The 28-day compressive strength derived from these studies was obtained by keeping all other parameters almost constant and varying only the percentage replacement of fly ash or slag. Therefore the compressive strengths of the reference material (100% Portland cement concrete) can be expected to be significantly higher than that of the fly ash or slag blended concrete.

$$f_{cm,x}(t) = \beta_{cc}(t) \cdot f_{cm,x} \qquad [3.4]$$

Where $f_{cm,x}(t)$ is the mean concrete compressive strength of FA or GGBS at an age of t days; $f_{cm,x}$ is the mean compressive strength at 28 days of FA and GGBS according to data from previous works; and βcc(t) is a coefficient which depends on the age of the concrete t.

Using the $f_{cm,x}$, tensile strength of the FA and GGBS could also be estimated as:

$$f_{ctm,x} = 0.3 \times f_{ck,x}$$

$$f_{ctm}(t) = \left[\beta_{cc}(t)\right]^{\alpha} \cdot f_{ctm,x} \qquad [3.5]$$

Where $\beta_{cc}(t)$ is as described in Equation 3.4; α =1 for t < 28 days; and f_{ck} is the characteristic strength of the FA and GGBS concrete estimated as follows:

$$f_{ck,x} = f_{cm,x} - 8(MPa) \qquad [3.6]$$

It is understood that the strength development of FA and GGBS may deviate from that estimated by the model. However, since this a preliminary study and the level of accuracy is not of much concern, this was considered to be an acceptable assumption. The data used to

determine the compressive strength development in the FA and GGBS concrete is presented in **Figure 3.6** and **Figure 3.7** respectively. The 28-day compressive strength was determined by extrapolating from these strength development curves. For example, for the reference concrete with 28-day compressive strength of 25 MPa, the slag concrete was estimated to have 28-day compressive strength of approximately 21 MPa.

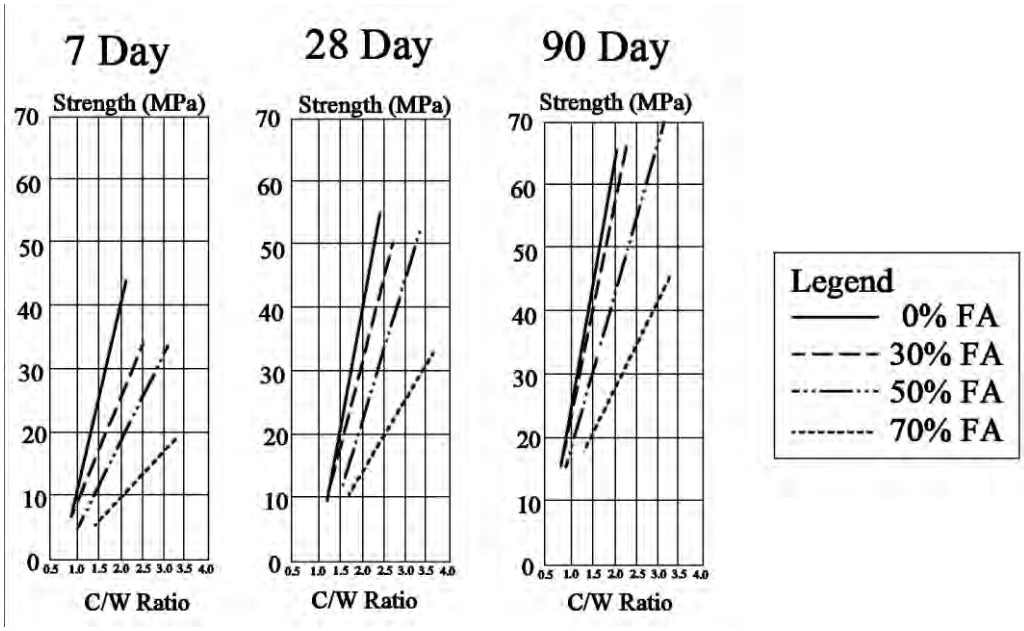

Figure 3.6: Compressive strength of mixes with classified Lethabo fly ash at 7, 28, and 90 days (Mukheibir, 1990).

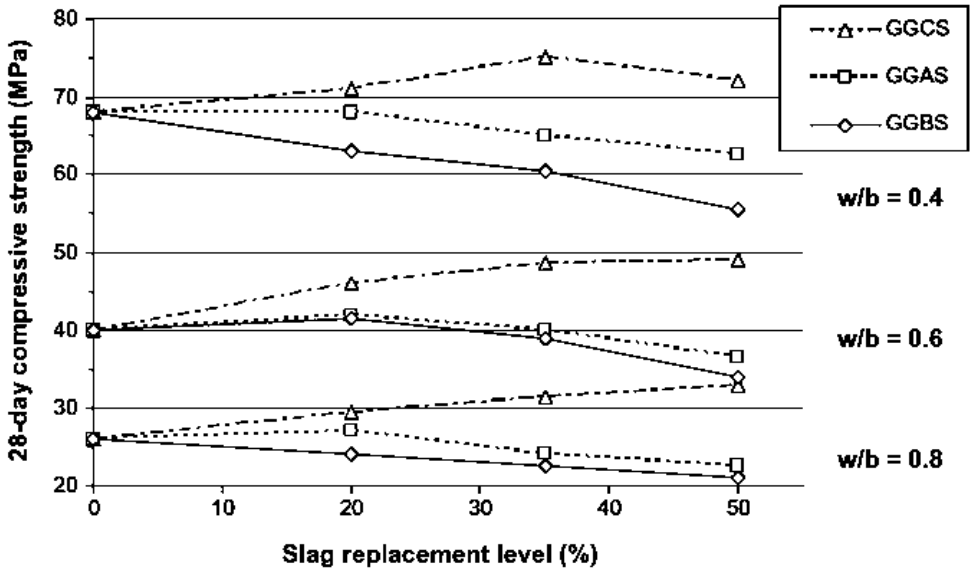

Figure 3.7: 28-day compressive strength of concrete mixes with various slag replacements at w/b = 0.60 & 0.8 (Beushausen, et al., 2012).

3.3.2 Elastic modulus

In the BS EN 1992-1-1:2004 code, the elastic modulus of concrete (E_{cm}) is linked to the mean compressive strength at 28 days (f_{cm}) and there is no difference between the elastic modulus in tension and compression. The elastic modulus is modelled as an exponential function based on time-development of compressive strength. This model was used to predict the elastic modulus of the concrete

The elastic modulus of the FA and GGBS concrete was estimated using information obtained by Krüger (2003) and Beushausen, et al. (2012) respectively. The development of the elastic modulus was estimated by inputting the obtained 28-day elastic modulus of the FA and GGBS concrete into the equation provided by the code. This was preferred to using the elastic modulus as predicted using the model equations as the modelled elastic moduli were higher (see **Table 3.1**). The 28-day elastic modulus derived from these studies was obtained by keeping all other parameters almost constant and varying only the percentage replacement of fly ash or slag. Therefore the elastic modulus of the reference material (100% Portland cement concrete) can be expected to be significantly higher than that of the fly ash or slag blended concrete.

Table 3.1: Comparison of elastic modulus

Reference concrete mix	E_{cm} (GPa) (Reference concrete)	Blended concrete mix	Elastic Modulus (GPa)	
			Measured	Modelled
25 MPa	30.0	50% FA	21	25,8
50 MPa	35.2	50% FA	27	29
25 MPa	30.0	50% GGBS	15.3	31.8
37 MPa	34.1	50% GGBS	26.6	27.5

The time-development of the elastic modulus of the GGBS was estimated according to Equation 3.7.

$$E_{cm,\mathrm{x}}(t) = \left(\frac{f_{cm,\mathrm{x}}(t)}{f_{cm,\mathrm{x}}} \right)^{0.3} \times E_{cm,\mathrm{x}} \qquad [3.7]$$

Where: $E_{cm,x}(t)$ = elastic modulus of FA or GGBS concrete at t days,

$f_{cm,x}(t)$ = compressive strength of FA or GGBS concrete at t days,

$f_{cm,x}$ = 28-day compressive strength of FA or GGBS concrete, and

$E_{cm,x}$ = 28-day elastic modulus of FA or GGBS concrete from previous research.

3.3.3 Shrinkage

Literature shows conflicting results with regards to the effects of FA and GGBS on the shrinkage of concrete (see Sections 2.4.1 and 2.4.2). It was therefore decided not to use any shrinkage results from previous research as input to model shrinkage strains. The shrinkage strains were predicted using the models provided in BS EN 1992-1-1:2004. The 28-day mean

compressive strength obtained from previous research was used to estimate the necessary coefficients.

3.3.4 Creep and relaxation

In the code, the creep coefficient, is dependent on mean compressive strength of concrete at 28 days (f_{cm}), RH, notional member size, the age at loading, and the cement class. In order to cater for the use of FA and GGBS, the estimated f_{cm} values of FA and GGBS were used to calculate the necessary coefficients.

Similar to Beushausen (2015), the tensile relaxation was modelled based on the prediction for compressive creep strain. Tensile relaxation was predicted based on creep properties using the principles of the Age Adjusted Effective Modulus Method (AAEM) recommended in the fib Model Code 2010. Linear creep models were used to predict the tensile relaxation irrespective of the stress levels. This is because non-linear creep resulted in very high creep coefficients which led to the prediction of crack-free members which was not useful for the research.

3.4 Results and discussion

3.4.1 Strength development and age at cracking

The results of the preliminary modelling of shrinkage-induced tensile stress in FA and GGBS bonded overlays is provided in this section. The results are presented as plots of the development in tensile strength and tensile stress with time. The intersection of the stress and strength curves indicate the age at cracking of the overlays. The results of the numerical modelling of the FA concrete for strength classes C25/30 and C40/50 are shown in **Figure 3.8** and **Figure 3.9**. The results of the numerical modelling of the GGBS concrete for strength classes C25/30 and C30/37 are shown in **Figure 3.10** and **Figure 3.11**. The predicted ages at cracking are presented in **Table 3.2**.

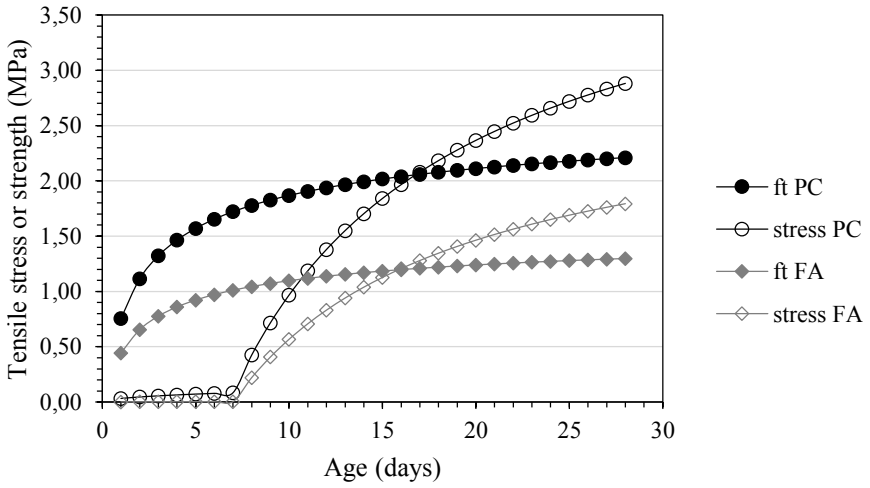

Figure 3.8: Development of tensile stress versus tensile strength for $f_{ck,cube}$ 30 MPa ($t_{overlay}$ = 40 mm, 50% RH, 7 days curing).

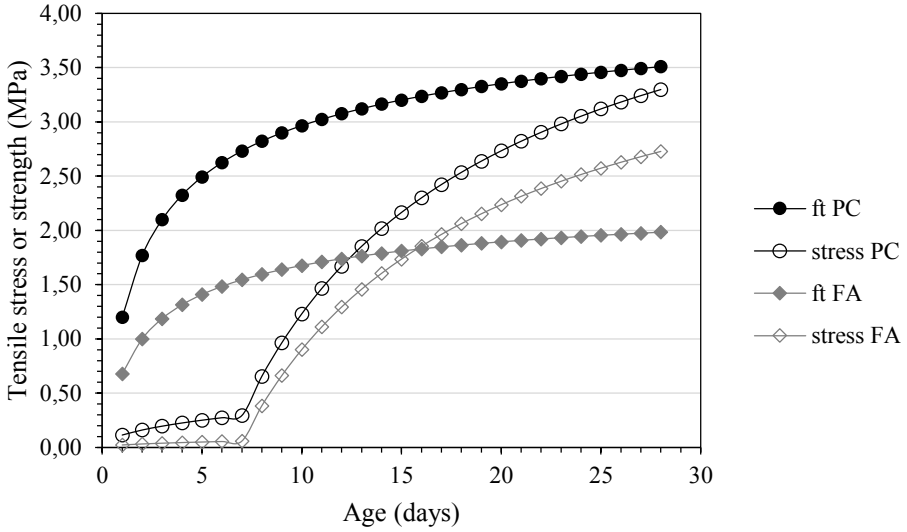

Figure 3.9: Development of tensile stress versus tensile strength for $f_{ck,cube}$ 50 MPa ($t_{overlay}$ = 40 mm, 50% RH, 7 days curing).

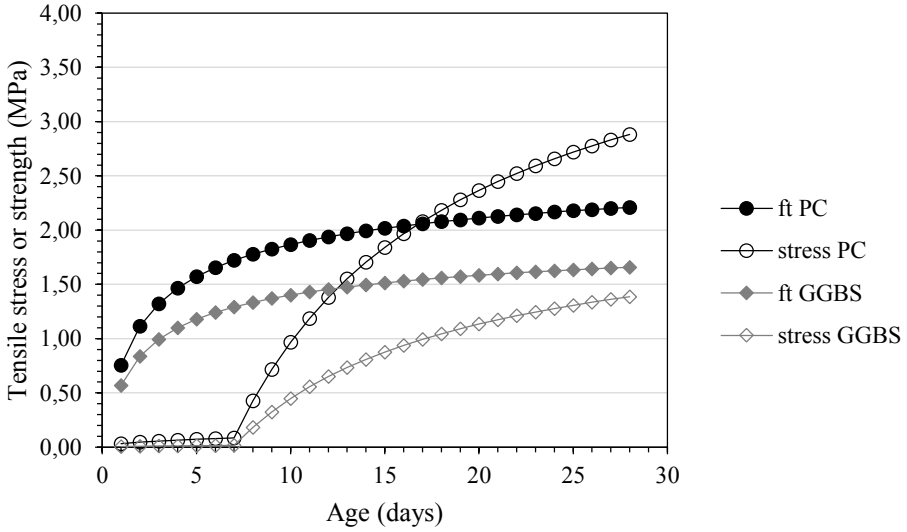

Figure 3.10: Development of tensile stress versus tensile strength for $f_{ck,cube}$ 25 MPa ($t_{overlay}$ = 40 mm, 50% RH, 7 days curing).

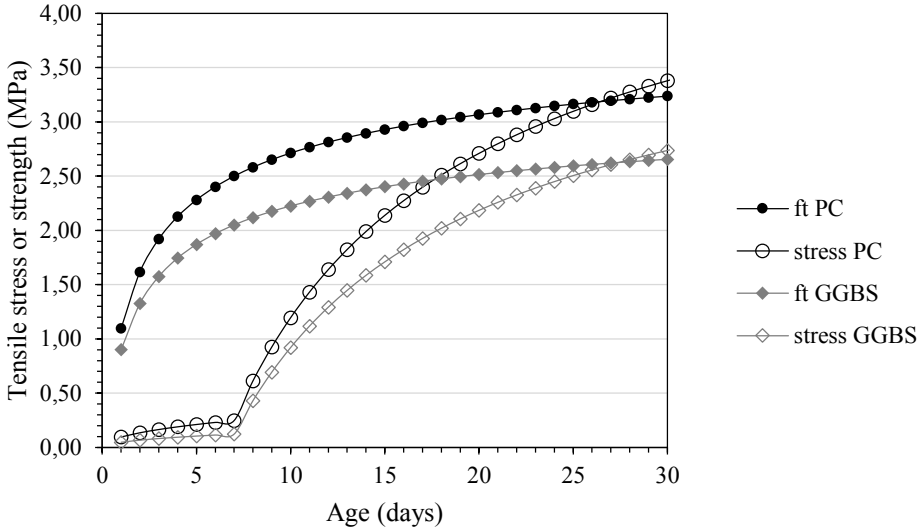

Figure 3.11: Development of tensile stress versus tensile strength for $f_{ck,cube}$ 37 MPa ($t_{overlay}$ = 40 mm, 50% RH, 7 days curing).

Table 3.2: Predicted age at cracking

Mix I.D	Age at cracking (days)
PC 25 MPa	17
FA 25 MPa	16
PC 50 MPa	> 28
FA 50 MPa	17
PC 25 MPa	16
GGBS 25 MPa	> 28
PC 37 MPa	27
GGBS 37 MPa	28

The results show that the predicted age at cracking for FA concretes is lower than the reference concrete for both strength classes. At lower strength, the age at cracking of the FA concrete is marginally lower to that of the reference concrete. However, at higher strength, the FA concrete is outperformed by the reference concrete. The figures also show that tensile strength development is significantly lower in the FA concrete than the reference concrete. For the GGBS concrete, the age at cracking is increased in comparison to the reference concrete. There is also an increase in age at cracking with increasing strength class unlike the FA concrete. Although the age at cracking is decreased at lower strengths, the relative difference between the slag and reference concrete is very significant. This finding suggests that GGBS has a larger positive impact on the age at cracking for lower strength concretes. The reduction in tensile strength in the GGBS concrete was not as high as that of the FA concrete.

3.4.2 Comments on material property results

This section provides brief comments on some of the observations made with regards to the development of the material properties.

1. Elastic modulus

The 28-day mean elastic modulus data that were used for the FA concretes were that of FA concretes wet cured for 28 days (Krüger, 2003). This is obviously an overestimation of the elastic modulus in comparison to a 28-day mean elastic modulus of concrete cured for only 7 days. This evidently affected the stress development of the FA concrete. The negative result observed in the FA concretes may thus have been as a result of this.

2. Tensile relaxation factor

The results of the development of the tensile relaxation factor with time are presented in **Figure 3.12** and **Figure 3.13**. The figures show that FA and GGBS concretes have lower mean relaxation factors, which corresponds to a higher relaxation capacity compared to the reference concretes. This is consistent with the findings from literature which suggest that FA and GGBS concretes exhibit higher stress relaxation. The results also show that the tensile relaxation of the concrete increases with decreasing strength. This is also as suggested in literature (see Section 2.4.5). It is also observed that FA and GGBS have a larger impact on the relaxation at lower strength values. This may have caused the improved performance of the FA and GGBS concrete at lower strength values.

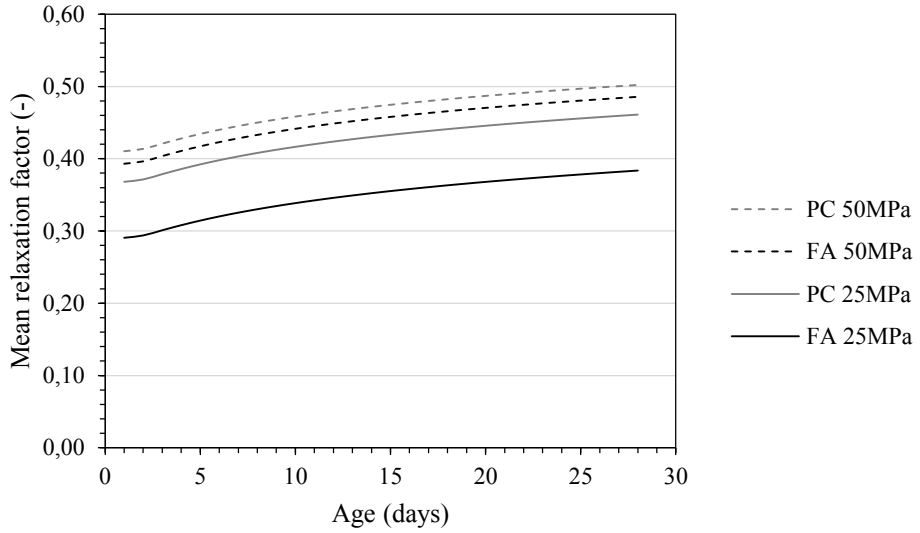

Figure 3.12: FA relaxation coefficients (ψ (t, t_0), ($t_{overlay}$ = 40 mm, 50% RH, 7 days curing).

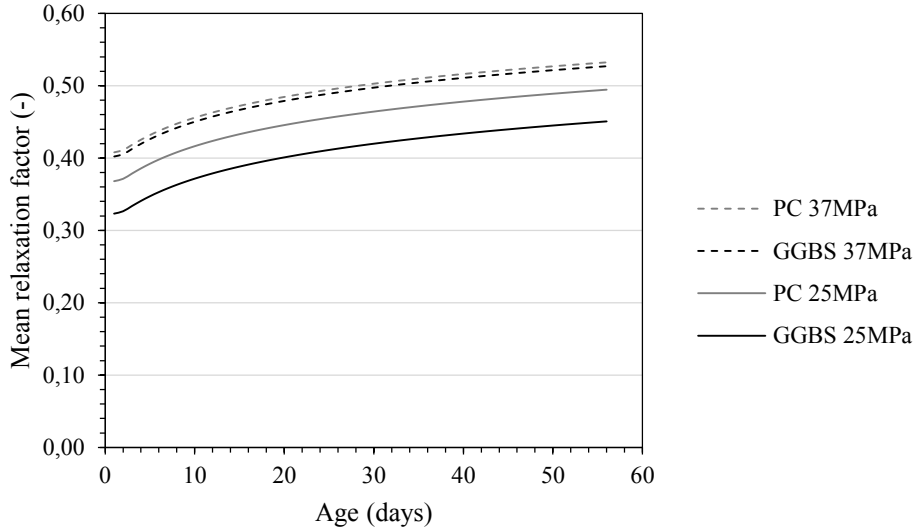

Figure 3.13: GGBS relaxation coefficients (ψ (t, t_0), ($t_{overlay}$ = 40 mm, 50% RH, 7 days curing).

3. Total shrinkage

The total shrinkage was taken as the sum of the autogenous shrinkage and drying shrinkage. The use of FA and GGBS resulted in very low autogenous shrinkage values. This is because the autogenous shrinkage is modelled as a linear function of the concrete strength. The autogenous shrinkage however, contributes a smaller fraction of the total shrinkage. The drying shrinkage results of the FA and GGBS concrete were higher than that of the reference concrete, more considerably in the FA concrete. This is because the basic drying shrinkage strain is modelled as a negative exponential function of the mean compressive strength. A decrease in mean compressive strength translates into a higher basic drying shrinkage coefficient.

It must be noted that the drying shrinkage model does not take into consideration the total paste volume. Literature shows that when fly ash or slag are substituted on an equal-weight basis, the lower specific gravity of the fly ash and slag compared to Portland cement results in higher paste volume which may lead to higher shrinkage. When corrected to compare mixtures on an equal paste content basis, fly ash and slag concrete may exhibit lower total shrinkage (Yuan, et al., 2015). The drying shrinkage results as modelled according to the code are presented in **Figure 3.14** and **Figure 3.15**.

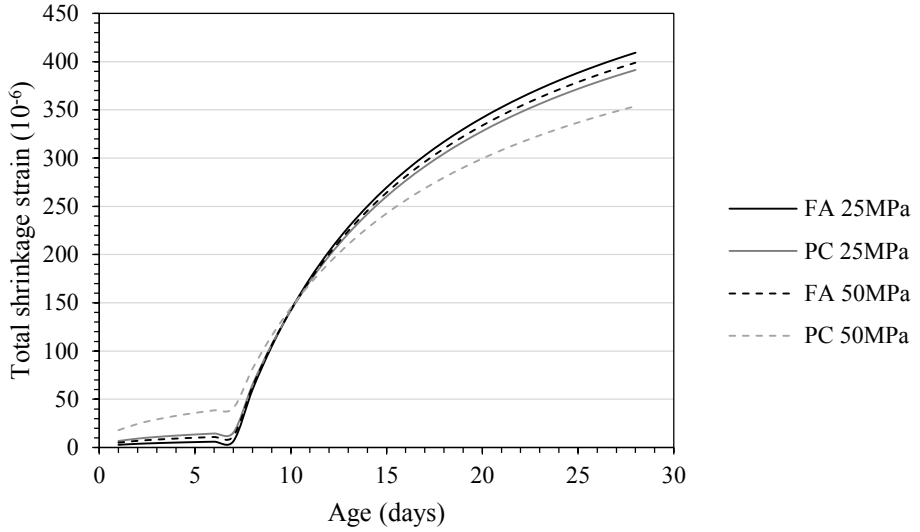

Figure 3.14: Development of total shrinkage strain ($\varepsilon_a(t) + \varepsilon_d(t)$) in FA concrete ($t_{overlay}$ = 40 mm, 50% RH, 7 days curing)

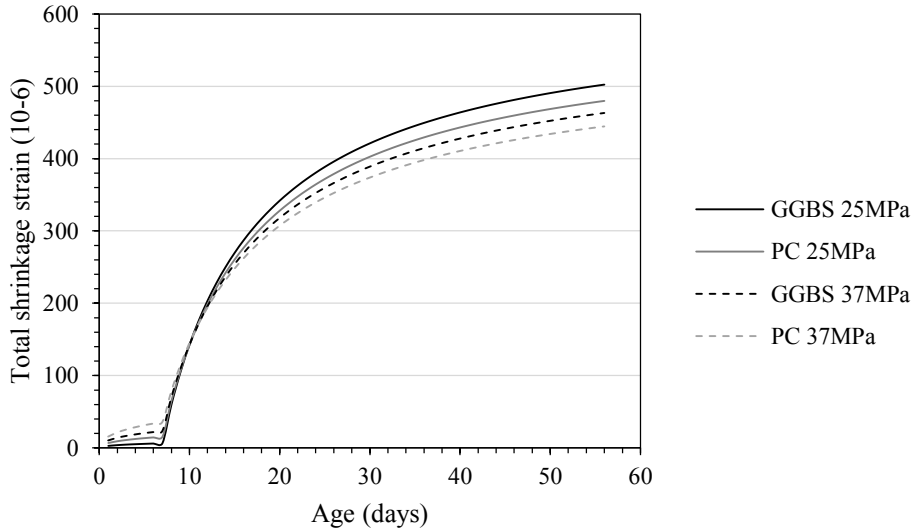

Figure 3.15: Development of total shrinkage strain (εa(t) + εd(t)) in GGBS concrete ($t_{overlay}$ = 40 mm, 50% RH, 7 days curing)

3.5 Conclusions

The results obtained from the preliminary investigation suggest that the age at cracking of bonded overlays can at least be increased with the use of GGBS. The FA results indicated otherwise. Conclusions on the influence of FA and GGBS on restrained shrinkage cracking cannot be made based on this information as the modelling approach used does not explicitly take into account mix compositions, binder types, or aggregate types and content. However, the results suggest that the research hypothesis is significant for further investigation. The main aspect carried forward into the experimental investigation from this preliminary modelling is the use of the worst case combination of external influences in order to ensure that any positive results obtained are as a result of the use of fly ash or slag.

CHAPTER FOUR

4 Experimental methodology

4.1 Introduction

This chapter provides a description on the experimental approach that was used in this research. It highlights the important aspects considered for both the experimental techniques and analysis of data for the attainment of the research goals. The chapter begins with a description of the pre-planning of the experimental phase, which was a necessary step in ensuring appropriate data was collected. This is followed by the material selection and concrete mix designs used in the investigation. The test procedures and data analysis techniques are then briefly explained.

4.2 Pre-experimental planning

4.2.1 Recognition of and statement of the problem

The objectives of the experimental investigation are as highlighted in research objective (6) given in Chapter 1. Bonded concrete overlays are a common method used to repair and rehabilitate damaged concrete structures. However, as highlighted in Chapters 1 and 2, their performance is impaired by the effects of surface cracking. Fly ash (FA) and ground granulated blastfurnace slag (GGBS) have been proposed as potential materials for the improvement of the performance of the overlay material with this respect. In Chapter 2, the various material parameters that affect cracking in concrete repair materials were identified. The influences of these two cement extenders on the material parameters were also documented. In order to draw meaningful conclusions, an experimental investigation is necessary to support the findings from literature.

The motivation of this experimental research is the exploration of materials to be used in concrete repairs. The experimental investigation is intended to:

- Quantify the difference in magnitude of the various material parameters when cement is replaced with high volumes of fly ash or GGBS,
- Determine which material parameter has the largest influence on the behaviour of the overlay when cement is replaced with high volumes of fly ash or GGBS, and
- Determine and analyse the overall effect on the susceptibility to cracking when cement is replaced with high volumes of fly ash or GGBS.

4.2.2 Scope of experimental investigation

The experimental investigation is intended to be a basis for a comparative study on the selected materials. The research does not look into the optimisation of the materials, but is rather focused on looking at differences in performance when different materials are used. The materials in question are ordinary Portland cement (PC), FA, and GGBS. The experimental investigation will only be applicable to overlays for which early-age strength is not a driving factor.

4.2.3 Selection of the response variable

The tests that were carried out in this investigation involved the determination of the following parameters: compressive and tensile strength, tensile relaxation, free shrinkage strains, elastic modulus, age at cracking, and crack characteristics. Each response was measured as described in the respective sections in Section 4.6.

4.2.4 Choice of factors, levels, and range of experiment

4.2.4.1 Design variables

The design variables are the variables selected for study in the experiments. For the purpose of this investigation, four design variables were identified: binder type, water-binder ratio, percentage replacement of cement, and curing duration. The expected effects and/or rationale behind the selection of these variables are described below.

Binder type

The motivation of this research is centred on the use of the following binder types:

- Portland cement
- Portland cement – fly ash blend
- Portland cement – GGBS blend

It was thus imperative that 'binder type' be selected as a design variable.

Water-binder ratio

Two water-binder ratios were selected for this study, 0.45 and 0.65. The water-binder ratio has a direct influence on the strength of the concrete. The strength of the concrete in turn has an influence on other material properties. Beushausen (2015) reported on the effects of strength class on the material properties of bonded overlays. Stronger overlays (associated with lower water-binder ratios) were found to develop higher stresses mainly due to a higher elastic modulus and lower relaxation in comparison to lower strength overlays. However, stronger overlays were also found to have higher tensile strengths. The research provided useful insights, however it was limited to analytical modelling and included overlays made with portland cement only. Thus, these findings may not be applicable to overlays made with blended cements and may not represent actual overlay behaviour.

The water-binder ratios were selected based on previous research (Masuku, 2009; Chilwesa, 2012) which indiated that these water-binder ratios generally cover the range of normal concretes that may be used in overlays. **Figure 4.1** shows the assumed effects of the water-binder ratios on the response variables.

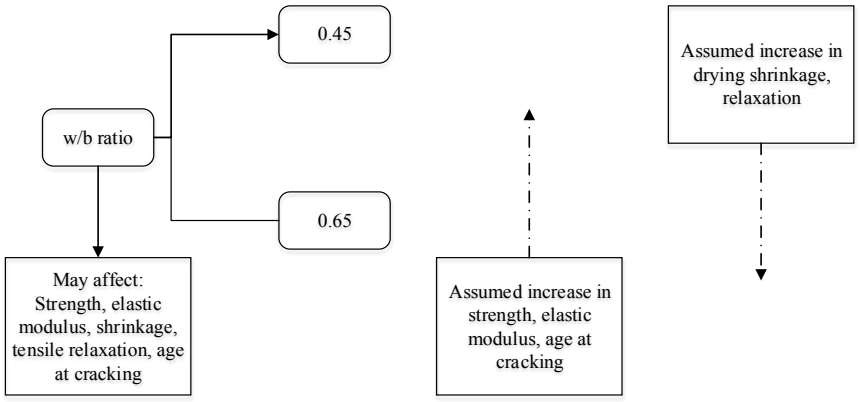

Figure 4.1: Assumed influence of water-binder ratio on main parameters

Percentage replacement of cement

Two percentage replacement ratios were used for each cement extender. For the FA blend, 30% and 50% replacement ratios were used, while 50% and 70% ratios were used for the GGBS blend. These replacement ratios were selected in order to determine the effects of high volumes of FA or GGBS on the cracking potential of concrete overlays. The ratios selected are in the range of the maximum values normally used (Addis, 1987). High volumes of extender are likely to magnify the effects and make observations more distinct. **Figure 4.2** and **Figure 4.3** show the assumed influence of the percentage replacement of cement by fly ash and slag respectively on the response variables.

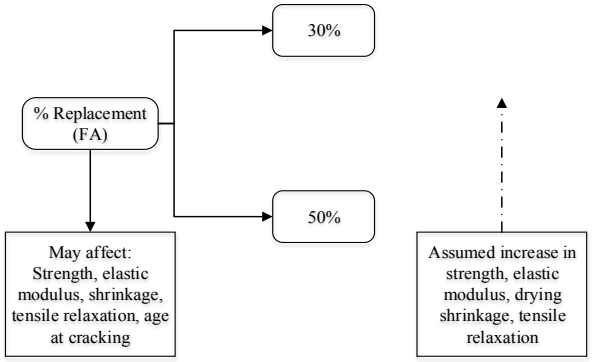

Figure 4.2: Assumed influence of % replacement of cement by fly ash on main parameters

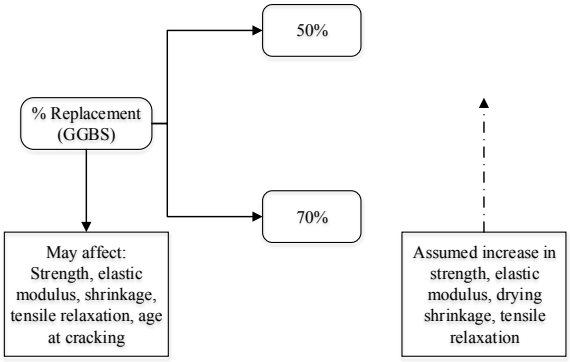

Figure 4.3: Assumed influence of % replacement of cement by slag on main parameters

4.2.4.2 Curing duration

Works carried out by Bester (2015) showed that the method of curing has an influence on the age at cracking of overlays subjected to restrained shrinkage. Air-cured specimens (0 days moist curing) experienced the greatest shrinkage at early ages and lower shrinkage at later ages in comparison to wet cloth cured specimens (2 and 7 days curing). Air curing was considered the least effective curing method as it resulted in the lowest ages at cracking and net age at cracking. Wet cloth curing resulted in increase in age at cracking in comparison to air curing suggesting that wet cloth curing provides an increase in crack resistance. However, this study

did not look into the effects of curing on FA or GGBS overlays. Research carried out by Beushausen (2015), studied the effects of longer curing on cracking of overlays by comparing the effects of curing for 1, 3 and 7 days. Only a very slightly positive effect on cracking behaviour was observed in low strength concretes, while high strength concretes cracked earlier when cured for longer. However, the study also did not take into account the effects of cement extenders and was only based on numerical modelling. It was therefore useful to investigate the influence of curing on cracking of the blended concretes to determine if similar trends would be observed. The two curing regimes invstigated were wet cloth curing and air curing. The effect of curing regime was only investigated in a limited number of samples because the effects of curing was not a primary objective for this research. For the majority of samples that constitute the main component of this investigation, the curing duration was set at 7 days (wet cloth curing), counting from the day of casting.

4.2.4.3 Fixed design factors

Fixed design factors are the factors that may exert some effect on the response but for purposes of the present experiment, are not of interest, and are thus held at a specific level. The environmental conditions, that is the ambient temperature and relative humidity were chosen as fixed design factors and were kept constant throughout.

4.3 Selected experimental approach

The experimental investigation was split into two components. The main component was designed to determine the influence of the cement extenders on the age at cracking and development of material properties. The minor component was focused at determining the effect of curing duration on the age at cracking for the blended concretes only.

Taking into consideration all the design factors selected, 10 different mixes were used in the main component of this research. To ensure homogeneity, all specimens for each mix were cast from the same batch. The ring test and material property test specimens were thus cast from the same batch for each mix. For each mix, 2 rings were cast for restrained shrinkage testing, resulting in a total of 20 rings. An additional 8 rings were cast to investigate the influence of curing duration on the age at cracking. **Figure 4.4** shows the breakdown of the mixes used in this experimental investigation.

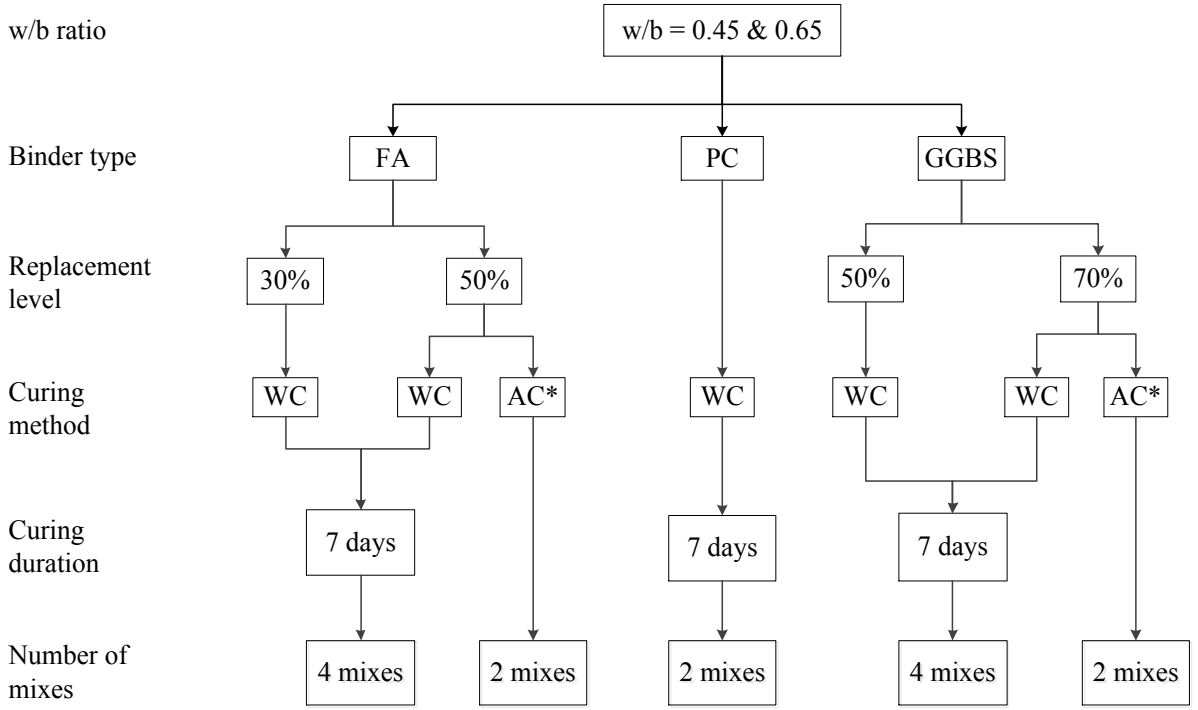

*Minor component of investigation; AC = Air curing; WC = Wet cloths curing; 1 mix/water-binder ratio.

Figure 4.4: Collated schematic of design factors for the two components of the experimental investigation

In order to determine the age at cracking for the various concrete mixes, ring tests were carried out. The ring test is the most common test for observing restrained shrinkage cracking. The test follows a very simple principle: the concrete is cast around a restraining core that restrains shrinkage thereby inducing tensile stresses that cause the concrete to crack. The performance of the mixes was determined by the characterisation and quantification of the cracks (i.e. average width, number of cracks, and time of cracking) (Bentur & Kovler, 2003). The ring test is commonly used for comparative studies making it specifically suitable for this research. The analysis of results from the ring test along with results from material parameter tests were used to draw conclusions on the influence of FA and GGBS on restrained shrinkage cracking.

The material parameter tests that were carried out were based on the response variables chosen for this research (Section 4.2.3). The tests were carried out on specimens cast from the 10 mixes shown in **Figure 4.4**. The tests were carried out over a period of 28 days in order to determine the time development of these properties. The results from the material property tests were then used to analytically model the development of stresses that lead to the cracking of the concrete. The results from the analytical modelling were compared to the results obtained from the ring test. **Figure 4.5** shows a detailed schematic of the experimental process.

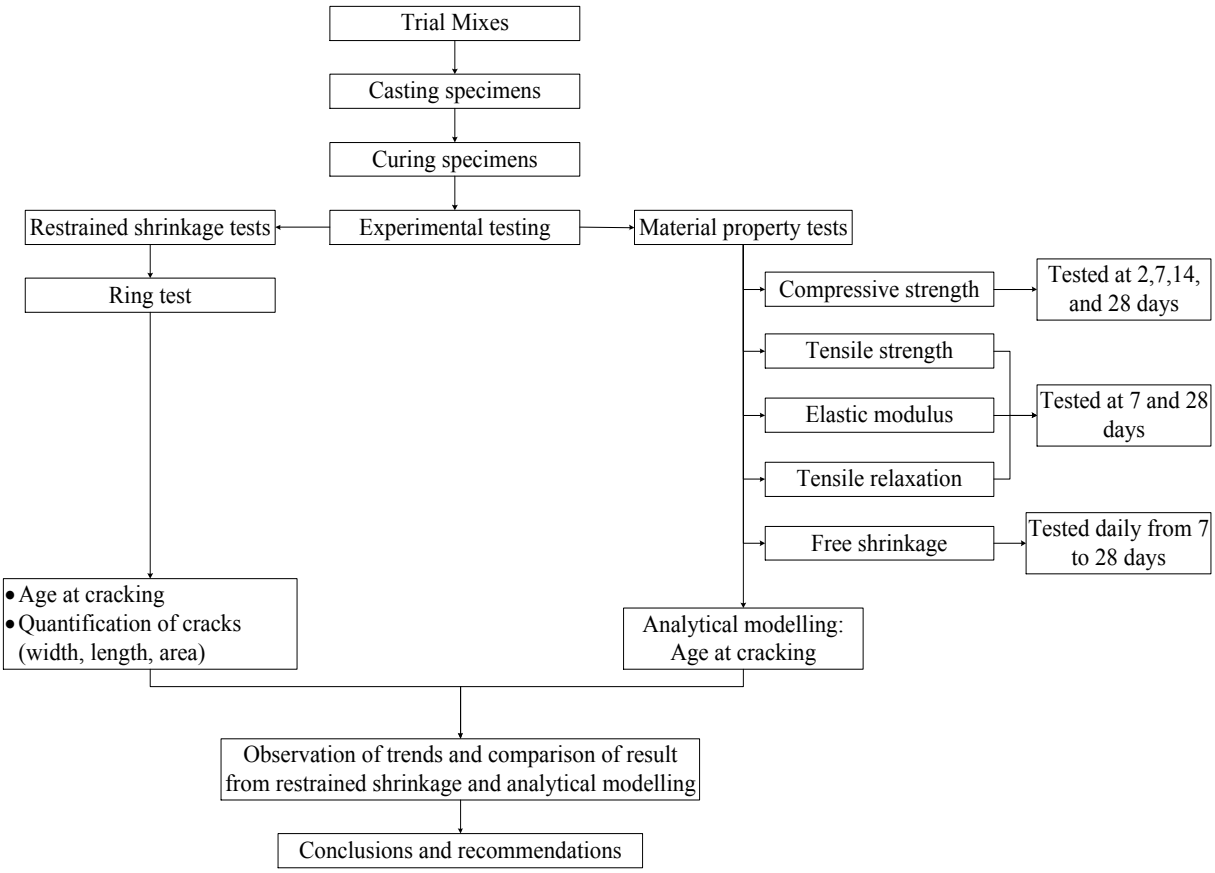

Figure 4.5: Schematic of complete experimental program.

4.4 Mix proportions and material selection

This section details the mix proportions and properties of the raw materials selected for this research. As indicated above, 10 different laboratory-made mixes were used in the investigation. The mixes are detailed in **Table 4.1** and **Table 4.2** for water-binder ratio 0.45 and 0.65 respectively.

4.4.1 Water content

The water content was kept constant at 250 l/m^3 for all 10 mixes. This was based on the fact that drying shrinkage is directly affected by water content. Therefore, to ensure the shrinkage trends observed were only due to different binder composition, it was necessary to fix the water content. The water content was determined using the method of the Cement and Concrete Institute (C&CI) mix design (Addis & Goodman, 1999). In this mix design method, the water content remains constant irrespective of the cement content, water-binder ratio, or aggregate proportions. The water content is dependent on the aggregate properties and the selected workability range.

4.4.2 Cement type

The cement used was CEM II/A-L 52,5N. This cement contains approximately 91% clinker and 9% limestone extender. CEM I 52,5N cement was the preferred cement type as it does not have any extender additions. However, this type of cement was not locally available and thus CEM II/A-L 52,5N was selected because it does not have any FA or GGBS additions that may influence the results obtained. The cement was obtained from PPC De-Hoek production factory in the Western Cape, South Africa.

4.4.3 Fine aggregate

Only fine aggregates were used in the mix design, that is, tests were carried out on mortar mixes. This is because coarse aggregates have significant influences on the key material properties influencing restrained shrinkage cracking. When coarse aggregates are present, the major contribution to the elastic modulus comes from the stiffness and volume concentration of the coarse aggregates. Coarse aggregates also have strong influences on shrinkage and creep by providing restraint to deformations (Alexander & Mindess, 2005). Hence, it was opted to carry out the tests on mortar rather than concrete in order avoid the influence of the coarse aggregates.

The fine aggregates readily available in the laboratory were Philippi dune sand and Greywacke crusher sand. In order to obtain well-graded fine aggregates, a 50/50 blend of Greywacke crusher sand and Philippi dune sand was used. Greywacke crusher sand is angular and therefore reduces the workability of the mixture and increases the water demand. Philippi dune sand on the other hand has spherical particles that increase the workability of the mixture. However, Philippi dune sand is singly graded with almost no fine particles (Particles < 75 μm) while Greywacke crusher sand has a better grading curve than Philippi dune as shown in **Figure 4.6**. According to Mehta & Monteiro (1993), aggregates that do not have a large deficiency or surplus of any particle size (well graded aggregates) tend to produce concrete mixtures with better workability. Consequently, these two types of sand were blended together to obtain an optimum particle distribution. The grading curves in **Figure 4.6** were obtained from a sieve analysis of the aggregates conducted according to SANS 3001 – GR2: 2011. The 50/50 blend was done volumetrically because the two sands have different particle relative densities. As a result, the final masses of sand used were not exactly the same.

The Philippi dune sand and Greywacke crusher sands were found to contain approximately 2.0% and 1.0% moisture respectively. Hence, it was necessary to dry the sand to remove all the additional moisture to ensure the water-binder ratio was not altered. The aggregates were oven dried at 80˚C for approximately 24 hours. The fine aggregates were then allowed to cool for an additional 24 hours prior to use.

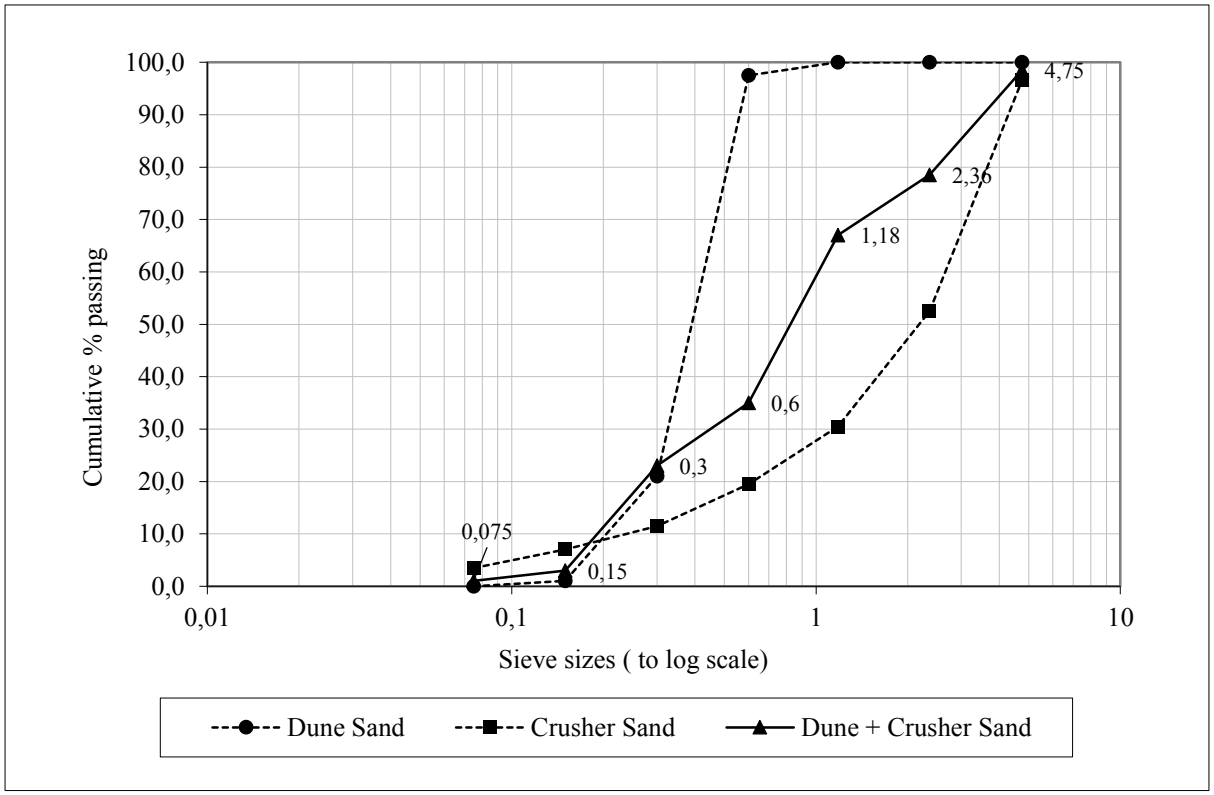

Figure 4.6: Grading curves of fine aggregates used.

4.4.4 Workability and consistence

The slump test in accordance to SANS 5862-1:2006 was used to assess the workability and consistence of the fresh mixes. A slump of 75±10 mm was selected for all the mixes. This slump was selected to allow for the mortar to properly fill the intricate shapes of some of the specimen moulds without the need for excessive vibration. Although this slump is not ideal for trowel application of mortars on vertical and overhead surfaces, it is still applicable for horizontal placement and was thus considered appropriate. The addition of a suitable amount of Chrysopremia 310 superplasticizer was used to meet the target slump for mixes that had low initial slumps. This is detailed in the concrete mix design in Section 4.4.5.

4.4.5 Mix Proportions

The concrete mix design was carried out according to the volumetric design method of the Cement and Concrete Institute (C&CI). This is the mix design that is typically used in South Africa. The mix designs have been split in two tables according to the water-binder ratio used. **Table 4.1** provides the mix proportions and key mix properties of the concrete mixes with w/b = 0.45, while **Table 4.2** for w/b = 0.65. Each mix is designated an identification number as shown by the first row of each table. The first character indicates the binder type (C: CEM I; F: FA blend; S: GGBS blend). The following two digits indicate the water-binder ratio (e.g.: 45: w/b =0.45). The last two digits indicate the percentage of cement replaced by an extender.

Table 4.1: Mix proportions and key mix properties for w/b = 0.45

Mix Proportions					
Mix ID	C45	F45_30	F45_50	S45-50	S45-70
Water content (kg/m^3)	250	250	250	250	250
Total binder content (kg/m^3)	556	556	556	556	556
CEM (kg/m^3)	556	389.2	278	278	166.8
Fly ash (kg/m^3)	0	166.8	278	0	0
Slag (kg/m^3)	0	0	0	278	389.2
Phillipe dune sand (kg/m^3)	759	738	723	745	739
Crusher sand (kg/m^3)	774	752	737	759	753
Superplasticizer (ml)	40	-	-	55	55
Key mix properties					
% cement extender	0	30	50	50	70
Paste content (%)	23.8	24.2	24.5	24.1	24.2
Measured slump (mm)	85 ± 5	70 ±5	90 ±5	80 ±5	80 ±5
Measured 28-day compressive strength (MPa)	53.8	46.1	32.6	47.2	37.7

Table 4.2: Mix proportions and key mix properties for w/b = 0.65

Mix proportions					
Mix I.D	C65	F65_30	F65_50	S65-50	S65-70
Water (kg/m^3)	250	250	250	250	250
Total binder content (kg/m^3)	385	385	385	385	385
CEM (kg/m^3)	385	269.5	192.5	192.5	115.5
Fly ash (kg/m^3)	0	115.5	192.5	0	0
Slag (kg/m^3)	0	0	0	192.5	269.5
Phillipe dune sand (kg/m^3)	831	816	806	822	818
Crusher sand (kg/m^3)	847	832	822	837	833
Superplasticizer (ml)	5	-	-	25	20
Key mix properties					
% cement extender	0	30	50	50	70
Paste content (%)	16.6	16.8	17.0	16.8	16.8
Measured slump (mm)	65 ±5	65 ±5	85 ±5	70 ±5	70 ±5
Measured 28-day compressive strength (MPa)	36.5	25.2	16.7	26.0	19.3

4.5 Curing and environmental conditions

4.5.1 Curing method

4.5.1.1 Initial curing

Initial curing was carried out on all specimens between the time of placement and de-moulding. Initial curing was necessary for the prevention of excessive moisture loss to the environment at the exposed surface of the fresh mortar. Although initial curing may or may not be practiced on site, for the purpose of this research, this was done in order to maintain consistency with respect to drying conditions. The specimens were kept in their moulds for approximately 24 hours to ensure the specimens had gained sufficient strength before they could be stripped from the moulds. During this 24-hour period, the specimens were protected from excessive moisture loss by covering with 125 μm black polyethylene sheeting. The sheeting was placed within 10 minutes of casting and compaction.

4.5.1.2 Saturated hessian sheets

The curing method considered for the main component of the experimental investigation was saturated hessian sheets. This is a fairly easy method to implement on horizontal and inclined concrete mortar overlays and was also easy to use on the test specimens. The hessian sheets were completely immersed in a bucket of water for at least 24 hours to ensure they were adequately saturated. Once the specimens were de-moulded, they were wrapped in the saturated hessian sheets within approximately 15 minutes. In order to secure the hessian sheets tightly, the specimens were further wrapped in plastic cling wrap. This also allowed for the prevention of moisture loss from the hessian sheets to the environment. The plastic cling wrap was then sealed using tape to adequately seal against moisture loss. The hessian sheets were removed following the specified curing duration and the specimens were allowed to air cure in the curing environment until the day of testing.

4.5.2 Curing duration

The curing duration was kept as a fixed parameter for all the specimens that constitute the main component of the research. These specimens were cured for 7 days using the method described in Section 4.5.1. The additional eight rings used to monitor the effects of curing duration were only cured during the initial 24-hour period before de-moulding as described in Section 4.5.1.1. The cube specimens used for compressive strength testing were cured in a water tank at 23°C until the day of testing. The cubes were tested at 2, 7, 14, and 28 days.

4.5.3 Environmental conditions

Temperature and relative humidity have a significant effect on the material properties. It is thus important to maintain constant laboratory conditions throughout the duration of testing. Changes in relative humidity affect the drying shrinkage and relaxation properties. Increasing relative humidity lowers the drying shrinkage and lessens the stress relaxation. Overall, an increase in relative humidity results in positive results with regards to cracking, mainly due to a decrease in shrinkage (Beushausen, 2015). The temperature affects the hydration of the cement and ultimately the development of material properties. An increase in concrete maturity results in increases in tensile and compressive strengths (Neville, 1996). Therefore for the purpose of this research, all test specimens were kept in a controlled environment room at

standard conditions of temperature and relative humidity (23.0 ± 2.00 C and 50 ± 4 %). This does not mirror realistic conditions, but was deemed adequate for the purpose of this research. Exposing the specimens to varying environmental conditions could result in covariates that may be difficult to isolate during analysis.

4.6 Test parameters and test methods

This section describes the various test methods carried out in this experimental investigation. The section describes how each response variable was measured, including, if applicable, how the measurement system was calibrated and how the calibration was maintained during the experiment. The gauge or measurement capability of the instrumentation to be used was also taken into account. Additional measurements or other mitigation strategies are specified where gauge capability was expected to be poor.

4.6.1 Compressive strength

Compressive strength tests were carried out on cube specimens (100 mm dimension) at 2, 7, 14, and 28 days. The focus on these ages is directly linked to practical applications. The 2-day strength is important when considering formwork turnaround, while 28-day strength is normally considered as the design strength of the concrete (Beushausen, Alexander, & Ballim, 2012). Monitoring the 2-day and 7-day strengths was important for the purpose of this research because blended cements have low compressive strengths in the early ages. This directly affects the tensile strength of the concrete and thus may negatively impact the resistance to cracking of the repair material.

The test was carried out according to SANS 5863: 2006. Three specimens were tested for each mix and each age of testing. The cube specimens were water cured at 23°C until the day of testing. The difference in curing regime from the rest of the test specimens (see Section 4.5) was considered to be acceptable in this research. The compressive strength results were primarily intended for the determination of compressive strength development and mortar material characterisation, and were not used in the subsequent analytical modelling. An Amsler Compression Machine was used to perform these tests.

4.6.2 Tensile strength

The uniaxial tensile strength test was carried out in order to determine the tensile strength of the concrete specimens. The tensile strength results were used to predict the age at cracking. Through analytical modelling (see Section 4.8), the tensile strength development was compared to the tensile stress development to determine the age at which cracking would be initiated. The results obtained from this test were also used for the estimation of stress-strength ratios for the tensile relaxation test described in Section 4.6.3.

4.6.2.1 Apparatus

The Zwick Roell Universal Testing Machine (UTM) of 20 kN capacity shown in **Figure 4.7**.

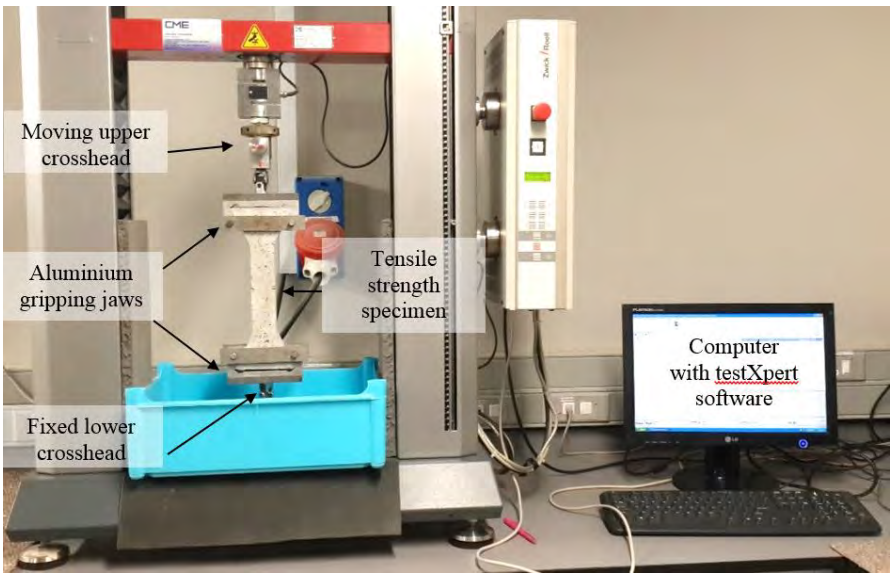

Figure 4.7: Test set-up for tensile strength and tensile relaxation

The machine is connected to a computer equipped with software (testXpert) that enables the recording of data as the test proceeds. The software enables the computer to plot graphs of Load vs Time (**Figure 4.8**), and captures the load at failure, which can then be used to determine the tensile strength of the specimen.

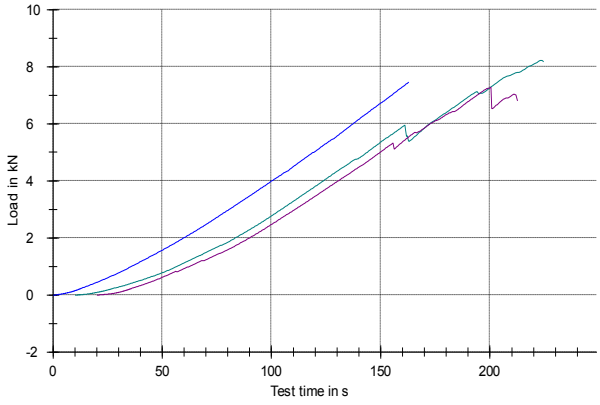

No.	R_m (N)	ε-F max (%)	Date	Time
1	7455.53	1.38	2015/09/08	12:02:40 PM
2	8221.76	1.82	2015/09/08	12:10:23 PM
3	7270.82	1.54	2015/09/08	12:30:02 PM

Figure 4.8: Sample of data-capture from UTM testXpert software for tensile strength test (28-day tensile strength of C45 mix)

4.6.2.2 Specimen preparation

Tensile strength tests were carried out on dog-bone specimens with dimensions as shown in **Figure 4.9**. To ensure failure occurred within the prismatic section, a notch was incorporated in the specimen. The notch induces a fracture plane at the mid-section of the specimen. Previous research (Magera, 2013) indicated that notched specimens produce consistent tensile stress values as opposed to un-notched specimens where the strength may be underestimated. The cross-section of the specimens at the location of the notch is 30 mm × 40 mm. After curing, the specimens were placed in the environment room until the day of testing at ages 7 and 28 days. Three specimens were tested at each age.

4.6.2.3 Test procedure

The tensile strength specimens were placed in the UTM, ensuring they were firmly secured between the gripping jaws of the machine. A tensile load was applied to the specimens through the upward movement of the upper crosshead while the lower crosshead remained fixed. The upper crosshead was set to move at a rate of 0.2 mm/min until failure occurred. The failure load was obtained from the UTM software, and recorded as the uniaxial tensile strength of the specimen. A typical failure through the notched section of the specimen is shown in **Figure 4.10**. In the instance in which failure occurred in the dovetail section of the specimen, the test result was disregarded. The ultimate tensile load was then recorded as the average value from the remaining 2 specimens.

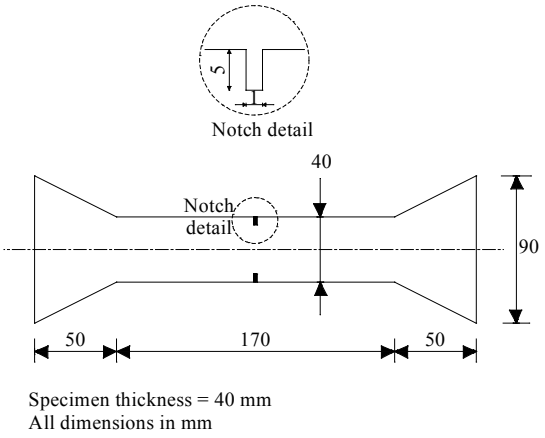

Figure 4.9: Tensile strength dog-bone specimen with central notch.

Figure 4.10: Tensile strength specimens showing fracture through the notched section.

4.6.3 Tensile relaxation

The tensile relaxation test was carried out to obtain the magnitude of relaxation with time, as well as the relaxation coefficient of the different mortar mixes. The same equipment used to determine the tensile strength (see Section 4.6.2.1) was used to simulate the relaxation behaviour of the concrete. The UTM software facilitated the monitoring of the tensile stress

decay within the specimen. The software plotted the curve of the stress relaxation, which could then be used for analysis.

4.6.3.1 Specimen preparation

Tensile relaxation tests were carried out on specimens of similar geometry as tensile strength test specimens with the exception of the notch (see **Figure 4.11**). After curing, the specimens were placed in the environment room until the day of testing at ages 7 and 28 days. All the tensile relaxation tests were carried out under sealed conditions. This was done to prevent moisture loss and the resulting shrinkage stresses during testing. On the day of testing, the specimens were sealed on all surfaces. The specimens were sealed by applying a thin coat of melted paraffin wax. Sealing the specimens does not prevent autogenous shrinkage from taking place. However, for the purpose of this investigation, autogenous shrinkage was considered negligible. For normal strength concretes with w/b greater than 0.4, autogenous shrinkage is usually small in comparison to drying shrinkage (Alexander & Beushausen, 2009) and can thus be considered insignificant.

4.6.3.2 Test procedure

Prior to carrying out the tensile relaxation test, the tensile strength of the specimen was determined as described in Section 4.6.2. This was done to estimate the magnitude of stress to be applied on the relaxation specimens. Similar to the tensile strength test, specimens were placed in the UTM, ensuring they were firmly secured between the gripping jaws of the machine. A tensile load was applied to the specimens through the upward movement of the upper crosshead while the lower crosshead remained fixed (see **Figure 4.12**). The upper crosshead was set to move at a rate of 0.2 mm/min until the required stress level was attained. The specimens were subjected to a stress level equivalent to 80% of the ultimate strength obtained from the tensile strength test. As soon as the load was reached, the upper crosshead was fixed in position and the stress decay in the specimen was electronically recorded. The test was carried out for 24 hours after which the test stopped automatically and the stress value at 24 hours recorded. The UTM software enables the capture of all the necessary data. The software monitors tensile stress decay, increase in strain, and the final strain reached by the loaded specimen. The gradient of the curve was used to determine the rate of stress relaxation. It should be noted that the 24-hour relaxation obtained is only approximately 80% of the ultimate relaxation value (Masuku, 2009). This however can be considered adequate for this research as the results are only meant for comparative purposes.

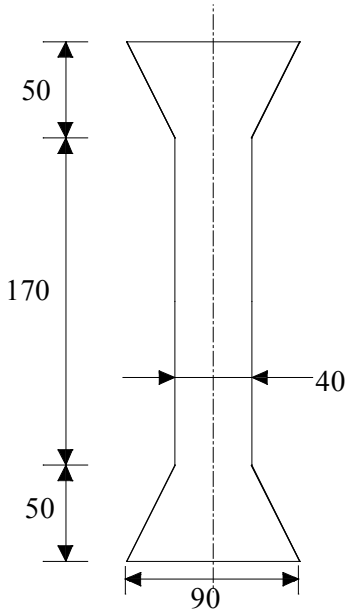

Specimen thickness = 40 mm
All dimensions in mm

Figure 4.11: Dog bone specimens used for tensile relaxation

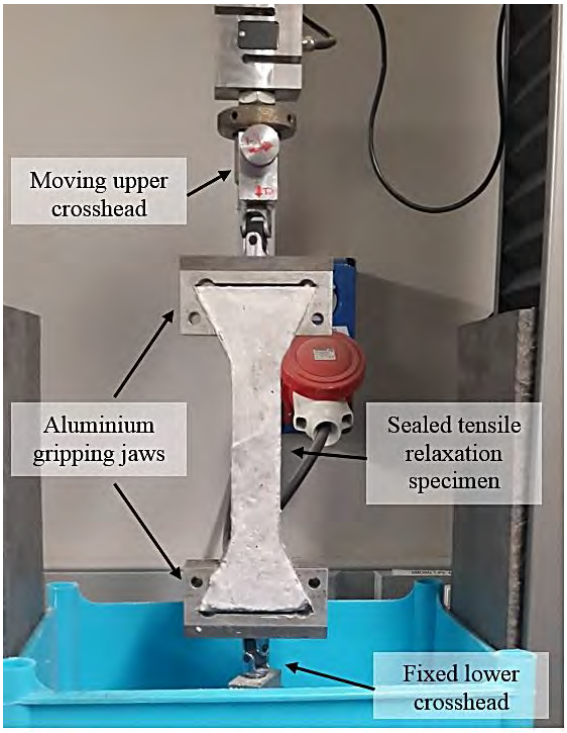

Figure 4.12: Test set-up for tensile relaxation

4.6.4 Elastic modulus

The elastic modulus was determined in compression due to the difficulty of accurately carrying out the test in tension. This approach was justified by (Beushausen & Chilwesa, 2013) stating that the elastic modulus is generally taken to be equal for tensile and compressive loading for normal strength concretes. The static modulus of elasticity in compression was determined from the secant modulus using the equation:

$$\frac{\Delta\sigma}{\Delta\varepsilon}$$

Where $\Delta\sigma$ and $\Delta\varepsilon$ are the differences in stress and strain, respectively, between a basic loading level of 0.5 N/mm^2 and an upper loading level of 30% of the compressive strength of the concrete.

4.6.4.1 Apparatus

The Zwick Roell Universal Testing Machine (UTM) of 100 kN capacity shown in **Figure 4.14** was used to apply the compression load onto the specimens. The Zwick Roell UTM allowed for the careful control of the imposed loads and loading rates. The machine is connected to a computer equipped with software that allows for the loading rate and maximum applied load to be set electronically. The elastic strain was measured using an electronic strain gauge with 100 mm gauge length. The strain gauge was calibrated before taking the initial measurements for each specimen.

4.6.4.2 Specimen preparation

The elastic modulus was carried out on cylindrical specimens of size Ø100 × 200 mm as shown in **Figure 4.13**. Once the specimens were cured, the top surfaces of the cylinders were ground in order to achieve the necessary flatness requirements. A flat surface ensures a uniform stress distribution over the cross-sectional area of the specimens during testing. Two pairs of strain targets were attached on opposite ends of the vertical side of the specimens. The targets were placed approximately 100 mm apart, equidistant from the two ends of the specimen. The strain targets allow for the measurement of the elastic strain due to the imposed load.

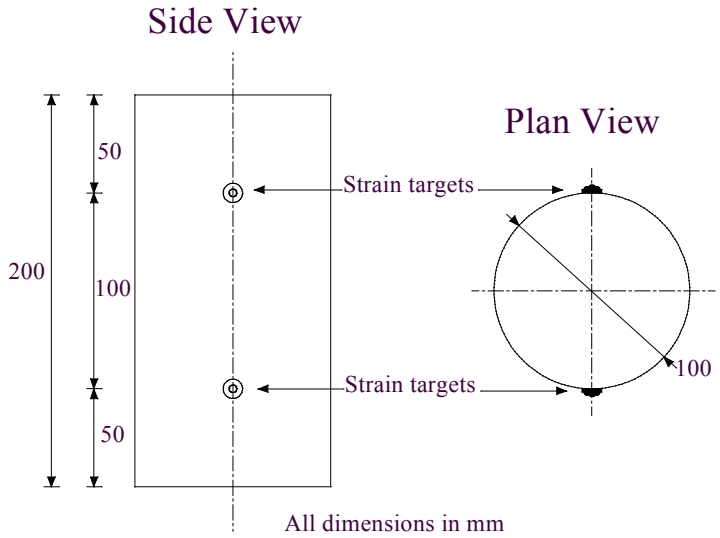

Figure 4.13: Elastic modulus specimen geometry

4.6.4.3 Test procedure

The elastic modulus test was carried out by first determining the compressive strength of the specimens. The compressive strength of the cylinders was estimated using the compressive strength of the companion cubes cast from the same batch. Prior to loading, the initial strain readings were taken. The specimens were then loaded to the basic stress and the strain readings recorded. The load was increased to 30% of their compressive strength at a loading rate of 0.1mm/min. Once the maximum load was achieved, the strain readings were measured as shown in **Figure 4.15**. For each specimen, an average secant modulus was calculated from the two pairs of strain targets. The static elastic modulus for each mix was then calculated from the average secant modulus of each specimen. The elastic modulus was tested at 7 and 28 days. Three specimens were tested for each mix and each age of testing, and the mean value was used in the analysis.

Figure 4.14: 100 kN Zwick Roell UTM used for elastic modulus testing.

Figure 4.15: Measurement of strain using digital strain gauge.

4.6.5 Free shrinkage strains

4.6.5.1 Apparatus

A Demec strain gauge with a measuring accuracy of 10 micro-strains was used to measure the linear strain. The strain gauge was calibrated against a reference bar before readings were taken. The specimens were marked to identify each end so as to ensure the same orientation was maintained throughout the measuring process.

4.6.5.2 Specimen preparation

Free shrinkage strain measurements were carried on the longitudinal edge of prismatic specimens with dimensions 300 × 50 × 50 mm as shown in **Figure 4.16**. After de-moulding, two pairs of strain targets were attached on opposite faces of the specimens. The targets were placed 100 mm apart, equidistant from the end of the specimen. The specimens were then cured as described in Section 4.5.1. Once cured, the specimens were exposed to the environmental conditions described in Section 4.5.3 and placed next to their respective ring specimens to ensure similar exposure.

The free-shrinkage specimens were left completely unsealed. Beushausen & Alexander (2006), emphasise that the boundary conditions experienced in the actual overlay are best represented by completely unsealed specimens. This is because the overlay loses moisture not only to the environment through the exposed surfaces, but also to the substrate. The substrate is relatively dry and as a result absorbs water from the overlay. Asad et al (1997) carried out free-shrinkage tests where drying was only allowed from the top surface of the specimen by sealing all of the other faces. However, this disregards the effects of moisture loss to the substrate and may therefore have underestimated the shrinkage strains.

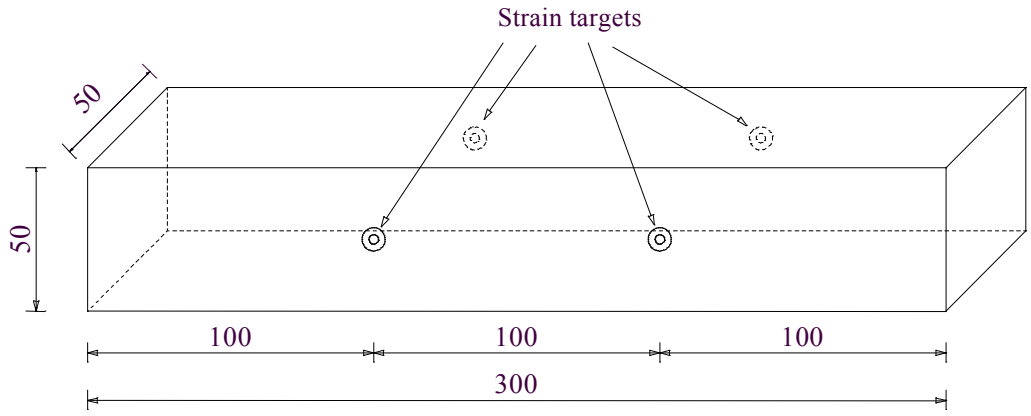

Figure 4.16: Free shrinkage strain specimen geometry.

4.6.5.3 Test procedure

Initial strain readings were taken immediately after curing. Thereafter, strain readings were taken daily for the period of 28 days (see **Figure 4.17**). Three specimens were cast for each mix and each specimen had two pairs of targets, therefore a total of 6 readings per mix were taken. The free-shrinkage strains of each mix and age of testing was calculated as the average of the readings taken from the 3 specimens.

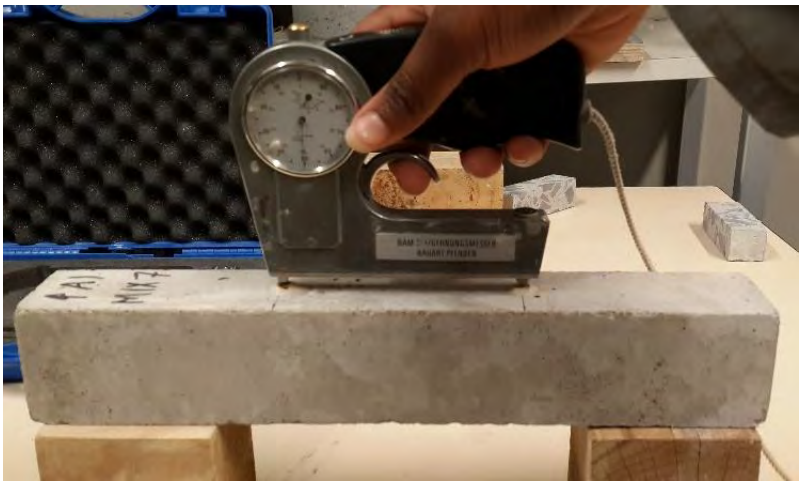

Figure 4.17: Measurement of free shrinkage strain using Demec strain gun

4.6.6 Ring test

The ring test is a method used for the determination of the age at cracking of mortar or concrete specimens under restrained shrinkage. The test is intended for relative comparison of materials and not to determine the actual age at cracking of mortar or concrete in any particular structure. The actual cracking tendency in service is dependent on various factors such as the degree of restraint, curing methods, and environmental conditions. The test method is therefore only useful for predicting the likelihood of cracking of different cementitious mixtures to aid the selection of materials less likely to crack under restrained shrinkage. The test determines the relative effects of material variations on cracking potential. Material variations include cement

type, cement content, water content and supplementary cementing materials (ASTM C1581-09a, 2009), making the test relevant for this particular research. The ring test also has the advantage of a well-defined and identical restraint as opposed to composite overlay-substrate specimens (Cärlsward, 2006). This was considered useful for this research, as it was best to keep variables such as the degree of restraint consistent to obtain meaningful comparisons.

4.6.6.1 Apparatus

The ring test comprised of a restraining steel ring with wall thickness t_{IS} of 12.7 mm and outer diameter D_o of 323.8 mm. The base is made of a 450 × 450 mm plywood board coated with a non-absorptive and non-reactive substance to prevent loss of moisture from the freshly cast concrete into the base. The outer steel ring has wall thickness t_{OS} of 3 mm, an inside diameter D_i of 400 mm, and a height h of 155 mm. The cross-section and plan view of the dimensions of the ring are shown in **Figure 4.18**.

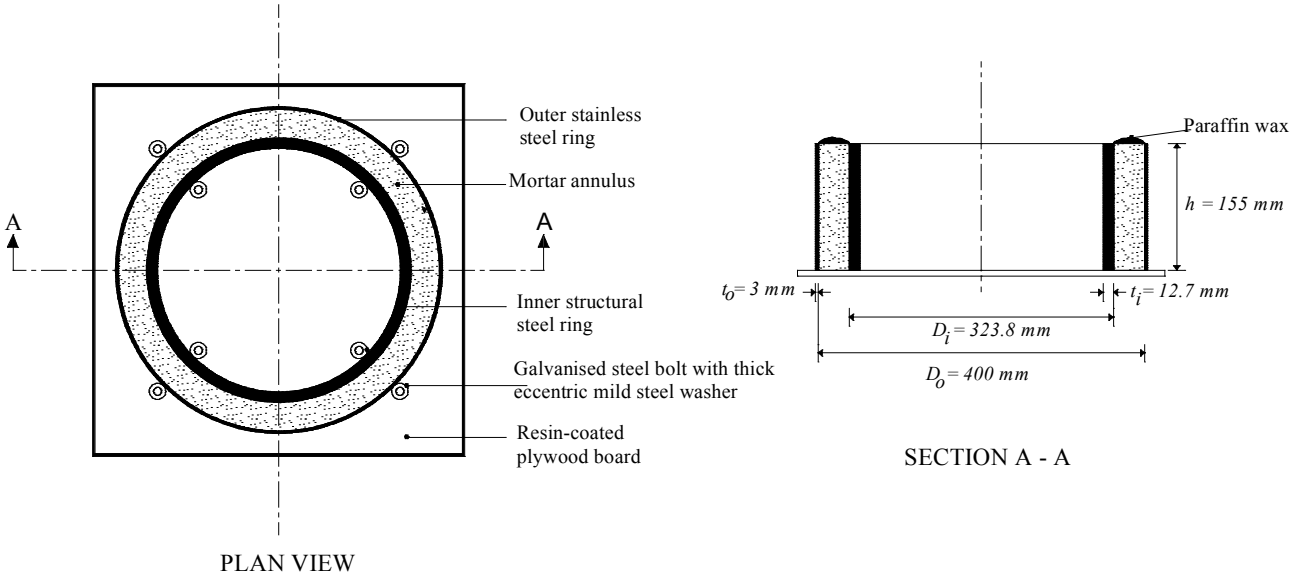

Figure 4.18: Schematic of ring test set-up

4.6.6.2 Specimen preparation

Two rings were prepared and monitored simultaneously for each batch of concrete. The ring moulds were coated with a thin layer of oil to allow for easy removal when de-moulding the specimens. Once assembled, the ring moulds were sealed with a silicone gel to prevent the leakage of the fresh concrete through the contact surfaces of the outer steel ring and base. The silicon was allowed to set for approximately 24 hours. **Figure 4.19** shows the assembled ring mould before casting. The respective mortar mix was then cast and placed in the ring mould. The moulds were filled with the mortar mixture in two approximately equal layers. The layers were each compacted with a tamping rod then vibrated on a vibrating table. A steel trowel was struck on the surface of the compacted mortar to achieve a smooth finish. After approximately 24 hours from the time of casting, the outer ring of the mould was removed. The specimens were then transferred to an environmentally controlled room (23 ± 2°C and 50 ± 4% relative humidity) within a 10 minute window. The specimens were subjected to moist curing for 7 days as described in Section 4.5.1.2. After curing, the top surface of the specimens was coated

with paraffin wax to prevent moisture loss. This was done to ensure that specimens only experienced circumferential drying.

Figure 4.19: Preparation of ring mould.

4.6.6.3 Cracking monitoring

The test specimens were monitored twice daily for the appearance of cracks until cracking occurred. This was done once in the morning and once in the evening using a handheld magnifying glass. The rings were not equipped with electrical strain gauges to monitor the strain development and age at cracking as prescribed in ASTM C1581-09a (2009). As such, the age at cracking was recorded to the nearest day. Once cracking had occurred, the age at cracking was recorded.

After the appearance of the cracks, the average crack widths were monitored for two weeks. The crack widths were measured using a handheld microscope with 4 mm gauge length and 0.02 mm accuracy. The crack width was determined by taking the average crack widths of the top, middle and bottom sections of the crack as shown in **Figure 4.20**.

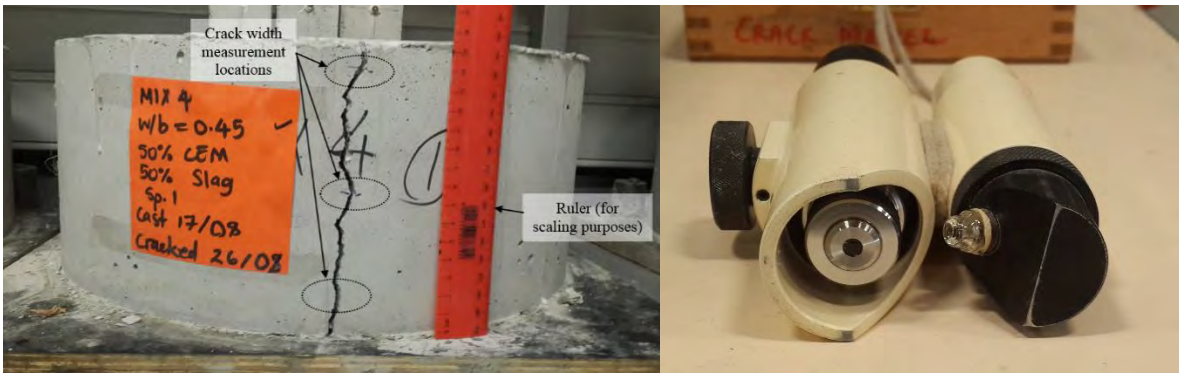

Figure 4.20: Ring specimen showing crack width measurement and hand microscope.

The crack lengths were determined by the taking a picture of the crack with a ruler placed next to it for scaling purposes. The picture was then imported into a CAD and Detailing programme (Prokon Padds) and the crack manually traced and measured. A screenshot of the length measuring technique is shown in **Table 4.3**.

Table 4.3: Crack measurement using Prokon Padds.

Insert image A photograph of the cracked ring specimen was taken and imported into Padds as a raster image.	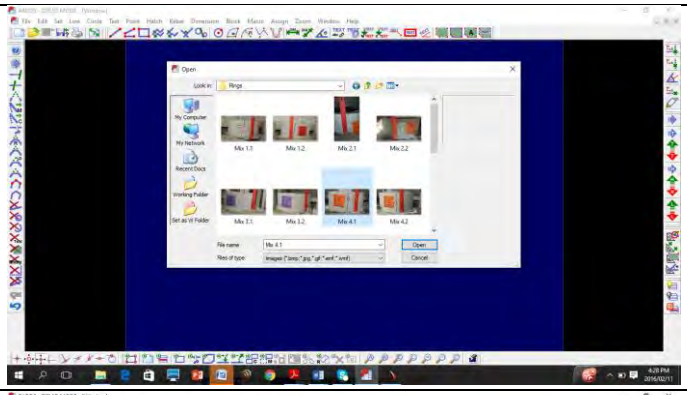
Manually trace crack The crack was then manually traced using a sketching tool.	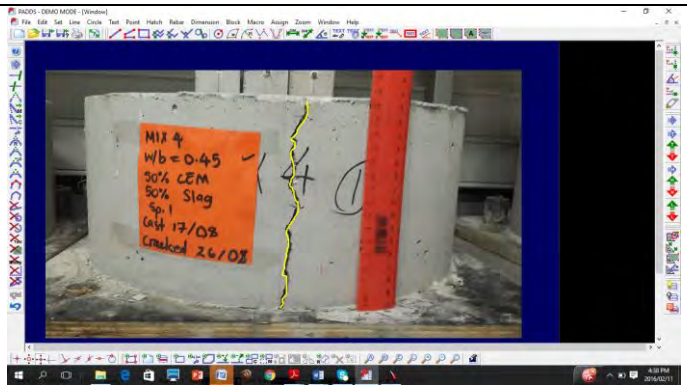
Measure crack length The length of the traced crack could then be determined by simply using a measuring tool that provided information on the full length of the segment. This was recorded as the measured length of crack, L_{mc}	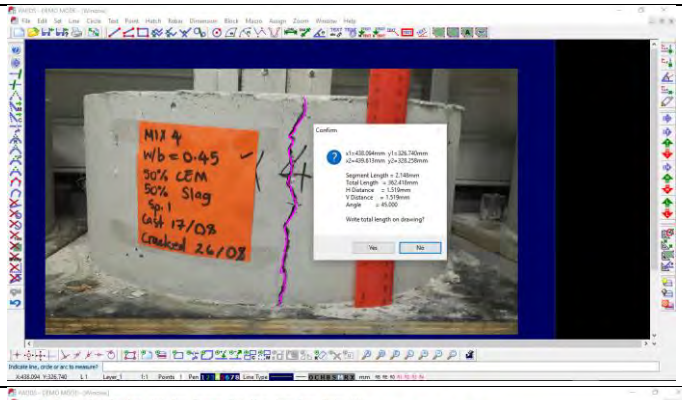
Measure length of ruler A ruler was placed next to the ring specimens to act as a reference for determining the scale. The length of the ruler between two known points (actual length of the ruler, L_{ruler}) was measured using the measuring tool. This was recorded as the mesured length of ruler, L_{mr}	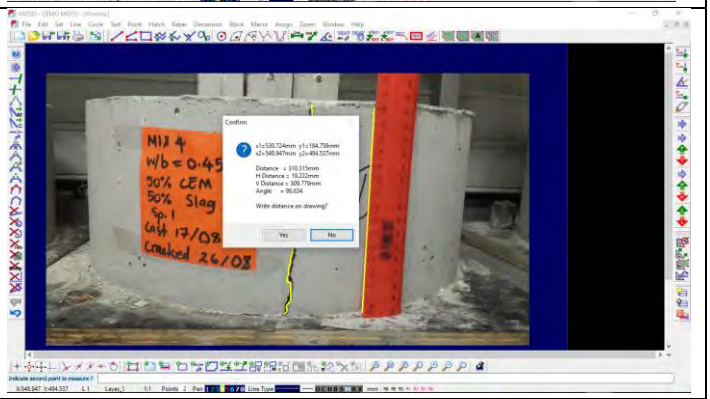
Calculate crack length Simple direct proportion was used to calculate the actual length of the crack as shown in the equation.	Mesured length of ruler, L_{mr}; Actual lengthof ruler, L_{ruler}; Measured length of crack, L_{mc}; Actual length of crack, L_{crack} $$L_{crack} = \frac{L_{mc} \times L_{ruler}}{L_{mr}}$$

This method was preferred over the simplistic method of placing a string between the cracks and measuring the length of string. This was mainly because some of the specimens only exhibited hairline cracks that would be difficult to measure using the string method. The crack area was then calculated using the measured width and length. The average crack area for each mix was determined as the average crack area of the two respective ring specimens.

4.7 Data analysis

Statistical methods were used to analyse the data to ensure results and conclusions were objective rather than judgemental in nature. Statistical methods do not allow anything to be proved experimentally, but allowed for the measurement of the likely error in the conclusions and attached a level of confidence to any statements made (Montgomery, 2013).

The results obtained from the above mentioned experimental investigation are detailed in Appendix A. The following methods were used to analyse the data collected:

- Detection of outliers. Due to the possibility of scatter in some of the results, it is imperative that outliers be detected. This was done using the inter-quartile range method as it is simplistic and can easily be used repetitively.
- Descriptive analysis. Preliminary answers to the research objectives are presented in the form of tables or graphs in Chapter 4.
- Regression analysis. The material parameters that were obtained experimentally were used for analytical modelling. Since these parameters were tested at specific ages only, regression functions were needed for the interpolation of values for the days when the properties were not measured.
- Analytical modelling to predict the age at cracking of the concrete. This is explained in detail in Section 4.8.
- Presentation of calculated error according to the standard deviation. The error was represented in the form of error bars.

4.8 Analytical modelling

The numerical model described in Chapter 3 was used to carry out analytical modelling to predict the age at cracking for the various mixes. Unlike the modelling approach used in Chapter 3, the inputs required for the analytical modelling were provided by the experimental component of the investigation. This modelling approach has been used in previous studies and has been found to yield reasonably accurate results (Chilwesa, 2012; Dittmer, 2013; Bester, 2015). The general numerical model and assumptions made to implement the model are provided in Section 3.2.1. The following sections discuss additional assumptions that pertain to the analytical modelling of the measured properties that were not applicable to the previous modelling approach discussed in Chapter 3.

4.8.1 Modelling assumptions

4.8.1.1 No shrinkage during curing

During curing, it assumed that no drying or autogenous shrinkage occurs. Effective curing is known to mitigate and delay drying shrinkage by preventing loss of moisture from the concrete to the environment. Although autogenous shrinkage is independent of the environmental

conditions and could still occur during the curing process, Alexander & Beushausen (2009) explained that at w/b ratios higher than 0.4, autogenous shrinkage is negligible. This simplifying assumption was applied by Chilwesa (2012) and was also considered in the current analytical modelling.

4.8.1.2 Small changes in material properties and cracking between data points

The material property tests (tensile strength, tensile relaxation, and elastic modulus) were only carried out 7 and 28 days. It could be argue that two data points are insufficient for curve fitting with regression functions (see Section 4.8.1.3). However, Bester (2015) argued that two data points (also 7 and 28 days) were sufficient for the analysis since cracking was expected to occur between these two measured data points. In addition, the change in material properties between these two measured points can be expected to be relatively small. The same argument was used in this research, and two data points were considered to be sufficient for the purpose of a simple analytical model. Dittmer (2013) also carried out similar analytical modelling with two data points at 7 and 28 days. In both cases, the age at cracking results obtained were fairly accurate.

4.8.1.3 Natural logarithmic functions

As previously mentioned, the data from the experimental investigation was the source of inputs for the analytical model. Since the tensile strength, tensile relaxation, and elastic modulus were only tested at 7 and 28 days, it was necessary to interpolate the values of these material properties at ages when test were not carried out. This was done using regression functions. An extensive literature survey carried out by Chilwesa (2012) showed that although several regression functions have been developed to model material property trends, logarithmic functions showed the best fit with experimental data. Based on this, logarithmic regression functions were also used in this investigation. The regression function used to analytically model the material properties were thus of the form:

$$f_{t,i}(t_i) = A \cdot \ln(t_i) + B$$
$$\psi_i(t_i) = C \cdot \ln(t_i) + D$$
$$\mathrm{E}_i(t_i) = E \cdot \ln(t_i) + F$$
$$\varepsilon_{FSS,i}(t_i) = \mathrm{G} \cdot \ln(\mathrm{t}_i) + H$$

Where $f_{t,i}(t_i)$ is the tensile strength at t_i; ψi(ti) is the mean tensile relaxation factor in the interval from $t_{1\text{-}i}$ to t_i; $E_i(t_i)$ is the mean elastic modulus in the interval from $t_{1\text{-}i}$ to t_i; $\varepsilon_{FSS,i}(t_i)$ is the mean free shrinkage strain in the interval from $t_{1\text{-}i}$ to t_i; and *A, B, C, D, E, F*, and *G*, are regression function constants.

Similar to Bester (2015), it was opted to use regression functions to the model the free shrinkage although free shrinkage strains were measured daily. This allowed for consistency and smooth stress development curves. Examples of the regression curves for mix F45_30 are shown in **Figure 4.21** – Typical shrinkage strain regression curve (obtained from mix F45_30).**Figure 4.24**. The regression constants for all the mixes are provided in Table B.1 of Appendix B.

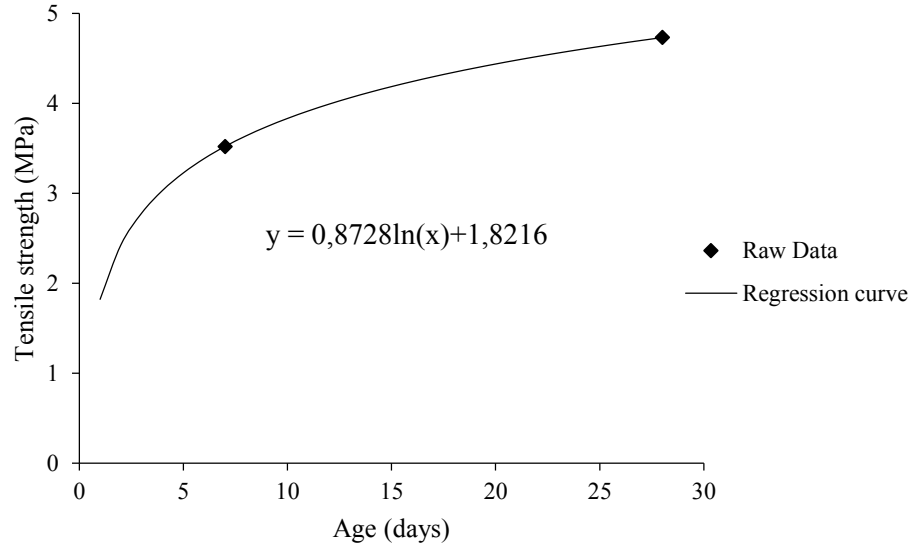

Figure 4.21: Typical tensile strength regression curve (obtained from mix F45_30).

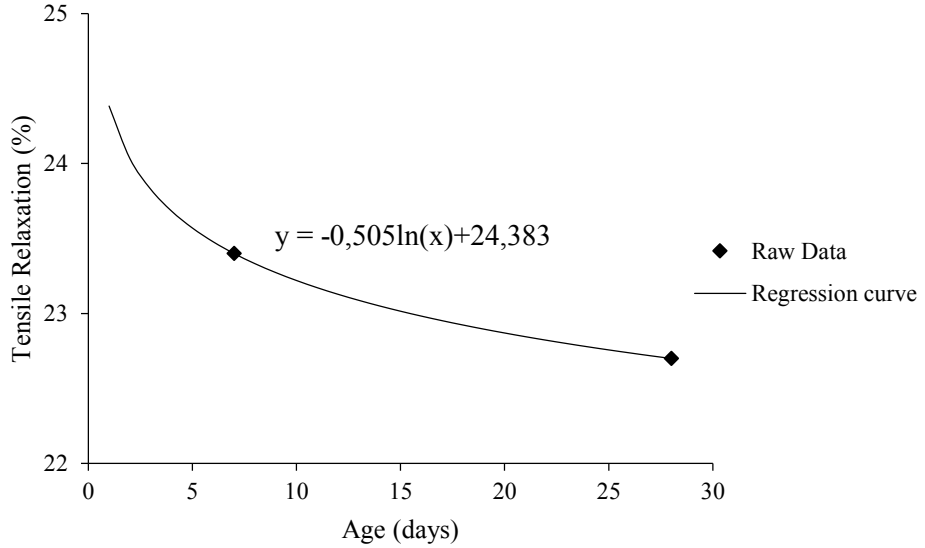

Figure 4.22: Typical tensile relaxation regression curve (obtained from mix F45_30).

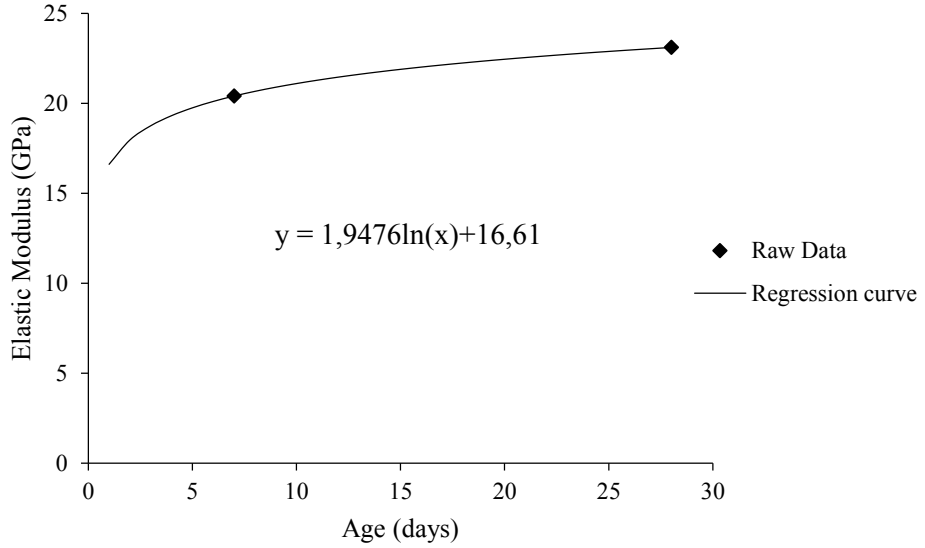

Figure 4.23: Typical elastic modulus regression curve (obtained from mix F45_30).

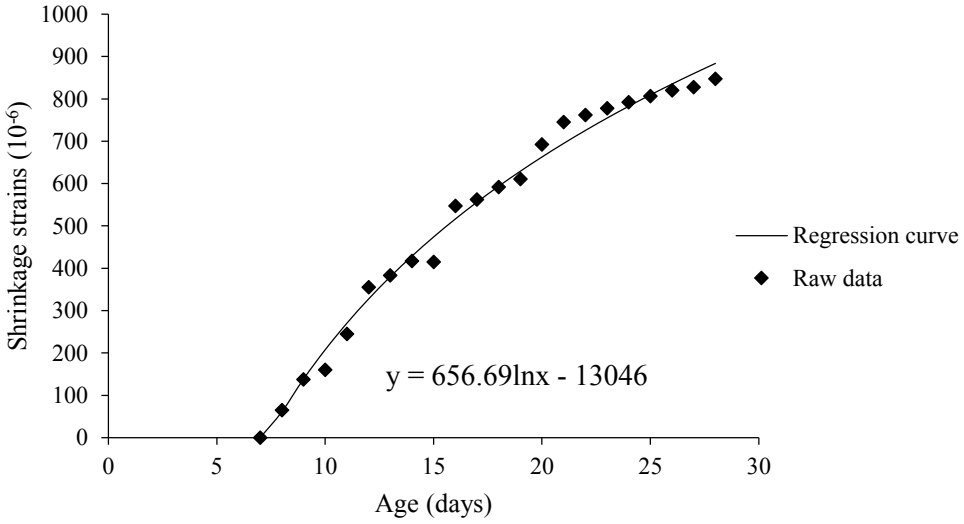

Figure 4.24: Typical shrinkage strain regression curve (obtained from mix F45_30).

4.9 Conclusion

The sections above provide information on the thought process behind the experimental investigation, the materials used, and the experimental tests carried out. A summary of the programme is given in the following paragraphs.

Four design variables were selected for this research: binder type, water-binder ratio, percentage replacement of cement, and curing duration. These design variables were considered for the measurement of the selected response parameters: compressive and tensile strength, tensile relaxation, free shrinkage strains, elastic modulus, age at cracking, and crack

characteristics. The method of curing and the environmental conditions were set as fixed factors.

Ten different laboratory-made mortar mixes were considered for experimentation. These mixes were composed of cement mixes blended with FA or GGBS. Two water-binder ratios of 0.45 and 0.65 were used, by means of fixed water content. One curing method (saturated hessian sheets) was used for all the mixes and only a minor component of the research focused on the effects of curing duration on the blended cement mixes.

Experimental test were conducted to determine the influence of FA and GGBS on the material properties that govern the performance of bonded concrete overlays subjected to restrained shrinkage cracking. These tests included tensile strength, tensile relaxation, elastic modulus, and free shrinkage tests. The experimental tests also included restrained shrinkage tests in the form of ring tests. From these tests, analytical modelling was carried out in order to determine the age at cracking. The results from these experiments are presented and discussed in Chapter 5.

CHAPTER FIVE

5 Results and discussion

5.1 Introduction

This chapter presents and discusses the results obtained from the experimental investigation documented in Chapter 4. To assess the susceptibility to cracking of materials used in BCOs, material property tests and restrained shrinkage tests were carried out. The compressive strength, tensile strength, tensile relaxation, elastic modulus, and free shrinkage results obtained from the material property tests are provided in Sections 5.2 to 5.6 respectively. The results from restrained shrinkage testing (ring tests) are provided in Section 5.7. Detailed results of these tests are provided in Appendix A. Analytical modelling is provided in Section 5.8 and comparisons of the age at cracking obtained from the analytical modelling and ring tests are provided in Section 5.9. Detailed results from the analytical modelling are provided in Appendix B. Conclusions and recommendations following the results detailed in this chapter are presented in Chapter 6. The notations given in **Table 5.1** were used throughout this chapter to distinguish the various mixes.

Table 5.1: Mix notation used in the results presented

Notation	Binder content	w/b ratio
C45	100% Portland cement	0,45
F45_30	30% Fly Ash	
F45_50	50% Fly Ash	
S45_50	50% Slag	
S45_70	70% Slag	
C65	100% Portland cement	0,65
F65_30	30% Fly Ash	
F65_50	50% Fly Ash	
S65_50	50% Slag	
S65_70	70% Slag	

Notation	Binder content
PC	100% Portland cement
F30	30% Fly Ash
F50	50% Fly Ash
S50	50% Slag
S70	70% Slag

5.2 Strength and strength development

5.2.1 Compressive strength

When it comes to restrained shrinkage cracking, compressive strength of the repair material becomes less important. The tensile strength is of more importance as discussed in Section 2.4.3. As such, the compressive strength tests were of little significance in the analysis of stresses. The tests were only carried out to determine the strength development for the purpose of material characterisation as well as for the determination of the load used in the testing of elastic modulus in compression. Compressive strength tests were carried out as detailed in Section 4.6.1 on 100 mm cube specimens at the age of 2, 7, 14 and 28 days. The 28-day strength development of the various mixes are shown in **Figure 5.1** and **Figure 5.2** for water-binder

ratios 0.45 and 0.65 respectively. The detailed compressive strength results are provided in Appendix A.1.

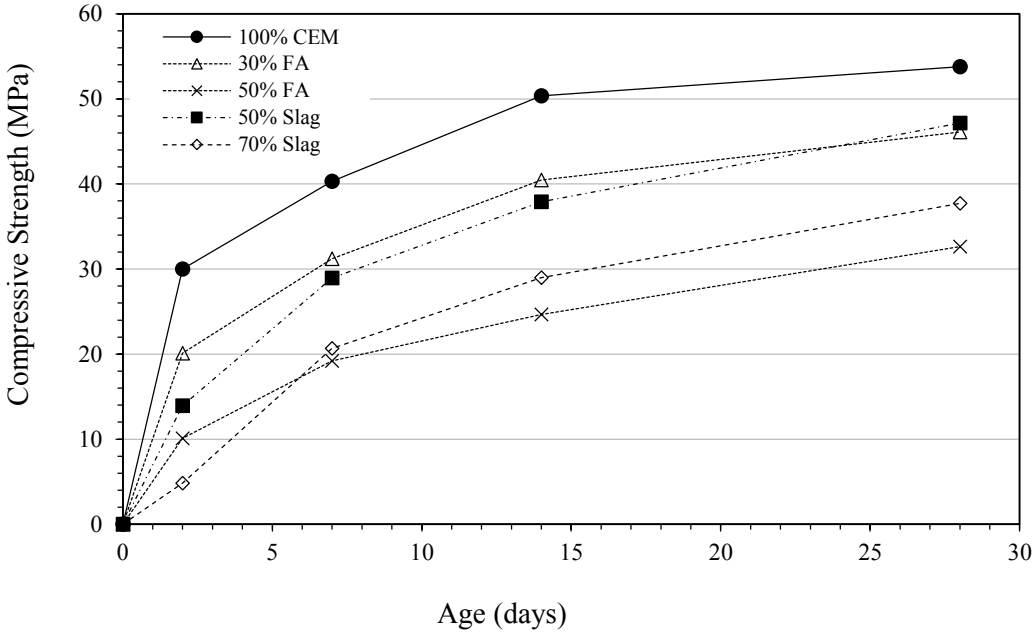

Figure 5.1: Compressive strength development of mortar mixes with w/b 0.45

Comparing the compressive strength development of the various mixes for w/b 0.45, it is evident that replacement of cement with FA or GGBS leads to decreased strength development, more significantly at early ages. This in agreement with the lower heat development and longer setting times associated with the use of FA and GGBS. The initial hydration reactions of cements blended with FA or GGBS are much slower compared with plain PC. As a result, the rate of strength development is retarded at early ages, with higher replacement levels resulting in lower strengths. At 2 days, the replacement of Portland cement with 30% and 50% FA resulted in 33% and 66% reduction in compressive strength as compared to the plain Portland cement mix. For the slag mixes at 2 days, substituting Portland cement with 50% and 70% slag resulted in 54% and 84% reductions in compressive strength respectively.

At 70% slag replacement level, the early-age strength was much lower in comparison to the other mixes. This can be explained as the result of reduced pH in the pore solution (Lothenbach, et al., 2011). The concentration of calcium hydroxide to drive the slag reaction is much lower, since the amount of PC present is only 30% that of the reference mix. This explains the strength decrease at early ages with increase in replacement level as the rate of calcium hydroxide generation is delayed. Though at 2 days the slag mixes exhibited lower compressive strengths, by 28 days their strengths were equivalent to or higher than the fly ash mixes. The compressive strength of the 50% slag mix (47.2 MPa) slightly exceeded that of the 30% fly ash mix (46.1 MPa), and the compressive strength of the 70% slag mix (37.7 MPa) exceeded that of the 50% fly ash mix. This result is due to the difference in reactivity between FA and GGBS. Fly ash and slag require different replacement levels in order to attain equivalent strengths. This is expected because FA is not a hydraulic binder like GGBS, it does not hydrate to produce cementitious material in itself, and thus more GGBS can be used than

fly ash because of its cementitious character. High replacement of fly ash results in excess fly ash that ends up as unreactive dilutant (Young, et al., 1998). This might explain why the 50% fly ash mixes exhibited the lowest compressive strength development of all the mixes.

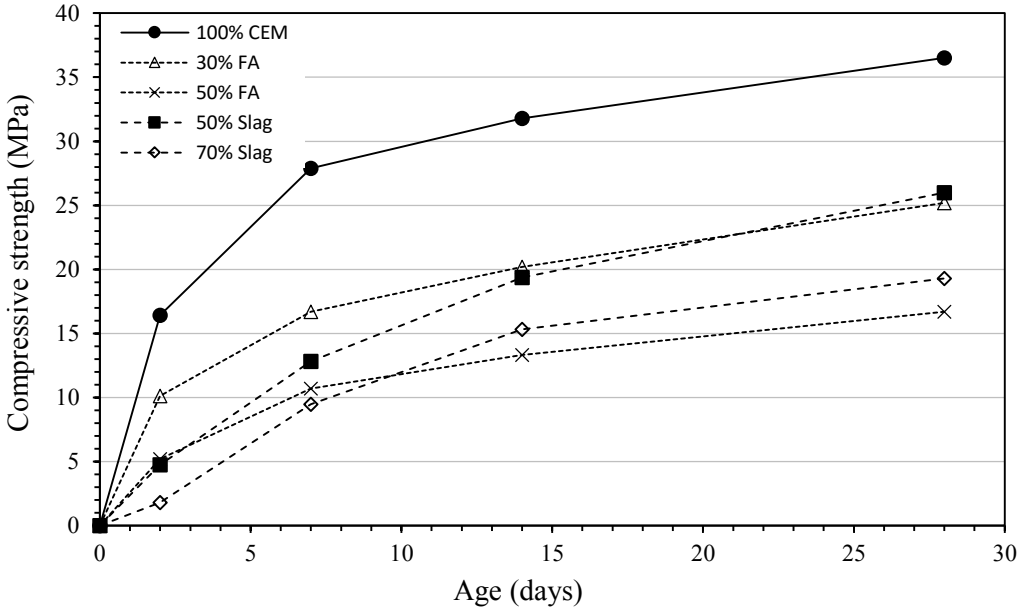

Figure 5.2: 28-day compressive strength development of overlay mixes with w/b = 0.65.

Similar trends were observed on specimens with w/b ratio 0.65. The replacement of PC with FA or GGBS led to an even more significant decrease in strength development.

The time-dependent change in the relationship between compressive strength of the FA or GGBS concrete ($f_{c,FA}$ or $f_{c,GGBS}$ respectively) and the plain PC concrete ($f_{c,PC}$) is further highlighted in **Figure 5.3** and **Figure 5.4**. The figures illustrate how the difference in strength between the blended concretes and the reference concretes reduce with time. The slag concretes show lower strength ratios than the fly ash concrete at early ages. However, the strength ratio of the slag concrete is seen to increase more rapidly than the fly ash concrete. This emphasises the theory that the two cement extenders have different reactivity. It was also noted that specimens with the same water-binder ratio and the same binder type had similar strength ratio developments. For example S45_50 and S45_70 had similar strength development curves, while S65_50 and S65_70 also had similar strength development curves. This was also true for fly ash specimens. The figures also clearly illustrate the decrease in compressive strength with an increase in water-binder ratio, as expected. The water-binder ratio is a key factor controlling the porosity of hardened cement paste. The porosity controls the strength and permeability of the hardened paste. Lower water-binder ratios lead to lower porosity and consequently higher compressive strengths.

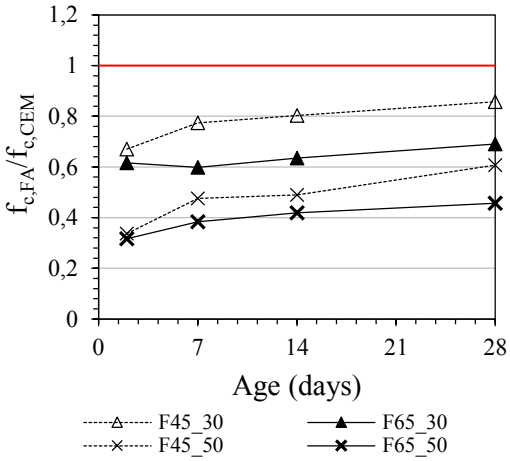

Figure 5.3: Development of the ratio between fly ash concrete compressive strength and reference concrete compressive strength (w/b 0.45 & 0.65).

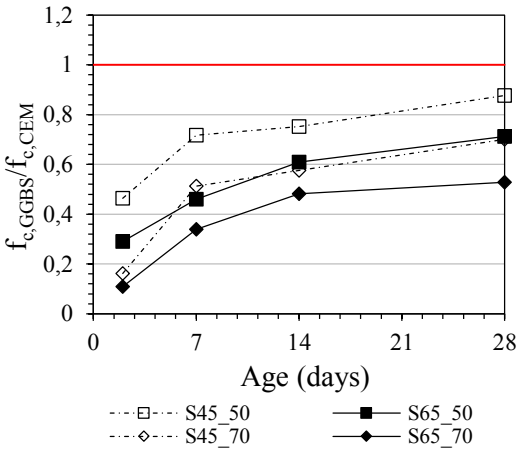

Figure 5.4: Development of the ratio between slag concrete compressive strength and reference concrete compressive strength (w/b 0.45 & 0.65).

5.2.2 Tensile strength

Tensile strength is a key material property to consider when determining the likelihood of restrained shrinkage cracking. If the shrinkage-induced tensile stresses exceed the tensile strength of the material, then cracking will occur. Tensile strength of concrete is considerably lower than its compressive strength. However, there is no simple relationship between compressive and tensile strength. This is because factors such as water-binder ratio, age, and mix proportions do not affect the compressive and tensile strength to the same extent (Perrie, 2009). Nonetheless, the 28-day tensile strength to compressive strength ratio (f_t/f_c) was seen to increase with increasing water-binder ratio as well as increasing replacement level as illustrated in **Figure 5.5**. This supports the theory that in general, the tensile/compressive strength ratio depends on the level of compressive strength. The higher the compressive strength, the lower the ratio. (Perrie, 2009).

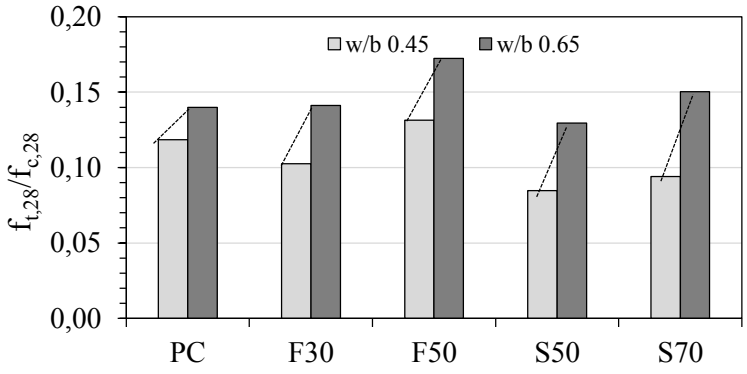

Figure 5.5: Ratio of tensile strength to compressive strength at 28 days for all mixes.

Uniaxial tensile strength tests were carried out as detailed in Section 4.6.2 on dog-bone specimens at ages 7 and 28 days. The results obtained from the tests are presented in **Figure 5.6** for both w/b ratio 0.45 and 0.65. The detailed tensile strength results are provided in Appendix A.2.

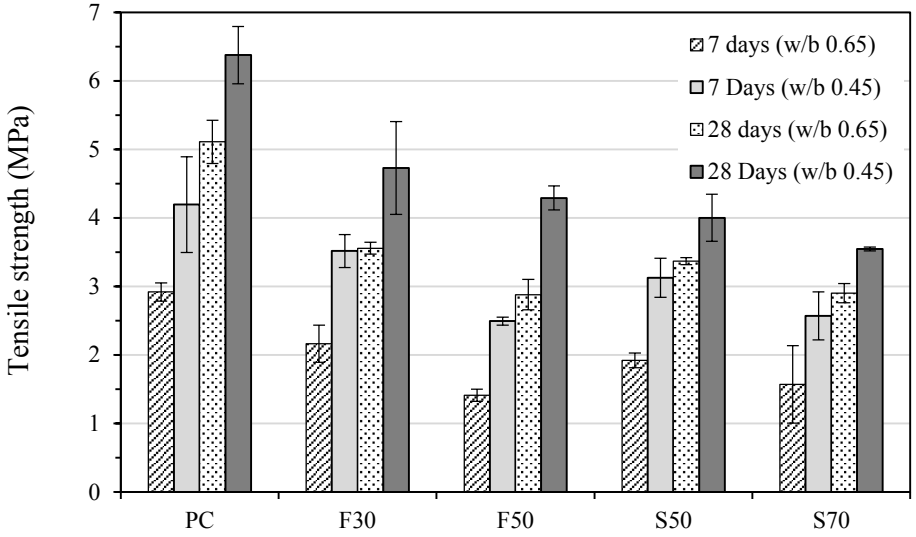

Figure 5.6: 7- and 28-day direct tensile strength results.

In general, the tensile strength increased with increase in age from 7 days to 28 days for all specimens. The specimens achieved on average 70% and 55% of their 28-day strength within the first 7 days for water binder ratios 0.45 and 0.65 respectively. As expected, the water-binder ratio had a significant effect on the tensile strength. The w/b ratio is a key factor controlling the porosity of hardened cement paste. The porosity controls the strength and permeability of the hardened paste. Lower water-binder ratios lead to lower porosity and consequently higher tensile strengths.

Comparing the tensile strength results of the various mixes, it is evident that replacement of cement with FA or GGBS leads to decreased strength development, more significantly at early ages. This is in agreement with the lower heat development and longer setting times associated with the use of FA and GGBS. The initial hydration reactions of cements blended with FA or GGBS are much slower compared with plain PC. As a result, the rate of strength development is retarded at early ages, with higher replacement levels resulting in lower strengths. As such, the 50% fly ash and the 70% slag specimens had the lowest tensile strengths, only achieving approximately 60% of the reference specimens' 28-day tensile strength.

Comment: On investigating the variability in the 7-day tensile strength of S70 w/b 0.65, it was observed that the average tensile strength was not much more than the difference between the maximum and the minimum values used to calculate the average. It was decided that the maximum value of tensile strength (1.57 MPa) was more representative than the average value (1.17MPa). Fortunately, the change in value of the tensile strength had little to no impact on the outcome of the analytical modelling discussed in Section 5.8.

5.3 Tensile relaxation

Tensile relaxation is of great importance when considering the development of tensile stresses in bonded overlays. It is considered one of most important factors for stress development in overlays subjected to restrained shrinkage (Beushausen & Alexander, 2006). The mechanism of tensile relaxation provides a relief in tensile stress, prolonging or even preventing the onset

of restrained shrinkage cracking (see Section 2.4.5). Tensile relaxation tests were carried out as detailed in Section 4.6.3 on dog-bone specimens at ages 7 and 28 days. The results obtained from the tests are presented in **Figure 5.7** for both w/b ratio 0.45 and 0.65. The detailed tensile relaxation results are provided in Appendix A.3.

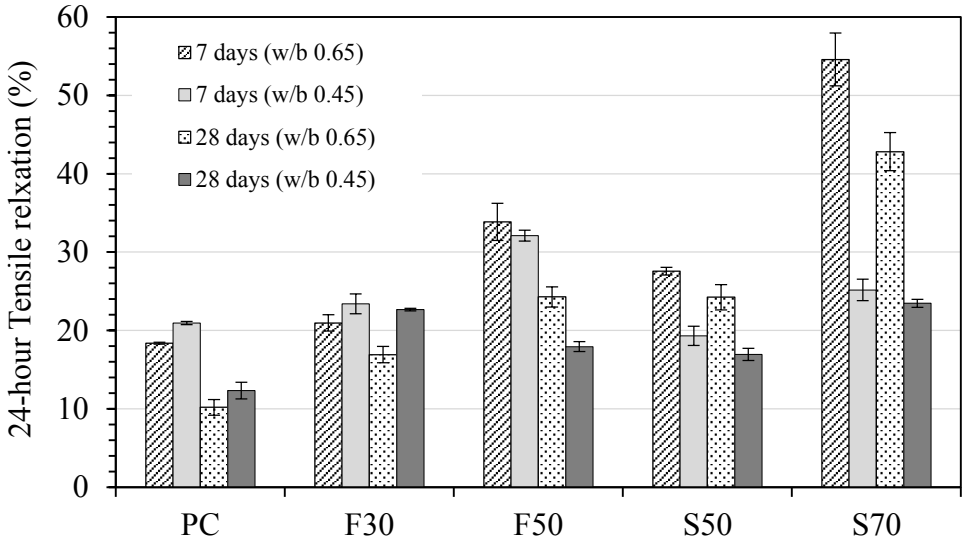

Figure 5.7: 7- and 28-day tensile relaxation results.

The results presented show general increase in tensile relaxation with increasing FA or GGBS content. This is in agreement with research carried out by Pane & Hansen (2008), in which FA and GGBS were observed to significantly increase the tensile relaxation. The viscous-shear theory and microcracking theory were used to explain the observed trends. According to the viscous-shear theory, creep is driven by the sliding of C-S-H sheets between layers of adsorbed water (Bazant & Chern, 1985). The mechanisms of tensile relaxation are assumed to be similar to those of creep (Magera, 2013). Using this theory, at lower degree of hydration in the FA and GGBS specimens, it is hypothesised that the there was sufficient thickness of water layers between the C-S-H particles to allow for increased slippage of the particles. According to the microcracking theory, tensile relaxation is a caused by the formation of microcracks. As the solid particles migrate out of the loaded regions into more stable parts of the microstructure, the loading on them is relaxed (Bazant, 1982). Using this theory, it is suggested that the presence of increased number of flaws in the FA or GGBS concrete due to the large presence of unreacted particles, led to increased formation of microcracks. This may have consequently resulted in increased stress relaxation.

Tensile relaxation in the reference specimens resulted in 21% stress relaxation at 7 days. The replacement of Portland cement with FA resulted in 23% and 32% stress relaxation in the 30% and 50% fly ash specimens respectively. The effect of GGBS on tensile relaxation was slightly less prominent compared to the FA specimens. The replacement of Portland cement with GGBS resulted in 19% and 25% stress relaxation in the 50% and 70% slag specimens respectively. From these results it can be observed that at lower replacement levels, the tensile relaxation of the FA or GGBS specimens was almost equivalent to the reference

specimens, with GGBS specimens showing slightly lower relaxation (10% difference) at 50% replacement level.

The results also indicate that the specimens had higher relaxation capacity at early ages. This is supported by the literature as discussed in Section 2.4.7. At 28 days, the tensile relaxation capacity decreased in all specimens. At low w/b ratio, the reduction of tensile relaxation in the reference specimens (41% reduction) was more distinct than in FA and GGBS specimens. This was with the exception of the 50% fly ash specimens that displayed results inconsistent with the expected behaviour (46% reduction). The reduction in tensile relaxation from 7 to 28 days was 3%, 12%, and 7% for F45_30, S45_50, and S45_70 specimens respectively. From this it can be seen that there is little reduction in tensile relaxation capacity at 28 days for the FA and GGBS specimens. This may be related to the lower degree in hydration and corresponding higher porosity as compared to the reference specimens. Judging from the lower strength development of the FA and GGBS specimens at 28 days, it can be assumed that the there is still a significant amount of unreacted FA or GGBS particles. This affects the microstructure of the hardened cement paste in a fashion that is favourable for the mechanisms of tensile relaxation both from the viscous-shear, and micro-cracking perspective.

Similar results were observed in specimens with w/b ratio 0.65 as illustrated in **Figure 5.7**. The relaxation capacity increased with increasing FA or GGBS replacement level. It was noted however, that the tensile relaxation in the reference mix decreased with increase in w/b ratio. However, the tensile relaxation increased with increase in w/b ratio as was expected for all the other specimens. The tensile relaxation also increased with increasing replacement level for both fly ash and slag mixes. Comparing with the reference specimens, the tensile relaxation was 10%, 93%, 47%, and 209% higher for the F65_30, F65_50, S65_50, and S65_70 specimens respectively.

Comment: The discrepancy in the 7-day tensile strength of S70 w/b 0.65 was carried forward into the calculation of the load applied on the test specimens during the 24-hour relaxation test. Using the maximum tensile strength as the ultimate tensile strength, it was found that the actual stress level of the sample was less than the planned 80% of the tensile strength. This could explain the extremely high relaxation value at 7 days. However, looking at the 28-day relaxation value, it can be deduced that the 7-day relaxation value was still significantly high. After running a sensitivity analysis in which the 7-day relaxation value was varied in the range between the 7-day value and 28-day values recorded, it was found that the impact on the analytical modelling results was minimal and the same trends were still observed.

5.4 Elastic modulus

Elastic modulus is another key material property to consider with regards to restrained shrinkage cracking of bonded overlays. The elastic modulus is directly proportional to the built-up stresses owing to the increase in strain caused by the shrinkage of the overlay material. Elastic modulus tests were carried out on cylindrical specimens as described in Section 4.6.4 at ages 7 and 28 days. The results obtained from the tests are presented in **Figure 5.8** for both w/b ratio 0.45 and 0.65. The detailed elastic modulus results are provided in Appendix A.4.

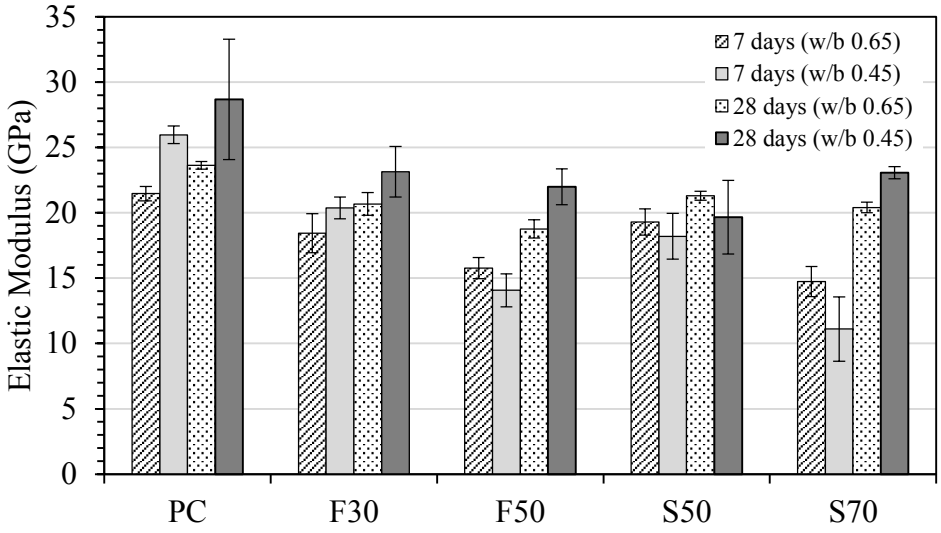

Figure 5.8: 7- and 28-day elastic modulus results.

A general decrease in elastic modulus was observed with the use of FA or GGBS as was expected. The elastic modulus of the hardened cement paste is directly linked to its porosity. The porosity of the hardened cement paste is in turn related to the degree of hydration. Therefore, the evolution of the elastic modulus is an increasing function of the degree of hydration (Sanahuja, et al., 2007). As the hydration reaction proceeds, the microstructure of the hardened cement paste becomes more refined, thereby decreasing the porosity and consequentially increasing the stiffness. This explains why the elastic modulus increases with age and can also be used to explain the effects seen in the FA and GGBS specimens. Partially replacing Portland cement with FA or GGBS delays the hydration reactions, and as such the cement paste is more porous and less stiff in comparison to the reference specimens. The same theory applies when explaining the results obtained when the water-binder ratio is increased. Since the elastic modulus of the hardened cement paste is determined by its porosity, then specimens with higher water-binder ratios would have lower elastic moduli due to the associated increase in porosity.

At the lower replacement levels of both FA and GGBS, the elastic modulus of the concrete did not show significant increases between 7 and 28 days for both w/b ratios. On average, the elastic modulus only increased by 13% and 9% in the FA and GGBS specimens respectively. In addition, increasing the percentage replacement level of both FA and GGBS by 20% did not drastically affect the 28-day elastic modulus. The difference in elastic modulus was 5 – 9% and 4 – 15% in the FA and GGBS specimens respectively.

5.5 Free shrinkage strain

Shrinkage generally leads to cracking which translates into durability issues. This is particularly true in the case of bonded concrete overlays in which the volume changes of the repair material are restrained both internally and externally (as discussed in Chapter 2). It was therefore important to investigate the influence of FA and GGBS on free shrinkage strains. Free shrinkage tests were carried out as described in Section 4.6.5 on prismatic specimens after 7 days of curing. The free shrinkage strains were assumed to be predominantly due to drying

shrinkage of the specimens, i.e. autogenous shrinkage was assumed to be negligible. The free shrinkage strains obtained from the experimental investigation are presented and discussed in this section. The 28-day free shrinkage strains for both w/b ratio mixes are presented in **Figure 5.9**. The free shrinkage strain results are also provided in Appendix A.5 and are illustrated with more clarity.

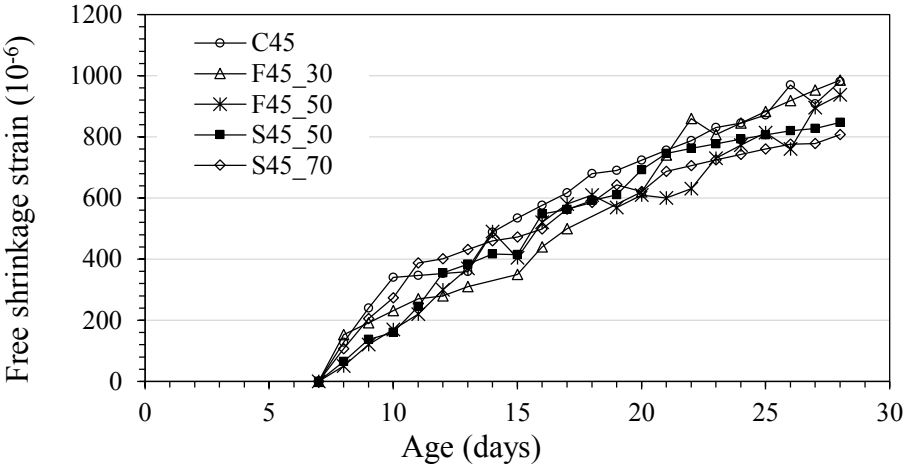

(a) 0.45 w/b ratio specimens

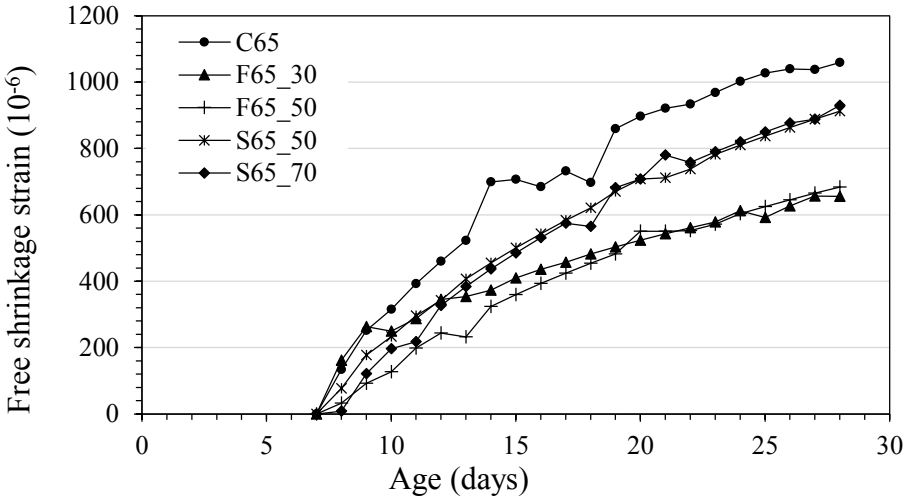

(a) 0.65 w/b ratio specimens

Figure 5.9: Free shrinkage results for all mixes

The results show that the partial replacement of Portland cement with FA or GGBS resulted in a decrease in the magnitude of free shrinkage strain. This observation was more obvious in the higher w/b ratio specimens. At w/b 0.65, the reference specimens exhibited higher shrinkage strains throughout the test duration, followed by the GGBS specimens. The FA specimens had the lowest shrinkage values. It should also be noted that there was very little change in shrinkage strain in the FA or GGBS specimens with increase in cement replacement level. **Figure 5.9(b)** shows three bands distinguishing the shrinkage strains of the different binder types. However, this was not observed in the lower w/b ratio specimens. The shrinkage strains of the lower w/b specimens were all more or less equivalent **Figure 5.9(a)**, with the reference

specimens showing slightly higher values. The free shrinkage results of the FA and GGBS specimens are discussed further in Sections 5.5.1 and 5.5.2 respectively.

5.5.1 Influence of FA on free shrinkage strains

The 28-day free shrinkage strains of the FA specimens are compared to that of the reference specimens. The results are presented in **Figure 5.10** and are discussed in this section.

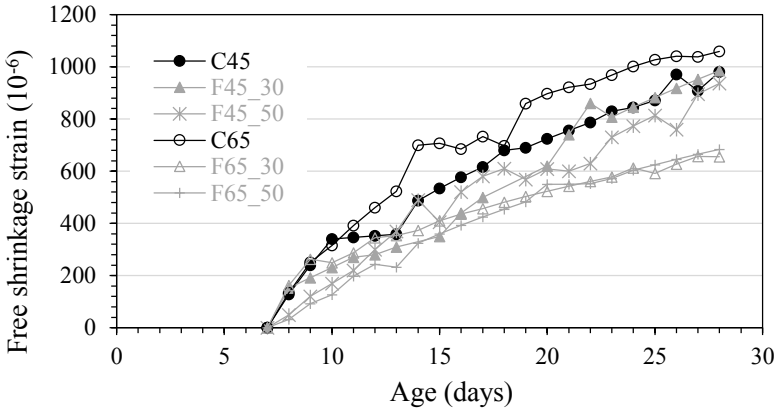

(a) Portland cement (comparison with GGBS mixes).

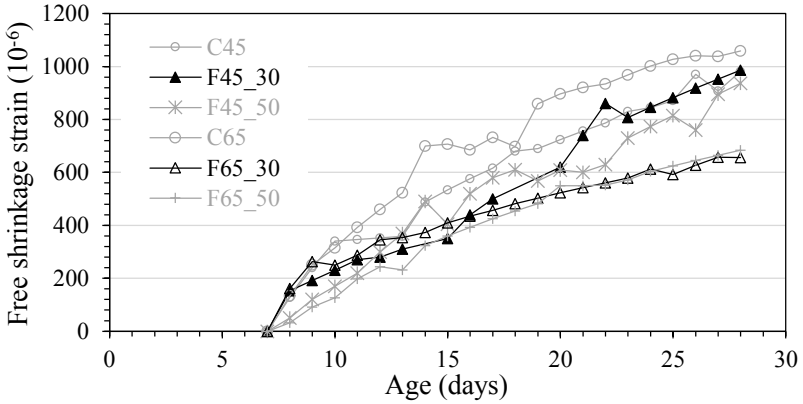

(b) 30% fly ash (w/b 0.45 & 0.65)

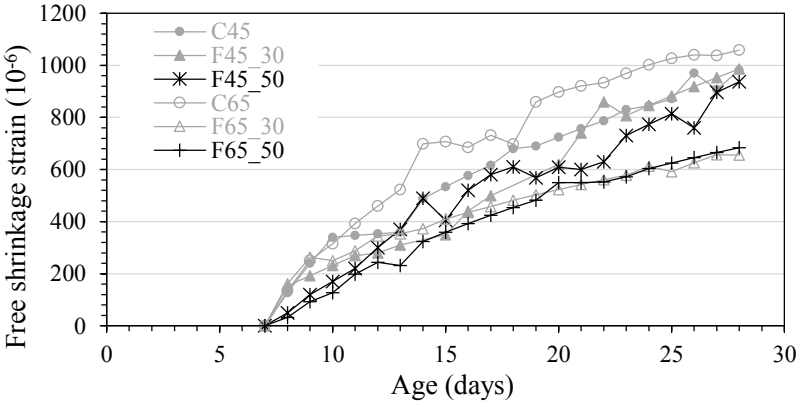

(c) 50% fly ash (w/b 0.45 & 0.65)

Figure 5.10: 28-Day free shrinkage strain development, from the completion of curing for the FA specimens.

The free shrinkage strains of the FA specimens were lower than the reference specimens at both w/b ratios (**Figure 5.10(a)**). At 30% replacement level, the shrinkage strains of the FA specimens were initially marginally higher in the 0.65 w/b ratio mix than at lower w/b ratio (**Figure 5.10(b)**). However, this effect was reversed at later ages and the 0.45 w/b ratio mixes exhibited significantly higher shrinkage strains. Similarly, at 50% replacement level, the shrinkage strains of the two w/b ratio specimens were almost equivalent at early ages. With time however, the 0.45 w/b ratio specimens exhibited noticeably higher shrinkage strains (**Figure 5.10(c)**). The similar shrinkage at early ages may be due to the initial loss of capillary water in both w/b ratio specimens. As explained by Alexander & Beushausen (2009), the loss of free water in the capillaries leads to smaller shrinkage strains than the loss of gel pore water. The low w/b ratio specimens had a greater gel volume owing to the increased paste content and this could explain the higher shrinkage strains at lower w/b ratio. So although the higher w/b ratio specimens had higher loss of free water (which causes smaller shrinkage strains), they also had a smaller loss of gel pore water (which causes larger shrinkage strains) resulting in less shrinkage overall. The low w/b ratio mixes had higher paste content (approximately 30% more cement paste) than the low w/b ratio mixes.

5.5.2 Influence of GGBS on free shrinkage strains

The 28-day free shrinkage strains of the GGBS specimens are compared to that of the reference specimens. The results are presented in **Figure 5.11** and are discussed in this section.

The free shrinkage strains in the GGBS specimens was lower than the reference specimens at both w/b ratios (**Figure 5.11(a)**). The reduction was more distinct at w/b 0.65. At 50% replacement level, the free shrinkage strains at both w/b ratios was very similar (**Figure 5.11(b)**). At 70% replacement level, the slightly higher shrinkage strains were observed in the lower w/b ratio specimens at early ages. This was however reversed at later ages and the 0.65 w/b ratio specimens showed higher shrinkage strains (**Figure 5.11(c)**). The observations in the GGBS specimens were unlike the trends seen in the FA specimens. The GGBS specimens comparatively showed similar shrinkage strains. The similar shrinkage strains in the GGBS specimens may have been as a result of the two influencing factors of increased free water and decreased paste content cancelling each other out.

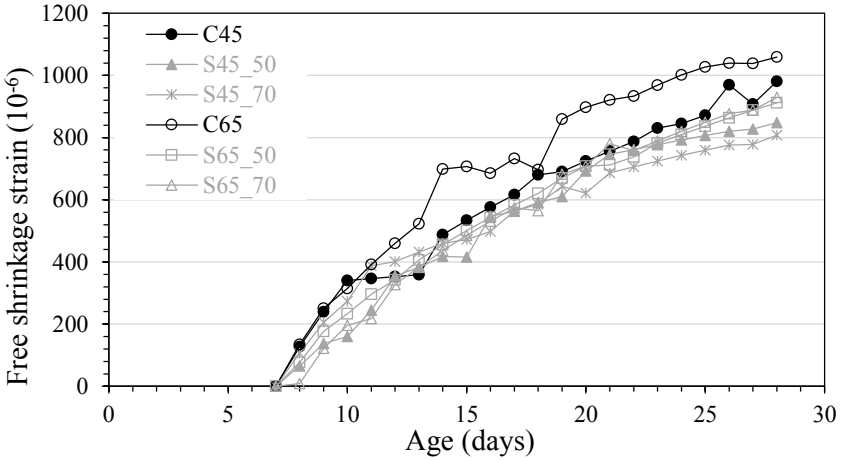

(a) Portland cement (comparison with GGBS mixes).

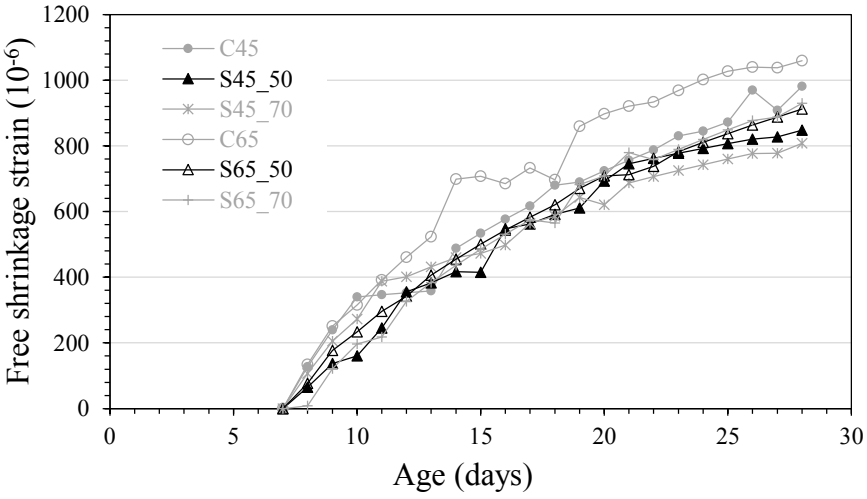

(b) 50% slag (w/b 0.45 & 0.65).

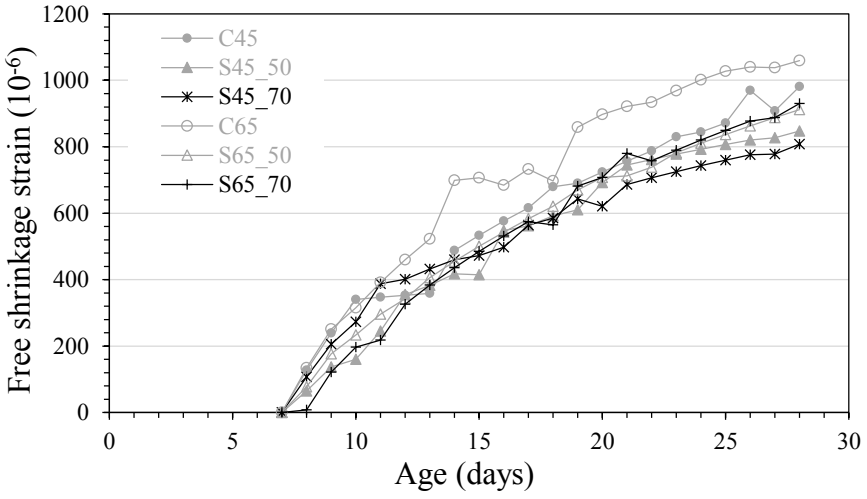

(c) 70% Slag (w/b 0.45 & 0.65).

Figure 5.11: 28-Day free shrinkage strain development, from the completion of curing for the GGBS specimens.

5.6 Summary of material property test results

Tensile strength, tensile relaxation, elastic modulus, and shrinkage properties were identified as key material parameters influencing the overlay material's susceptibility to cracking. Material property tests were thus carried out to investigate the influence of FA and GGBS on these properties in an attempt to understand and predict the restrained shrinkage behaviour. The results obtained are presented and discussed in the preceding sections (Sections 5.1 – 5.5). This section provides a brief summary of all the material property results obtained. **Table 5.2** shows the effect of FA and GGBS on the material properties. The arrow indicates whether the magnitude of the material property increased (↑), decreased (↓) or was almost equal (≈) to the reference specimen values. The number in brackets quantifies this difference.

Table 5.2: Change in material properties with FA and GGBS in comparison to the reference specimens.

Mix I.D	Tensile strength		Tensile relaxation		Elastic modulus		Free shrinkage strains
	7 days	28 days	7 days	28 days	7 days	28 days	
Water-binder ratio 0.45							
30% FA	↓ (16%)	↓ (26%)	↑ (12%)	↑ (84%)	↓ (22%)	↓ (19%)	≈↓
50% FA	↓ (41%)	↓ (33%)	↑ (53%)	↑ (45%)	↓ (46%)	↓ (23%)	≈↓
50% GGBS	↓ (26%)	↓ (37%)	↓ (8%)	↑ (37%)	↓ (30%)	↓ (31%)	≈↓
70% GGBS	↓ (39%)	↓ (44%)	↑ (20%)	↑ (90%)	↓ (57%)	↓ (20%)	≈↓
Water-binder ratio 0.65							
30% FA	↓ (26%)	↓ (30%)	↑ (14%)	↑ (66%)	↓ (14%)	↓ (13%)	↓
50% FA	↓ (52%)	↓ (44%)	↑ (84%)	↑ (138%)	↓ (27%)	↓ (21%)	↓
50% GGBS	↓ (34%)	↓ (34%)	↑ (50%)	↑ (138%)	↓ (10%)	↓ (10%)	↓
70% GGBS	↓ (60%)	↓ (43%)	↑ (197%)	↑ (320%)	↓ (31%)	↓ (14%)	↓

The results indicate that FA and GGBS had significant effects on the material properties of the specimens. Although the tensile strength was negatively affected by the partial replacement of Portland cement with FA or GGBS, the overall effects on tensile relaxation, elastic modulus, and free shrinkage were positive for the reduction of shrinkage-induced tensile stresses. The implication of these results are investigated using the analytical model discussed in Chapter 4. The results of the analytical modelling are provided in Section 5.8.

5.7 Ring test

The ring test is a simple test method used to determine susceptibility to cracking of concrete under restrained shrinkage conditions. The test can be used to study the relative effects of material variations on cracking potential. Ring tests were carried out as described in Section 4.6.6. The results of the ring tests are presented and discussed in this section. Results on the influence of fly ash and slag on the age at cracking and crack area are presented in Section 5.7.1 and 5.7.2 respectively. The detailed ring tests results are provided in Appendix A.6.

5.7.1 Net age at cracking

The age at cracking of the specimens gives an indication on the material's susceptibility to cracking under restrained shrinkage conditions. The age at cracking represents the age at which cracking is initiated in the specimen. Therefore, the age at cracking can be used as an indication of the influence of FA or GGBS on restrained shrinkage cracking. The results can also be expressed in terms of 'net age at cracking'. The net age at cracking does not include the duration of curing, and is thus useful when comparing results of two different curing regimes as is the case in Section 5.7.1.2. **Figure 5.12** provides an overview of the net age at cracking results of all the mixes. The net age at cracking of the FA and GGBS specimens is generally higher than that of the reference mixes. At w/b 0.45, the 50% FA specimens had the highest net age at cracking, while at w/b 0.65 the net age at cracking of the 70% GGBS specimens exceeded all the other specimens. The results are discussed further in the subsections that follow.

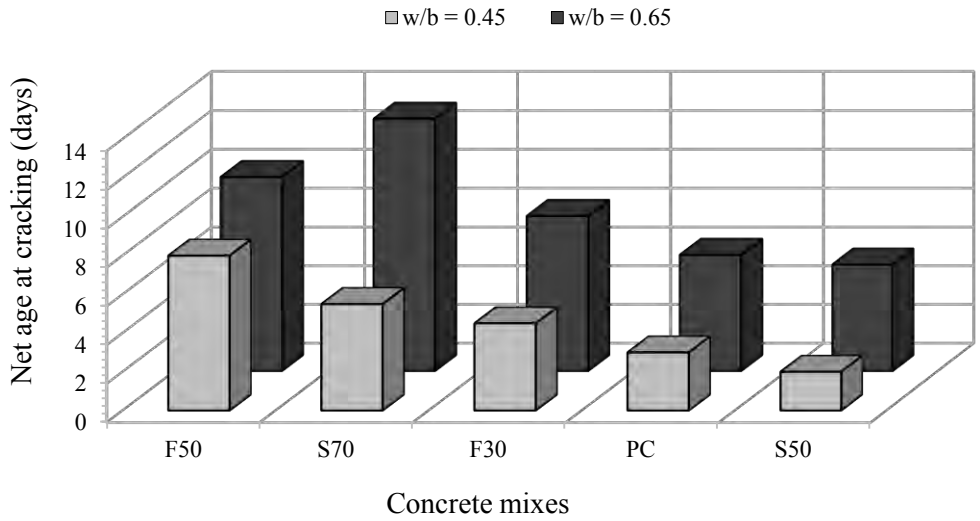

Figure 5.12: Overview of net age at cracking results of ring specimens.

5.7.1.1 Influence of FA and GGBS

The net age at cracking results of the FA specimens are presented in **Figure 5.13**. The net age at cracking increases with increasing fly ash content. At lower w/b ratio, the age at cracking is increased by 2 days and 5 days for 30% and 50% partial replacement of Portland cement,

respectively. This may be due to the increase in tensile relaxation and reduction in elastic modulus having a net positive effect on the age at cracking. Although the tensile strength in the FA specimens maybe be lower than the reference specimens, the tensile stresses have probably decreased significantly (this will be discussed further in Section 5.8). Similar results were observed at higher w/b ratio. The net age at cracking however increased with increasing w/b ratio. This outcome may have been caused by the combination of decreased shrinkage, decreased stiffness, and increased relaxation capacity. Increasing the w/b ratio from 0.45 to 0.65 led to 100%, 77%, and 25% increase in net age at cracking for 0%, 30%, and 50% partial replacement of Portland cement. Bester (2015), observed similar trends with regards to increasing age at cracking with increase in w/b ratio.

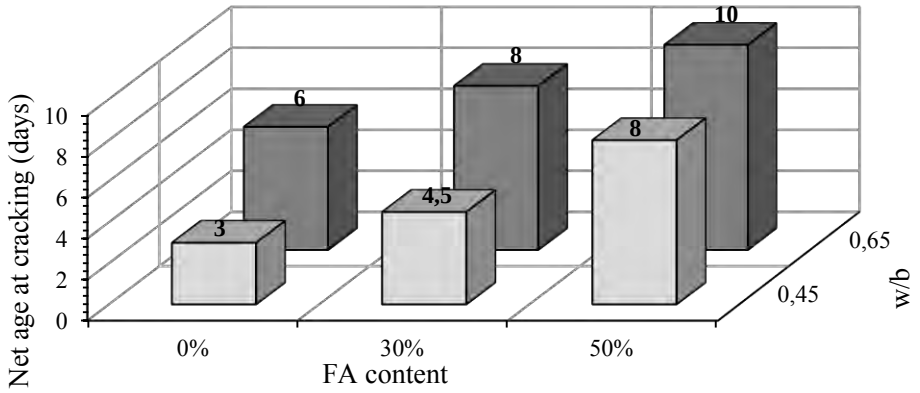

Figure 5.13: Influence of fly ash on the net age at cracking of ring test specimens.

The net age at cracking results of the GGBS specimens are presented in **Figure 5.14**. Similar to the FA specimens, the net age at cracking increased with increasing slag content, but only at 70% replacement. At w/b 0.45, the age at cracking is decreased by 1 day and increased by 2.5 days for 50% and 70% partial replacement of Portland cement. Increasing the w/b ratio from 0.45 to 0.65 led to 100%, 125%, and 136% increase in net age at cracking for 0%, 50%, and 70% partial replacement of Portland cement, respectively. Interestingly, 50% GGBS specimens showed lower (almost equivalent) net ages at cracking in comparison to the reference specimens at both w/b ratios. Judging from the material property data obtained, it can be assumed that the development of the material properties in the 50% GGBS specimens was not favourable for the reduction of tensile stresses in comparison to the reference specimens. At w/b ratio 0.45, despite the reduction in elastic modulus, the tensile relaxation was lower in the GGBS specimens than the reference specimens. At w/b ratio 0.65, the tensile strength was greatly reduced, and the elastic modulus was sufficiently high to possibly counteract the positive effects of increased relaxation. At 70% GGBS replacement level, the same argument used to explain the observations made in the fly ash specimens applies.

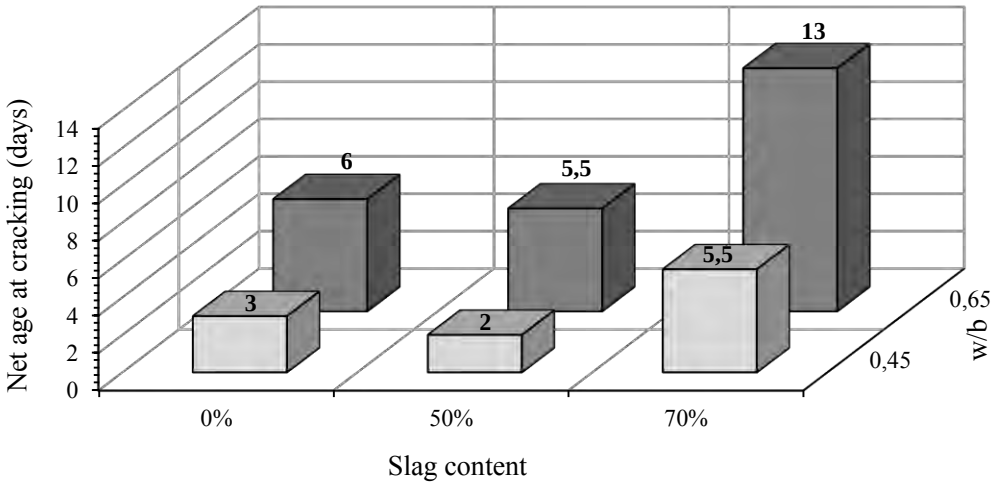

Figure 5.14: Influence of GGBS on the net age at cracking of ring test specimens.

Following the above discussion, one important aspect that must be noted is that the ability of a repair material to resist cracking is dependent on the combined influence of the all material properties.

5.7.1.2 Influence of curing

The influence of curing on restrained shrinkage cracking was investigated on a select number of ring specimens only. The overlay mixes selected were those of 50% FA and 70% GGBS composition, at both w/b ratios. These mixes were selected because of their overall positive performance on the net age at cracking when cured for 7 days with wet cloths. Moreover, these mixes had the highest replacement levels and any effects may be more distinguished and magnified. The specimens were either cured for 7 days using wet hessian sheets or allowed to air cure in an environmentally controlled room (see Section 4.5). The influence of curing regime on the age and net age at cracking of the ring test specimens are provided in **Figure 5.15**. The air cured specimens exhibited lower age at cracking than the wet cloths cured specimens for both w/b ratios. However, the net age at cracking of the specimens did not follow the same trend. The air cured specimens did not always exhibit the lowest net age at cracking. For the FA specimens, net age at cracking of the air cured specimens was equivalent to or greater than (20% higher) the wet cloth cured specimens. The GGBS specimens showed a marginal increase in net age at cracking when cured with wet cloths (9% higher) at lower w/b ratio, but a very significant increase (54% higher) at higher w/b ratio. Moist curing with wet cloths may have resulted in higher shrinkage strains since there was more water in the specimens that could dry out once curing was completed. Beushausen (2015), argued that the magnitude of shrinkage is not influenced by curing, and that a later onset of drying does not reduce the shrinkage strain development. In fact, increased curing merely delays the shrinkage strain development to a time when the relaxation coefficient is smaller and the elastic modulus is higher resulting in higher stresses.

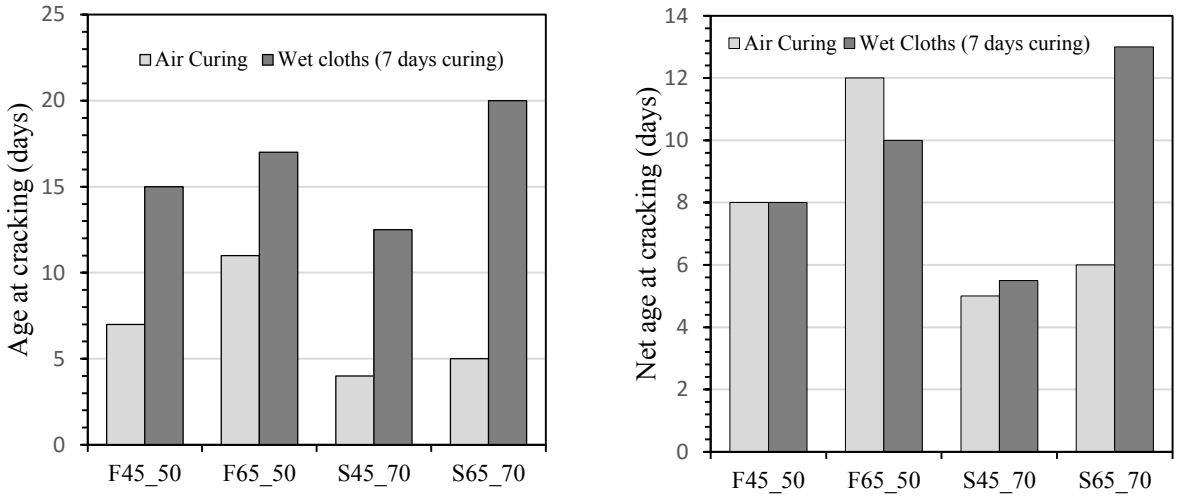

Figure 5.15: Influence of curing on net age at cracking of ring specimens with maximum.

5.7.2 Crack Area

The crack area is a quantity that serves as an indicator of the extent of cracking once cracking occurs. The crack area was calculated by multiplying the average measured crack widths by the average measured crack length. The crack area was calculated at 3 and 14 days after the first occurrence of the crack. The subsections that follow discuss the influence of FA and GGBS on the crack area, the effect of different curing regimes, and the relationship between crack areas and age at cracking.

5.7.2.1 Influence of FA and GGBS

The influence of FA on the crack area is illustrated in **Figure 5.16**. The crack area decreases with increase in FA content at both w/b ratios, with reference specimens showing the largest crack areas.

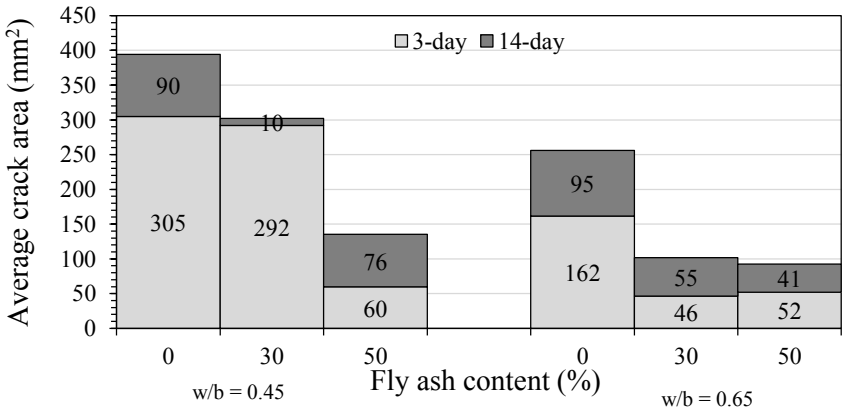

Figure 5.16: Influence of fly ash on 3- and 14-day crack area of ring specimens.

The low w/b ratio mixes had significantly larger crack areas in comparison to the higher w/b ratio mixes. This observation was also noted by Bester (2015). The greater part of the 14-day crack area was developed in the first three days following the occurrence of the cracks. Similar trends were observed on the GGBS specimens. The influence of GGBS on the crack area is

illustrated in **Figure 5.17**. The crack area decreases with an increase in GGBS content with the exception of the 50% GGBS specimens at 0.45 w/b ratio.

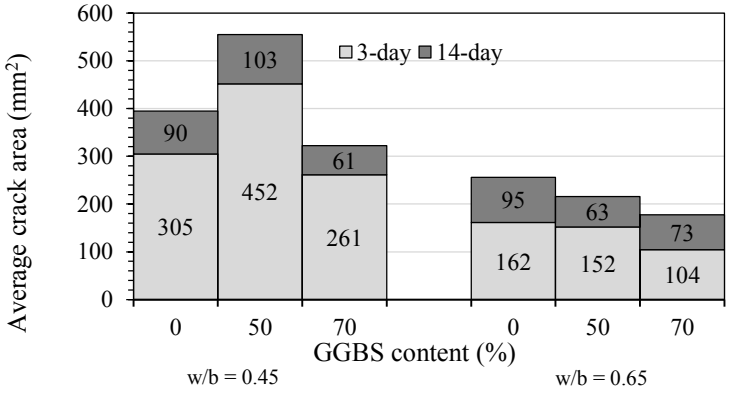

Figure 5.17: Influence of blastfurnace slag on 3- and 14-day crack area of ring specimens.

5.7.2.2 Influence of curing

The influence of curing on the crack area of the selected ring specimens is provided in **Figure 5.18**. The crack areas measured on the air cured specimens are varyingly lower than the crack area of the wet cloth cured specimens. The wet cloth cured specimens may have experienced greater shrinkage than the air cured specimens due to the absorption of curing water by the wet cloth cured specimens. The increased shrinkage may have then translated into increased crack growth. This behaviour could not be further explained as no free shrinkage tests were carried out on the air cured specimens.

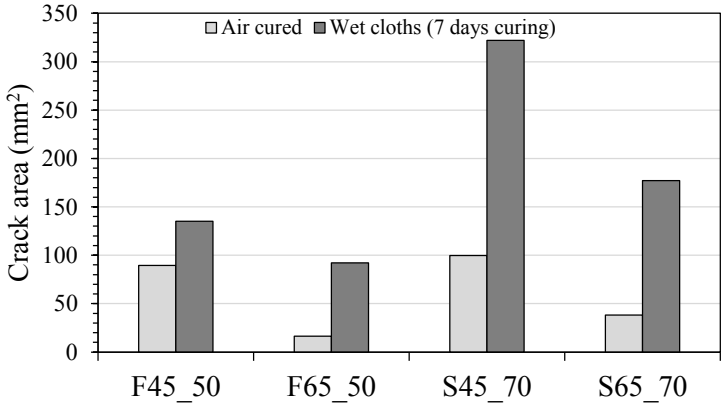

Figure 5.18: Influence of curing regime on 14-day crack area of ring specimens.

5.7.2.3 Correlation between net age at cracking and crack area

The analysis of the combined results of net age at cracking and crack area revealed a correlation between the two results. **Figure 5.20** shows the net age at cracking and crack area results alongside each other. Generally, specimens with higher net age at cracking exhibited the smallest crack areas. Similar observations were recorded by Chilwesa (2012) & Bester (2015),

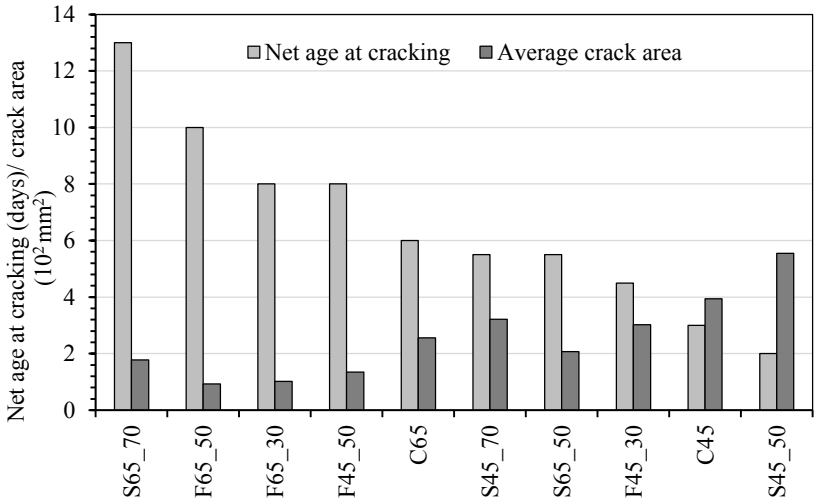

Figure 5.19: Comparison of average crack area and net age at cracking.

The relationship between the net age at cracking and the crack areas is illustrated graphically in **Figure 5.20**.

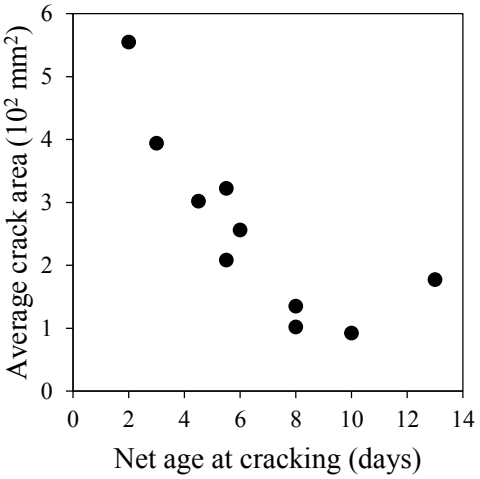

Figure 5.20: Correlation between 14-day crack area and net age at cracking.

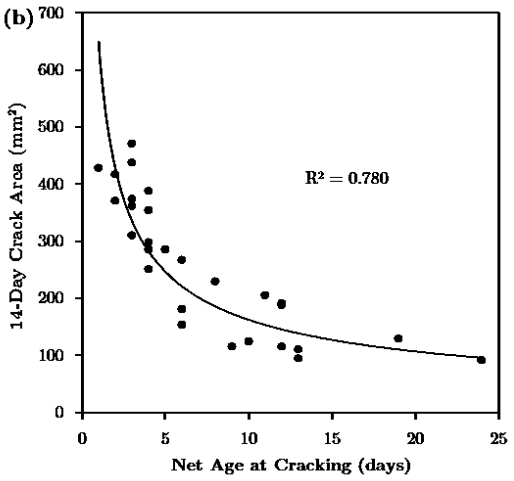

Figure 5.21: Correlation between 14-day crack area and net age at cracking (Bester, 2015).

The curve obtained resembles a negative hyperbolic function. This is similar to the results obtained by Bester (2015) in which a negative hyperbolic curve was used to best describe the correlation between the net age at cracking and crack area. It was suggested that the net age at cracking is directly related to the stress rate at cracking. The stress rate is highest at lower net age at cracking thereby resulting in wider cracks. Using this reasoning, it can thus be said that the influence of FA and GGBS on the crack area depends largely on the influence of FA and GGBS on the net age at cracking.

5.8 Analytical modelling of tensile stresses

The age at cracking was predicted based on the analytical model described in Chapter 4. This was carried out using the time-dependent material properties obtained from the experimental investigation (results detailed in Sections 5.2 – 5.6). These material properties were considered to be the main properties governing retrained shrinkage cracking. Regression analysis was carried out in order to estimate the time-development of these material properties between the ages of 7 and 28 days. The results of the analytical modelling are presented in **Figure 5.22** and **Figure 5.24** for water-binder ratios 0.45 and 0.65 respectively. The results are presented as plots of the development in tensile strength and tensile stress with time. The intersection of the stress and strength curves indicate the age at cracking of the mixes. The predicted ages and net ages at cracking from the analytical modelling are displayed in **Figure 5.23** and **Figure 5.25** for water-binder ratios 0.45 and 0.65 respectively. The detailed analytical modelling results are provided in Appendix B.

The predicted age at cracking from the analytical modelling for water-binder ratio 0.45 show an increase in age at cracking with increase in FA or GGBS replacement levels. The mixes with 50% fly ash and 70% slag showed an increase in the age at cracking of 4 days and 3 days respectively in comparison to the reference mix. Although the reference mix had higher tensile strength than the other mixes, it also exhibited higher stiffness, higher shrinkage strains, and lower relaxation capacity. This most likely resulted in more rapid development in tensile stresses and consequently exceeded the tensile strength at an earlier age. Mixes with FA or GGBS exhibited relatively lower tensile strengths in comparison to the reference mix. However, these mixes also showed general increases in tensile relaxation and reductions in stiffness and shrinkage strains to counteract the decrease in tensile strength, resulting in overall positive performance. These effects were more pronounced with an increase in replacement level and thus mixes with the highest replacements had higher ages at cracking for both FA and GGBS. This is further illustrated in **Figure 5.23**, which shows the age and net age at cracking of the mixes with water-binder ratio 0.45. The fly ash mixes showed slightly better performance than the slag mixes. This may be attributed to the higher relaxation values obtained in the fly ash mixes in comparison to the slag mixes.

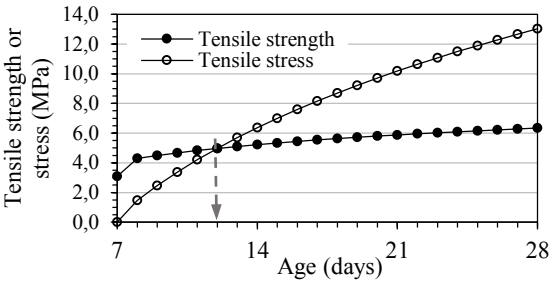

(a) C45 – 100% Portland cement.

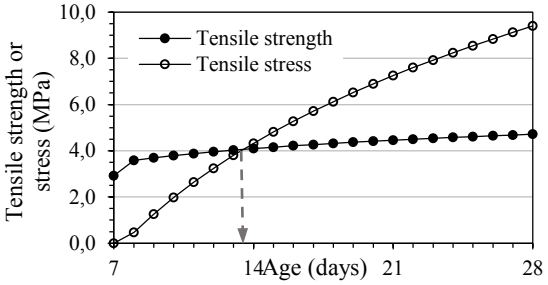

(b) F45_30 – 30% Fly ash.

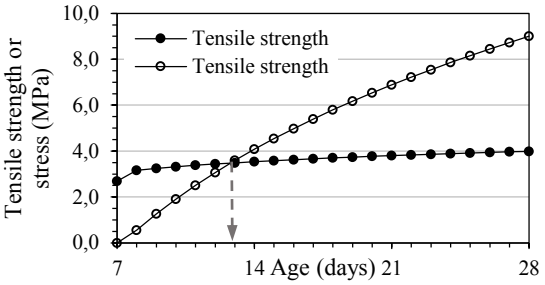

(d) S45_70 – 70% Slag

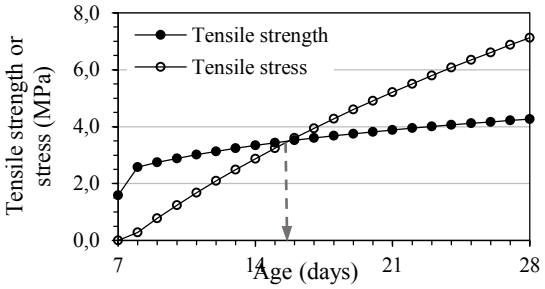

(c) F45_50 – 50% Slag.

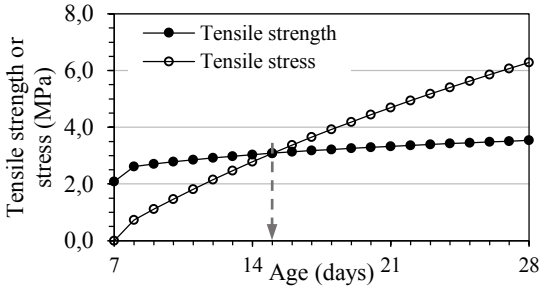

(e) S45_70 – 70% Slag

Figure 5.22: Analytical modelling results of the mixes with w/b 0.45.

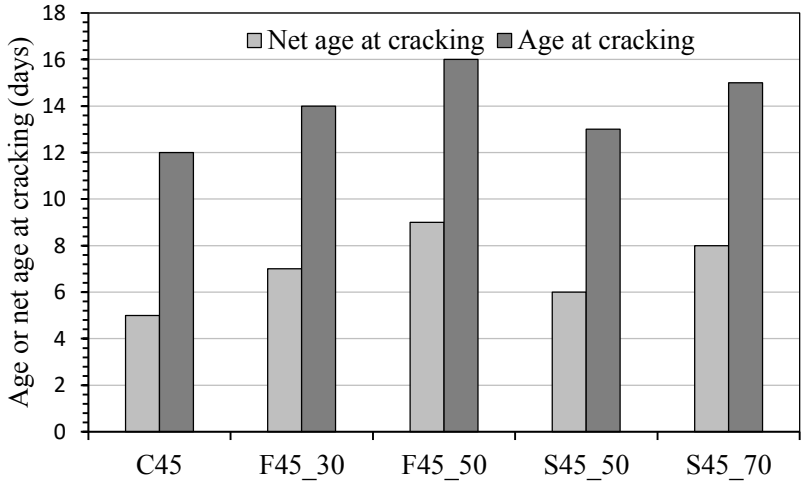

Figure 5.23: Net age at cracking predicted from analytical modelling for w/b 0.45.

Similar results were obtained when the water-binder ratio was increased as shown in **Figure 5.24**. However, at higher water-binder ratio, the 50% slag mix had the lowest age at cracking

of all the mixes. This may have been because the increase in tensile relaxation (33% higher than the reference mix) and the decrease in elastic modulus (10% lower than the reference mix) may not have been sufficient to counteract the massive reduction in tensile strength (54% lower than the reference mix).

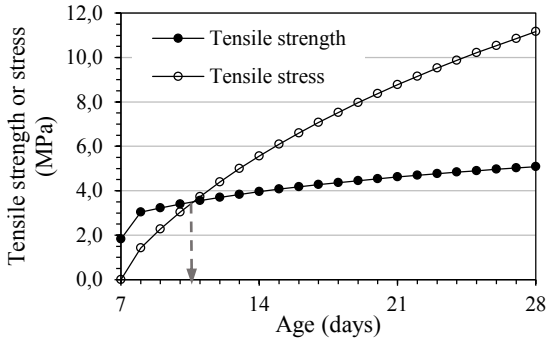

(a) C65 – 100% Portland cement.

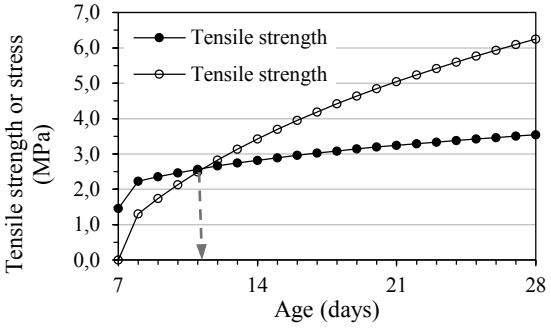

(b) F65_30 – 30% Fly ash.

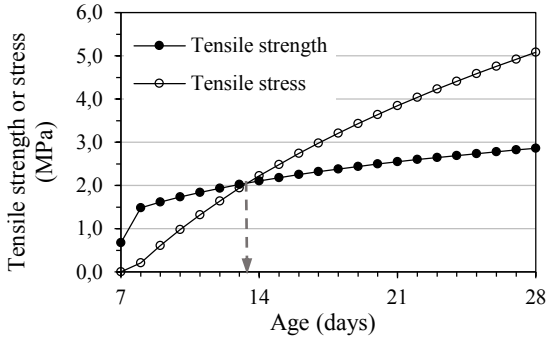

(c) F65_50 – 50% Fly ash.

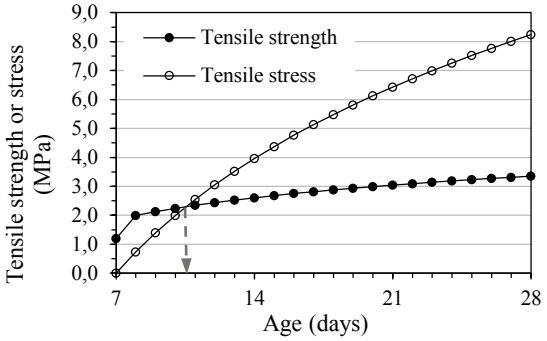

(d) S65_50 – 50% Slag.

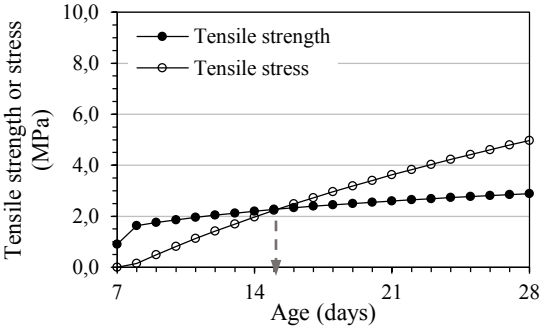

(e) S65_70 – 70% Slag.

Figure 5.24: Analytical modelling results of the mixes with w/b 0.65.

This is further illustrated in **Figure 5.25**, which shows the age and net age at cracking of the mixes with water-binder ratio 0.65. In contrast with the lower water-binder ratio results, the 70% slag mix showed the best performance of all the mixes. This may be attributed to the exceedingly high tensile relaxation displayed in this mix. Overall, there was also an increase in age at cracking with increasing fly ash content as previously discussed. Generally, the analytical modelling results show improvements in performance with the use of fly ash or slag.

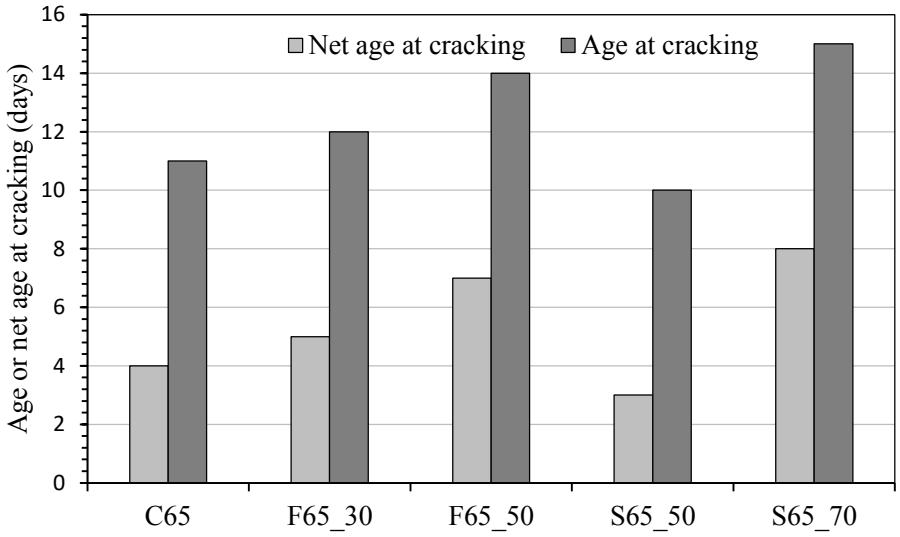

Figure 5.25: Net age at cracking predicted from analytical modelling for w/b 0.65.

5.9 Comparison of net age at cracking

The comparisons of net age at cracking results obtained from the ring tests and analytical modelling are provided in this section. The comparison is necessary for the assessment of the accuracy of the experimental results obtained and analytical modelling carried out. The assessment provides validation in the use of the experimental results obtained to explain the age at cracking observed. This allows for the key research questions to be effectively answered.

The comparisons of net age at cracking for water-binder ratio 0.45 are presented in **Figure 5.26** and **Table 5.3**. The results of both the ring tests and analytical modelling show a similar trend, the net age at cracking is observed to increase with the use of FA or GGBS. The net age at cracking also increases with an increase in FA or GGBS content in both results.

Table 5.4 displays the order of ranking of the repair mortars according to age at cracking. The mortars are listed in descending order, that is, the mortar with the highest age at cracking is positioned at the top of the table. The number in brackets represent the net age at cracking of each of the mortars. With the exception of the 50% slag mix and the reference mix, there is a general agreement in the order of ranking of the mortars between the ring test and the analytical modelling results. In any case, the difference in net age at cracking between the reference mix and the 50% slag mix is one day for both test methods. It can perhaps be concluded that these two mixes have very similar age at cracking, and their performance is nearly identical.

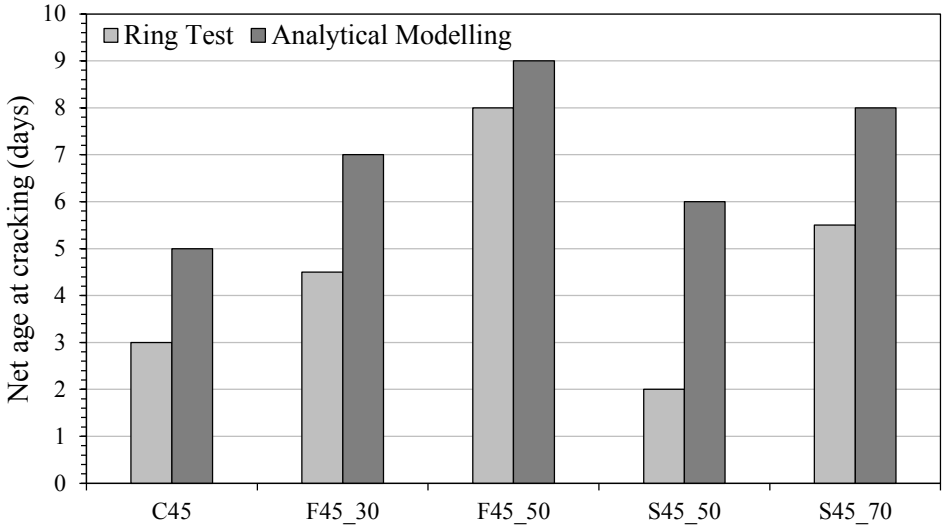

Figure 5.26: Comparison of net age at cracking for mixes with w/b 0.45.

Table 5.3: Comparison of the net age at cracking results of the mixes with w/b 0.45.

Test Type	Mix Type				
	C45	F45_30	F45_50	S45_50	S45_70
Ring test	3	4,5	8	2	5,5
Analytical modelling	5	7	9	6	8

Table 5.4: Ranking of mixes according to age at cracking (7-day curing, w/b 0.45).

Ranking	Ring test	Analytical modelling
1	50% FA (8)	50% FA (9) 70% GGBS (9)
2	70% GGBS (5,5)	30% FA (7)
3	30% FA (4,5)	50% GGBS (6)
4	100% PC (3)	100% PC (5)
5	50% GGBS (2)	

The comparison of net age at cracking for water-binder ratio 0.65 are presented in **Figure 5.27** and **Table 5.5**, while **Table 5.6** displays the order of ranking of the repair mortars according to age at cracking similar to **Table 5.4**.

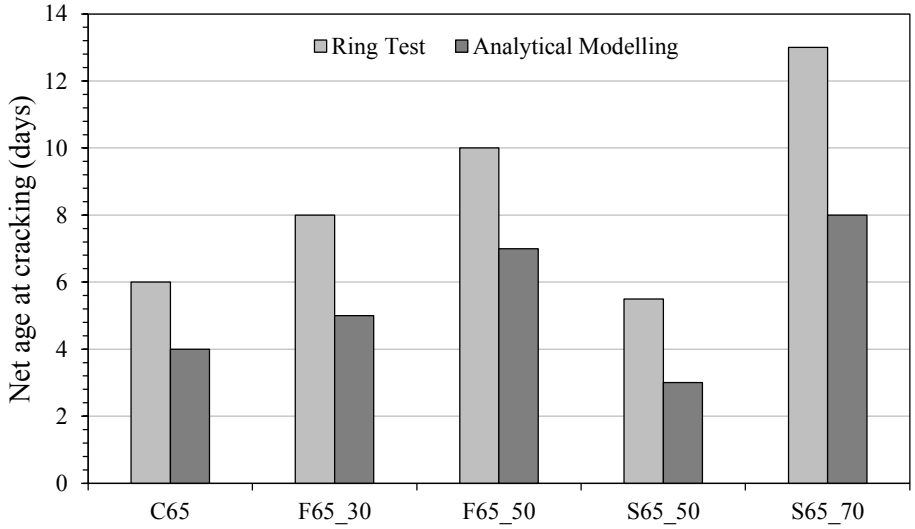

Figure 5.27: Comparison of net age at cracking for mixes with w/b 0.65.

Table 5.5: Comparison of the net age at cracking results of the mixes with w/b 0.65.

Test Type	Mix Type				
	C65	F65_30	F65_50	S65_50	S65_70
Ring test	6	8	10	5,5	13
Analytical modelling	4	5	7	3	8

Table 5.6: Ranking of mixes according to age at cracking (7-day curing, w/b 0.65).

Ranking	Ring test	Analytical modelling
1	70% GGBS (13)	70% GGBS (9)
2	50% FA (10)	50% FA (7)
3	30% FA (8)	30% FA (5)
4	100% PC (6)	100% PC (4)
5	50% GGBS (5,5)	50% GGBS (3)

The net age at cracking results of the ring test were considerably lower than that of the analytical modelling for the low water-binder ratio mixes. This effect was however reversed in higher water-binder ratio mixes. A difference in age at cracking between the two methods was expected. This is because the analytical model does not represent the geometry and degree of restraint present in the ring tests. Previous research (Bester, 2015; Chilwesa, 2012) also showed differences between the two tests methods, the ring test results were also lower than the analytical modelling results. However, it cannot be explained why the results for the analytical modelling were underestimated at higher water-binder ratio. Research carried out by (Molefe, 2015) on rubberised concrete also displayed lower values in the analytical modelling results.. **Figure 5.28** illustrates the correlation between the ring test and the analytical modelling results.

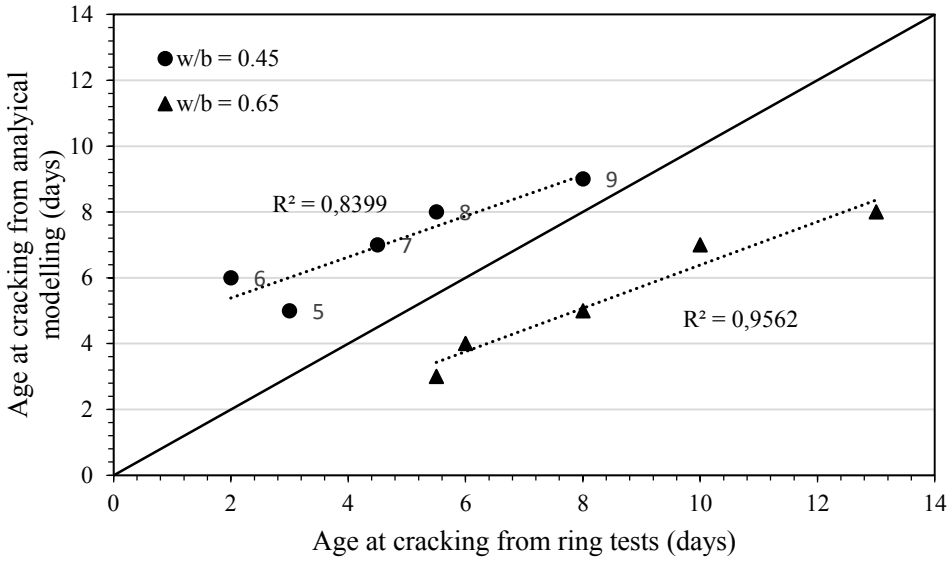

Figure 5.28: Correlation between ring test and analytical modelling results

A reasonably good correlation between the ring test and the analytical modelling age at cracking results was observed for both water-binder ratios. The figure also clearly shows that the age at cracking is overestimated by the analytical model in w/b 0.45 mixes (above the line of equality) and underestimated in w/b 0.65 mixes (below the line of equality). The age at cracking of the ring specimens in is on average 62 ± 7% that of the analytical modelling result for w/b ratio 0.45. At w/b ratio 0.65, the age at cracking from the analytical modelling is on average 66 ± 7% that of the ring test results**.**

.

CHAPTER SIX

6 Conclusions and recommendations

6.1 Introduction

The research was aimed at determining the influence of fly ash and slag on the cracking potential of bonded overlays. To achieve this, material property tests, restrained shrinkage tests, and analytical modelling were employed to predict the age at cracking of fly ash- and slag-blended mortars. The principal objective was to determine whether the performance of bonded overlays was improved by the use of fly ash or slag, with particular reference to age at cracking and crack characteristics.

The chapter summarises the results of the experimental investigation and analytical modelling. Conclusions are drawn and recommendations are made based on these results. A summary of the influence of fly ash and slag on the material properties that govern restrained shrinkage cracking, the age at cracking and crack area, is provided in Section 6.2. This is followed by other additional findings gathered from the investigation in Section 6.3. Finally, the conclusions drawn and recommendations made are summarised in Sections 6.4 and 6.5 respectively.

6.2 The Influence of FA and GGBS on restrained shrinkage cracking of bonded overlays

6.2.1 Effect on material properties

It was generally observed that the replacement of cement with FA or GGBS resulted in lower tensile strength values at both ages, for both water-binder ratios. Furthermore, the tensile strength decreased with an increase in fly ash or slag content. Overall, the elastic modulus decreased with the use of FA or GGBS as was expected. At the lower replacement levels of both FA and GGBS, the elastic modulus of the concrete did not show significant increases between 7 and 28 days for both w/b ratios. In addition, increasing the percentage replacement level of both FA and GGBS by 20% did not drastically affect the 28-day elastic modulus. Tensile relaxation increased with increasing FA or GGBS content. The effect of GGBS on tensile relaxation was slightly less prominent in comparison to FA at low w/b ratio. At lower replacement levels, the tensile relaxation of the FA or GGBS specimens was almost equivalent to the reference specimens. The results also indicate that the specimens had higher relaxation capacity at early ages. At 28 days, the tensile relaxation capacity decreased in all specimens. The reduction of tensile relaxation in the reference specimens was more distinct than in FA and GGBS specimens. The partial replacement of Portland cement with FA or GGBS resulted in a decrease in the magnitude of free shrinkage strain. This observation was more apparent in the higher w/b ratio specimens.

6.2.2 Effect on age at cracking and crack area

The net age at cracking of the FA and GGBS specimens was generally higher than that of the reference mixes. The net age at cracking increased with increasing fly ash content and slag

content with the exception of the 50% slag mix which had the lowest age at cracking at both w/b ratios. Crack areas were decreased with increase in FA content at both w/b ratios, with reference specimens showing the largest crack areas. Similar observations were made in the GGBS ring tests, with the exception of the 50% GGBS specimens at 0.45 w/b ratio which showed the largest crack area. The crack areas measured on the air cured specimens were varyingly lower than the crack area of the wet cloth cured specimens. The wet cloth cured specimens may have experienced greater shrinkage than the air cured specimens.

6.2.3 Analytical modelling

The predicted age at cracking from the analytical modelling show an increase in age at cracking with increase in FA or GGBS replacement levels. The analytical modelling did not give the exact age at cracking, but did however give an identical order of cracking when comparing the different materials. This suggests that the ring test is sufficient for the assessment of relative susceptibility to cracking of FA and GGBS bonded overlays.

6.3 Additional findings

Additional findings that were not directly linked to the influence of FA and GGBS on restrained shrinkage cracking area provided in this section. These include the correlation between net age at cracking and crack area, and the correlation between ring test and analytical modelling results

- The analysis of the combined results of net age at cracking and crack area revealed a correlation between the two results. Generally, specimens with higher net age at cracking exhibited the smallest crack areas.
- The net age at cracking results of the ring test were considerably lower than that of the analytical modelling for the low water-binder ratio mixes. This effect was however reversed in higher water-binder ratio mixes. The age at cracking of the ring specimens in is on average 62 ± 7% that of the analytical modelling result for w/b ratio 0.45. At w/b ratio 0.65, the age at cracking from the analytical modelling is on average 66 ± 7% that of the ring test results.

6.4 Conclusions

The following are the conclusions drawn from the experimental investigation and analytical modelling on the influence of fly ash and slag on restrained shrinkage cracking:

1. Partial replacement of cement with FA or GGBS had the effect of decreasing the tensile strength, elastic modulus, and free shrinkage of the specimens. The degree of reduction in these material properties was directly related to the replacement level. Higher replacement levels resulted in larger reductions.
2. Partial replacement of cement with FA or GGBS had the effect of generally increasing the tensile relaxation of the specimens. The tensile relaxation was also seen to increase with increasing fly ash or slag content in the binder material.
3. In general, FA and GGBS had a positive influence on restrained shrinkage cracking with the exception of the 50% slag mixes. The net age at cracking increased with increasing fly ash or slag content in the binder material.

4. Increase in w/b ratio had a positive effect on restrained shrinkage cracking for all binder types. The net age at cracking increased with increasing w/b ratio.
5. Increased curing duration was observed to increase the age at cracking of the 50% FA and 70% FA specimens. However, the net age at cracking was only improved in the 70% GGBS specimens. Increased curing duration thus only improved the crack resistance of the 70% GGBS specimens.
6. The influence of FA and GGBS on the crack area depended largely on the influence of FA and GGBS on the net age at cracking. Generally, specimens with higher net age at cracking exhibited the smallest crack areas. Increased curing duration resulted in higher crack areas.
7. The net age at cracking of the ring tests showed a correlation to the age at cracking obtained through analytical modelling. The analytical modelling was seen to overestimate the age at cracking at w/b 0.45, and underestimate at w/b 0.65. The age at cracking of the ring specimens in is on average 62 ± 7% that of the analytical modelling result for w/b ratio 0.45. At w/b ratio 0.65, the age at cracking from the analytical modelling is on average 66 ± 7% that of the ring test results.

The overall results of this experimental investigation indicate promising results with regards to the use of high volumes of fly ash or slag to improve the resistance to cracking of bonded overlays. However, the investigation also reveals that the issue of predicting the susceptibility to cracking for these materials is a complex problem that requires a higher level of sophistication. This is evident from the reversal of trends observed between the lower and higher water-binder ratio specimens. A higher level of correlation of results can perhaps be achieved by taking into account the recommendations detailed in the section that follows.

6.5 Recommendations for future research

The following recommendations for future research are suggested for the improvement in understanding of the influence of fly ash and slag on restrained shrinkage cracking, and the factors that govern their behaviour under such conditions:

1. **Hydration and development of material properties**
   The central theory behind this research is that fly ash and slag influence the hydration reactions and thus have an effect on the development of the mechanical properties that influence restrained shrinkage cracking. It is therefore recommended that the time-development of the material properties be investigated as a function of the hydration reaction. It is also suggested that efforts be made at linking the pore structure to the material resulting material properties through a study of the microstructure so as to reinforce understanding.
2. **Observation of trends over longer time period**
   The current research was limited to an experimental investigation that was narrowed to a window of 28 days. For future research, it would be beneficial to observe the trends over a period longer than 28 days in order to determine the long-term effects of fly ash and slag on restrained shrinkage cracking and the crack characteristics.
3. **Variation in mix design**
   The current research is limited to specific concrete mix designs. The influence of fly ash and slag on restrained shrinkage cracking were only investigated for w/b ratios 0.45 and

0.65, and replacement levels of 30% and 50% for fly ash specimens, and 50% and 70% for slag specimens. It is clear that this is a very narrow window of the vast concrete mixtures possible. It is obviously impractical and non-beneficial to investigate over the entire spectrum of mix designs. However, mix design optimisation can be employed to realise the maximum benefits of fly ash and slag in overlay materials

4. **Durability tests**
   Restrained shrinkage cracking has several implications on the durability of the overlay material, and the system as a whole. It is thus suggested that durability tests be carried out to accompany the restrained shrinkage tests. This is essential in order to have a holistic understanding on the influence of fly ash and slag on the long-term performance of the bonded concrete overlays.
5. **Curing methods and duration**
   The study was limited to only one curing duration (7 days) for the major component of the research, the effect of curing duration (1 or 7 days) was only investigated on a fraction of the ring tests. Moreover, the effect of curing duration was not investigated on specimens used to carry out material property tests. This limited the analysis of the effects of curing on fly ash and slag overlay materials. The curing method used was wet hessian sheets, additional curing methods should be investigated in order to broaden understanding as different curing methods may yield different results to the current research.
6. **Variation in environmental conditions**
   The time-dependent material properties are influenced by the prevalent environmental conditions. This is particularly important when considering the tensile relaxation and shrinkage as they are significantly influenced by the temperature and relative humidity. Varying the environmental conditions would thus have an effect on restrained shrinkage, more especially for slag concretes which are more sensitive to temperature. It would thus be beneficial to investigate the influence of varying relative humidity and temperature on restrained shrinkage cracking of FA and GGBS concrete.
7. **Sensitivity study**
   A sensitivity study to better understand which material properties have the largest influence on restrained shrinkage cracking of fly ash and slag bonded overlays should be carried out. This would assist in model refinement allowing for more accurate predictions of age at cracking.
8. **Use of better test methods**
   Refinement of the obtained results through the use of more advanced test methods would be beneficial. For instance, the determination the tensile elastic modulus could be improved by using the tensile strength testing equipment to determine the initial loading phases rather than relying on the compressive strength test which are less representative.

7 References

Addis, B. & Goodman, J., 1999. Concrete Mix Design. In: G. Owens, ed. *Fulton's Concrete Technology.* Midrand: Cement & Concrete Institute, pp. 219-228.

Addis, B. J., 1987. Portland cement, milled granulated blasfurnace slag, fly ash, and silica fume: development and properties. In: B. J. Addis, ed. *Practical guidelines on the selection and use of portland cement, mgbs, fly ash, and silica dume in concrete.* Midrand: Portland Cement Institute, pp. 1-32.

Alexander, M. & Beushausen, H., 2009. Deformation and volume change of hardened concrete. In: O. Gill, ed. *Fulton's Concrete Technology.* 9 ed. Johannesburg: Cement and Concrete Institute, pp. 111-154.

Alexander, M. & Beushausen, H., 2009. Deformation and volume change of hardened concrete. In: G. Owens, ed. *Fultons Concrete Technology.* Midrand: Cement & Concrete Institute, pp. 111-154.

Alexander, M. & Mindess, S., 2005. *Aggregates in Concrete.* New York: Taylor and Francis.

Aly, T. & Sanjayan, J. G., 2008. Factors contributing to early age shrinkage cracking of slag concretes subjected to 7-days moist curing. *Materials and Structures,* Volume 41, pp. 633-642.

Asad, M., Baluch, M. H. & AI-Gadhib, A. H., 1997. Drying shrinkage stresses in concrete patch repair systems. *Magazine of Concrete Research,* 49(181), pp. 283-293.

ASTM, 2009. *Standard Test Method for Determining Age at Cracking and Induced Tensile Stress Characteristics of Mortar and Concrete under Restrained Shrinkage.* West Conshohocken, PA: s.n.

Atis, D. C., 2003. High-Volume Fly Ash Concrete with High Strength and Low Drying Shrinkage. *Journal Of Materials In Civil Engineering,* Issue March/April, pp. 153-156.

Ballim, Y. & Graham, P. C., 2009. The effects of supplementary cementing materials in modifying the heat of hydration of concrete. *Materials and Structures,* Volume 42, p. 803–811.

Bazant, Z. P., 1982. Mathematical Models for Creep and Shrinkage of Concrete. In: Z. P. Bazant & F. H. Wittmann, eds. *Creep and Shrinkage in Concrete Structures.* New York: John Wiley and Sons Ltd, pp. 163-256.

Bazant, Z. P. & Chern, J. C., 1985. Concrete creep at variable humidity: constitutive law and mechanism. *Materiaux et Constructions,* 18(103), pp. 1-20.

Bentur, A. & Kovler, K., 2003. Evaluation of early age cracking characteristics in cementitious systems. *Materials and Structures,* pp. 183-190.

Bentz, D. P., 2008. A review of early-age properties of cement-based materials. *Cement and Concrete Research,* Volume 32, pp. 196-204.

Bester, N., 2015. *The Influence of Curing on Restrained Shrinkage Cracking of Bonded Overlays,* Cape Town: s.n.

Beushausen, H., 2005. *Long-term performance of bonded concrete overlays subjected to differential shrinkage,* Cape Town: s.n.

Beushausen, H., 2015. A parameter study on the age at cracking of bonded concrete overlays subjected to restrained shrinkage. *Materials & Structures,* 49(5), pp. 1905-1916.

Beushausen, H. & Alexander, M., 2006. Failure mechanisms and tensile relaxation of bonded concrete overlays subjected to differential shrinkage. *Cement and Concrete Research,* Volume 36, pp. 1908-1914.

Beushausen, H., Alexander, M. & Ballim, Y., 2012. Early-age properties, strength development and heat of hydration of concrete containing various South African slags at different replacement ratios. *Construction and Building Materials,* Volume 29, pp. 533-540.

Beushausen, H. & Alexander, M. G., 2007. Localised strain and stress in bonded concrete overlays subjected to differential shrinkage. *Materials and Structures,* Volume 40, pp. 189-199.

Beushausen, H. & Chilwesa, M., 2013. Assessment and prediction of drying shrinkage cracking in bonded morta overlays. *Cement and Concrete Research,* Volume 53, pp. 256-266.

Beushausen, H., Masuku, C. & Moyo, P., 2012. Relaxation characteristics of cement mortar subjected to tensile strain. *Materials and Structures ,* Volume 45, pp. 1181-1188.

Bharatkumar, B. H. et al., 2005. Effect of fly ash and slag on the fracture characteristics of high performance concrete. *Materials and Structures,* January-February, Volume 38, pp. 63-72.

Bijen, J., 1996. Benefits of slag and fly ash. *Construction and Building Materials,* 10(5), pp. 309-314.

Bissonnette, B., Pierre, P. & Pigeon, M., 1999. Influence of key material parameters on drying shrinkage of cementitious materials. *Cement and Concrete Research,* Volume 29, pp. 1655-1662.

Bullard, J. W. et al., 2011. Mechanisms of cement hydration. *Cement and Concrete Research,* Volume 41, pp. 1208-1223.

Cärlsward, J., 2006. *Shrinkage cracking of steel fibre reinforced self compacting concrete overlays,* Luleå,: s.n.

Cementitious Slag Makers Association, 2010. *Cementitious Slag Makers Association.* [Online] Available at: www.ukcsma.co.uk [Accessed 20 May 2013].

Chen, W., 2006. *Hydration of Slag Cement: Theory, Modeling and Application,* Enschede: s.n.

Chilwesa, M., 2012. *Assessing the age at cracking of concrete repair mortars/overlays subjected to restrained shrinkage cracking,* Cape Town: s.n.

Chindaprasirta, P., Homwuttiwongb, S. & Sirivivatnanonc, V., 2004. Influence of fly ash fineness on strength, drying shrinkage and sulfate resistance of blended cement mortar. *Cement and Concrete Research,* Volume 34, pp. 1087-1092.

Darquennes, A. et al., 2012. Long-term deformations and cracking risk of concrete with high content of mineral additions. *Materials and Structures,* 45(11), pp. 1705-1716.

Denarie, E. & Silfwerbrand, J., 2004. *Structural behaviour of bonded concrete overlays.* Stockholm, s.n.

Dittmer, T. J., 2013. *The effect of aggregate on the age at cracking of bonded concrete overlays subjected to restrained deformation,* Cape Town: s.n.

Emmons, P. H. & Vaysburd, A. M., 1996. System concept in design and construction of durable concrete repairs. *Construction and Building Materials,* 0(1), pp. 69-75.

Fowler, D. & Trevino, M., 2011. Overlay Design Process. In: *Field Application and Performance of Concrete Overlay for the Repair, the Lining or the Strengthening of Slabs and Pavements.* s.l.:s.n.

Gagne, R., Aouad, I., Shen, J. & Poulin, C., 1999. Development of a new experimental technique for the study of the autogenous shrinkage of cement paste. *Materials and Structures,* 32(November), pp. 635-642.

Gilbert, R. I., 1988. *Time effects in concrete structures.* Netherlands: Elsevier.

Gogol, V. R., 1994. *The compressive strength of fly ash concrete and its mineralogy,* Cape Town: s.n.

Greensmith, C. G., 2005. *The effects of cement extenders and water to binder ratio on the heat evolution characteristics of concrete,* Johannesburg: s.n.

Grieve, G., 2009. Cementitious Materials. In: G. Owens, ed. *Fulton's Concrete Technology.* 9th ed. Midrand: Cement and Conrete Institute, pp. 1-16.

Grieve, G. R. H., 1987. The properties of fresh concrete made with portland cemcents, milled granulated blastfurnace slag, fly ash, or silica fume. In: *Practical guidelines on the selection and use of portland cement, mgbs, fly ash and silica fume in concrete.* Midrand: Portland Cement Institute, pp. 33-49.

Hassan, K. E., Brooks, J. J. & Al-alawi, L., 2001. Compatibility of repair mortars with concrete in a hot-dry environment. *Cement and Concrete Composistes,* Volume 23, pp. 93-101.

Hooton, R. D., Stanish, K., Angel, J. P. & Prusinski, J., 2009. *The effect of ground granulated blast furnace slag (slag cement) on the drying shrinkage of concrete - a critical review of the literature.* Michigan, American Concrete Institute.

Hover, K., 2011. The influence of water on the performance of concrete. *Construction and Building Materials.*

Hwang, K., Noguchi, T. & Tomosawa, F., 2004. Prediction model of compressive strength development of fly-ash concrete. *Cement and Concrete Research,* Volume 34, p. 2269–2276.

Jaouadi, I., Amor, G. & Scrivener, K., 2008. *Modellng Autogenous shrinkage of hydrating cement paste.* Delft, s.n.

Ji, G., 2008. *Cracking risk of concrete structures in the hardening phase: Experiments, material modeling and finite element analysis,* Trondheim: s.n.

Kolani, B. et al., 2012. Hydration of slag-blended cements. *Cement & Concrete Composites,* Volume 34, p. 1009–1018.

Kourounis, S. et al., 2007. Properties and hydration of blended cements with steelmaking slag. *Cement and Concrete Research,* Volume 37, p. 815–822.

Krüger, J. E., 2003. *South African Fly Ash: A Cement Extender.* Silverton: The South African Coal Association.

Kumar, B., Tike, G. K. & Nanda, P. K., 2007. Evaluation of Properties of High-Volume Fly-Ash Concrete for Pavements. *Journal Of Materials In Civil Engineering,* Issue October, pp. 906-911.

Lee, J.-H. & Yoon, Y.-S., 2014. The Effects of Cementitious Materials on the Mechanical and Durability Performance of High-Strength Concrete. *KSCE Journal of Civil Engineering,* 00(0), pp. 1-9.

Lee, K. M., Lee, H. K., Lee, S. H. & Kim, G. Y., 2006. Autogenous shrinkage of concrete containing granulated blast-furnace slag. *Cement and Concrete Research,* Volume 36, pp. 1279-1285.

Leung, P. W. C. & Wong, H. D., 2011. *Final report on durability and strength development of ground granulated blastfurnace slag concret,* Kowloon, Hong Kong: s.n.

Li, G. & Zhao, X., 2003. Properties of concrete incorporating fly ash and ground granulated blast-furnace slag. *Cement & Concrete Composites,* Volume 25, p. 293–299.

Li, M. & Li, V. C., 2009. Influence of Material Ductility on Performance of Concrete Repair. *ACI Materials Journal,* September-October.pp. 419-428.

Li, Z., 2011. *Advanced Concrete Technology.* New Jersey: John Wiley & Sons, Inc.

Lothenbach, B., Scrivener, K. & Hooton, R. D., 2011. Supplementary cementitious materials. *Cement and Concrete Research,* Volume 41, pp. 1244-1256.

Lukovic, M., Ye, G. & Breugel, K. v., n.d. *Reliable Concrete Repair - A Critical Review,* s.l.: s.n.

Magera, N. K., 2013. *Predicting and Testing the Tensile Relaxation of concrete,* Cape Town: s.n.

Maia, L., Azenha, M., Faria, R. & Figueiras, J., 2011. Influence of the cementitious paste composition on the E-modulus and heat of hydration evolutions. *Cement and Concrete Research,* Volume 41, pp. 799-807.

Maia, L., Azenha, M., Geiker, M. & Figueiras, J., 2012. E-modulus evolution and its relation to solids formation of pastes from commercial cements. *Cement and Concrete Research,* Volume 42, pp. 928-936.

Mantel, D. G., 1992. *The manufacture, properties, and applications of Portland cements, cement additives, and blended cements.* Pretoria: Pretoria Portland Cement.

Masuku, C., 2009. *Tensile relaxation of bonded concrete overlays,* Cape Town: s.n.

Mheta, P. K. & Monteiro, P. J. M., 2001. *Concrete: Microstructure, Properties and Materials.* s.l.:s.n.

Mindess, S., Young, J. F. & Darwin, D., 2003. *Concrete.* 2nd ed. s.l.:Prentice Hall.

Molefe, T. D., 2015. *Optimizing the content and gradation of recycled tyre rubber particles to improve cracking resistance of concrete mortars,* Cape Town: s.n.

Montgomery, D. C., 2013. *Design and Analysis of Experiments.* 8th ed., International Student Version. ed. New York: John Wiley & Sons, Inc..

Morgan, D. R., 1996. Compatibility of concrete repair materials and systems. *Construction and Building Materials,* 10(1), pp. 57-67.

Mounanga, P., Baroghel-Bounyb, V., Loukili, A. & Khelidj, A., 2006. Autogenous deformations of cement pastes: Part I. Temperature effects at early age and micro–macro correlations. *Cement and Concrete Research,* Volume 36, pp. 110-122.

Mukheibir, P. V., 1990. *The deformation properties of concrete with classified Lethabo fly ash,* Cape Town: s.n.

Pane, I. & Hansen, W., 2002. Early age creep and stress relaxation of concrete containing blended cements. *Materials and Structures,* Volume 35, pp. 92-96.

Pane, I. & Hansen, W., 2008. Investigation on key properties controlling early-age stress development of blended cement concrete. *Cement and Concrete Research,* Volume 38, pp. 1325-1335.

Pane, I. & Hansen, W., 2008. Predictions and verifications of early-age stress development in hydrating blended cement concrete. *Cement and Concrete Research ,* Volume 38, pp. 1315-1324.

Perrie, B., 2009. Strength of hardened concrete. In: O. Gill, ed. *Fulton's concrete technology.* 9 ed. Midrand: Cement & Concrete Institute, pp. 97-110.

Pigeon, M. et al., 2000. Equipment for the analysis of the behaviour of concrete under restrained shrinkage at early ages. *Magazine of Concrete Research,* 52(4), pp. 297-302.

Plannerer, M. & Brandes, C., n.d. *Influence of binders and admixtures on autogenous shrinkage of high performance conrete.* s.l., s.n., pp. 179-190.

Sanahuja, J., Dormieux, L. & Chanvillard, G., 2007. Modelling elasticity of a hydrating cement paste. *Cement and Concrete Research,* Volume 37, p. 1427–1439.

SANS 201, 2008. *SANS 201: Sieve analysis fines, content and dust content of aggregates.* Pretoria: South African National Standards..

SANS 5863, 2006. *SANS 5863: Concrete tests - Compressive strength of hardened concrete.* Pretoria: South African National Standards.

Schieβl, P., Plannerer, M. & Brandes, C., 2000. *Influence of binders and admixtures on autogenous shrinkage of high performance concrete.* Paris, RILEM, pp. 179-190.

Scrivener, K. L. & Nonat, A., 2011. Hydration of cementitious materials, present and future. *Cement and Concrete Research,* Volume 41, p. 651–665.

Shah, S. P., 1997. An overview of the fracture mechanics of concrete. *Cement, Concrete, and Aggregates,* 19(2), pp. 79-86.

Siddique, R., 2004. Performance characteristics of high-volume Class F fly ash concrete. *Cement and Concrete Research,* Volume 34, p. 487–493.

Silfwerbrand, J. & Beushausen, H., 2006. Bonded concrete overlays – bond strength issues. *Concrete Repair, Rehabilitation and Retrofitting ,* pp. 53-61.

Slag Cement Association, 2013. *Effect of slag cement on shinrkage in concrete,* Michigan: Slag Cement Association.

Tao, Z. & Weizu, Q., 2006. Tensile creep due to restraining stresses in high-strength concrete at early ages. *Cement and Concrete Research,* Volume 36, pp. 584-591.

Tayeh, B. A., Bakar, A. B., Johari, M. M. A. & Voo, Y. L., 2012. Mechanical and permeability properties of the interface between normal concrete substrate and ultra high performance fiber concrete overlay. *Construction and Building Materials,* Volume 36, pp. 538-548.

Tazawa, E., Sato, R., Sakai, E. & Miyazawa, S., 2000. *Work of JCI Committee on Autogenous Shrinkage.* Paris, RILEM, pp. 21-40.

Termkhajornkita, P. et al., 2005. Effect of fly ash on autogenous shrinkage. *Cement and Concrete Research,* Volume 35, pp. 473-482.

The Concrete Society, 2011. *Cementitious Materials,* s.l.: The Concrete Society.

Theiner, Y. & Hofstetter, G., 2012. Evaluation of the effects of drying shrinkage on the behavior of concrete structures strengthened by overlays. *Cement and Concrete Research,* Volume 42, pp. 1286-1297.

Trevino, M. & Fowler, D. W., 2004. *The bonded concrete overlay process and a case study.* Stockholm, s.n.

Vaysburd, A. & Emmons, P., 2000. How to make today's repairs durable for tomorrow - corrosion protection in concrete repair. *Construction and Building Materials,* Volume 14, pp. 189-197.

Vaysburd, A. M., Carino, N. J. & Bissonette, B., 2000. *Predicting the Performance of Concrete Repair Materials,* Durham, New Hampshire: s.n.

Vaysburd, A. M. & Emmons, P. H., 2006. Concrete repair – a composite system: Philosophy, engineering and practice. In: *Concrete Repair, Rehabilitation and Retrofitting.* London: Taylor & Francis Group, pp. 19-26.

Wang, X. Y., 2013. Properties prediction of fly ash blended concrete using hydration model. *Science China Technological Sciences,* 56(9), p. 2317–2325.

Young, F., Mindess, S. & Bentur, A., 1998. *The science and technology of civil engineering materials.* New Jersey: Prentice Hall.

Yuan, J., Lindquist, W., Darwin, D. & Browning, J., 2015. Effect of Slag Cement on Drying Shrinkage of Concrete. *ACI Materials Journal,* Issue March/April, pp. 267-276.

Yun, K.-k. & Suh, Y.-c., 1999. Field Application and Performance of Concrete Overlay for Pavement Rehabilitation. *KSCE Journal of Civil Engineering,* September, 3(3), pp. 233-241.

Zajac, M. & Haha, M. B., 2014. Experimental investigation and modeling of hydration and performance evolution of fly ash cement. *Materials and Structures,* Volume 47, p. 1259–1269.

Zhang, X., Li, Y. & Wu, K.-r., 2000. *Study on autogenous shrinkage and AC impedance of paste with additives.* Paris, RILEM, pp. 547-557.

Zhou, J., Ye, G., Schlangen, E. & Van Breugel, K., 2006. *Autogenous deformation of portland cement paste blended with blast frunace slag measured by mini TSTM.* Lyngby, s.n.

APPENDIX A

A. Detailed experimental results

A.1 Compressive strength results

Table A.1: Compressive strength results for mortar mix C45 (100% Portland cement; w/b = 0.45).

Specimen Reference	Age (days)	Cube Dim. (mm)	Saturated Density (kg/m^3)	Mean Saturated Density (kg/m^3)	Failure Load (kN)	Comp. Str. (MPa)	Mean Comp. Str. (MPa)	CoV[1] (%)
C45-2D-1	2	100	2160	2175	360	36,0	35,0	2,86
C45-2D-2		100	2200		340	34,0		
C45-2D-3		100	2165		350	35,0		
C45-7D-1	7	100	2205	2175	408	40,8	40,3	2,59
C45-7D-2		100	2170		391	39,1		
C45-7D-3		100	2150		410	41,0		
C45-14D-1	14	100	2275	2290	503	50,3	50,4	0,23
C45-14D-2		100	2325		505	50,5		
C45-14D-3		100	2270		503	50,3		
C45-28D-1	28	100	2225	2238	540	54,0	53,8	0,92
C45-28D-2		100	2260		532	53,2		
C45-28D-3		100	2230		541	54,1		

Table A.2: Compressive strength results for mortar mix F45_30 (70% Portland cement & 30% FA; w/b = 0.45).

Specimen Reference	Age (days)	Cube Dim. (mm)	Saturated Density (kg/m^3)	Mean Saturated Density (kg/m^3)	Failure Load (kN)	Comp. Str. (MPa)	Mean Comp. Str. (MPa)	CoV (%)
F45/30-2D-1	2	100	2205	2225	255	25,5	25,1	1,61
F45/30-2D-2		100	2245		247	24,7		
F45/30-2D-3		100	2225		250	25,0		
F45/30-7D-1	7	100	2235	2225	308	30,8	31,2	1,88
F45/30-7D-2		100	2205		310	31,0		
F45/30-7D-3		100	2235		319	31,9		
F45/30-14D-1	14	100	2295	2240	404	40,4	40,5	0,29
F45/30-14D-2		100	2230		404	40,4		
F45/30-14D-3		100	2195		406	40,6		
F45/30-28D-1	28	100	2255	2247	435	43,5	46,1	5,05
F45/30-28D-2		100	2260		480	48,0		
F45/30-28D-3		100	2225		468	46,8		

Table A.3: Compressive strength results for mortar mix F45_50 (50% Portland cement & 50% FA; w/b = 0.45).

Specimen Reference	Age (days)	Cube Dim. (mm)	Saturated Density (kg/m^3)	Mean Saturated Density (kg/m^3)	Failure Load (kN)	Comp. Str. (MPa)	Mean Comp. Str. (MPa)	CoV (%)
F45/50-2D-1	2	100	2205	2195	157	15,7	15,1	3,66
F45/50-2D-2		100	2195		147	14,7		
F45/50-2D-3		100	2185		148	14,8		
F45/50-7D-1	7	100	2185	2203	193	19,3	19,2	0,52
F45/50-7D-2		100	2210		191	19,1		
F45/50-7D-3		100	2215		192	19,2		
F45/50-14D-1	14	100	2170	2182	249	24,9	24,7	1,02
F45/50-14D-2		100	2205		244	24,4		
F45/50-14D-3		100	2170		247	24,7		
F45/50-28D-1	28	100	2225	2213	317	31,7	32,6	3,71
F45/50-28D-2		100	2185		340	34,0		
F45/50-28D-3		100	2230		322	32,2		

Table A.4: Compressive strength results for mortar mix S45_50 (50% Portland cement & 50% GGBS; w/b = 0.45).

Specimen Reference	Age (days)	Cube Dim. (mm)	Saturated Density (kg/m^3)	Mean Saturated Density (kg/m^3)	Failure Load (kN)	Comp. Str. (MPa)	Mean Comp. Str. (MPa)	CoV (%)
S45/50-2D-1	2	100	2190	2203	137	13,7	13,9	1,49
S45/50-2D-2		100	2215		141	14,1		
S45/50-2D-3		100	2205		140	14,0		
S45/50-7D-1	7	100	2205	2238	291	29,1	28,9	1,63
S45/50-7D-2		100	2245		284	28,4		
S45/30-7D-3		100	2265		293	29,3		
S45/50-14D-1	14	100	2220	2237	391	39,1	37,9	3,04
S45/50-14D-2		100	2250		368	36,8		
S45/50-14D-3		100	2240		378	37,8		
S45/50-28D-1	28	100	2205	2222	486	48,6	47,2	2,88
S45/50-28D-2		100	2255		459	45,9		
S45/50-28D-3		100	2205		470	47,0		

Table A.5: Compressive strength results for mortar mix S45_70 (30% Portland cement & 70% GGBS; w/b = 0.45).

Specimen Reference	Age (days)	Cube Dim. (mm)	Saturated Density (kg/m^3)	Mean Saturated Density (kg/m^3)	Failure Load (kN)	Comp. Str. (MPa)	Mean Comp. Str. (MPa)	CoV (%)
S45/70-2D-1	2	100	2215	2203	51	5,1	4,8	5,21
S45/70-2D-2		100	2190		48	4,8		
S45/70-2D-3		100	2205		46	4,6		
S45/70-7D-1	7	100	2250	2203	210	21,0	20,7	1,48
S45/70-7D-2		100	2185		206	20,6		
S45/70-7D-3		100	2175		204	20,4		
S45/70-14D-1	14	100	2170	2188	279	27,9	29,0	3,98
S45/70-14D-2		100	2205		289	28,9		
S45/70-14D-3		100	2190		302	30,2		
S45/70-28D-1	28	100	2170	2187	374	37,4	37,7	2,47
S45/70-28D-2		100	2185		369	36,9		
S45/70-28D-3		100	2205		387	38,7		

Table A.6: Compressive strength results for mortar mix C65 (100% Portland cement; w/b = 0.65).

Specimen Reference	Age (days)	Cube Dim. (mm)	Saturated Density (kg/m^3)	Mean Saturated Density (kg/m^3)	Failure Load (kN)	Comp. Str. (MPa)	Mean Comp. Str. (MPa)	CoV (%)
C65-2D-1	2	100	2215	2170	165	16,5	16,4	0,35
C65-2D-2		100	2165		164	16,4		
C65-2D-3		100	2130		164	16,4		
C65-7D-1	7	100	2175	2165	287	28,7	27,9	2,71
C65-7D-2		100	2145		272	27,2		
C65-7D-3		100	2175		278	27,8		
C65-14D-1	14	100	2240	2203	323	32,3	31,8	1,57
C65-14D-2		100	2230		318	31,8		
C65-14D-3		100	2140		313	31,3		
C65-28D-1	28	100	2190	2157	365	36,5	36,5	1,51
C65-28D-2		100	2150		370	37,0		
C65-28D-3		100	2130		359	35,9		

Table A.7: Compressive strength results for mortar mix F65_30 (70% Portland cement & 30% FA; w/b = 0.65).

Specimen Reference	Age (days)	Cube Dim. (mm)	Saturated Density (kg/m^3)	Mean Saturated Density (kg/m^3)	Failure Load (kN)	Comp. Str. (MPa)	Mean Comp. Str. (MPa)	CoV (%)
F65/30-2D-1	2	100	2200	2173	103	10,3	10,1	1,51
F65/30-2D-2		100	2150		101	10,1		
F65/30-2D-3		100	2170		100	10,0		
F65/30-7D-1	7	100	2135	2160	163	16,3	16,7	2,40
F65/30-7D-2		100	2140		167	16,7		
F65/30-7D-3		100	2205		171	17,1		
F65/30-14D-1	14	100	2185	2192	197	19,7	20,2	2,48
F65/30-14D-2		100	2185		207	20,7		
F65/30-14D-3		100	2205		202	20,2		
F65/30-28D-1	28	100	2200	2198	249	24,9	25,2	1,65
F65/30-28D-2		100	2220		257	25,7		
F65/30-28D-3		100	2175		251	25,1		

Table A.8: Compressive strength results for mortar mix F65_50 (50% Portland cement & 50% FA; w/b = 0.65).

Specimen Reference	Age (days)	Cube Dim. (mm)	Saturated Density (kg/m^3)	Mean Saturated Density (kg/m^3)	Failure Load (kN)	Comp. Str. (MPa)	Mean Comp. Str. (MPa)	CoV (%)
F65/50-2D-1	2	100	2210	2210	52	5,2	5,2	7,69
F65/50-2D-2		100	2180		48	4,8		
F65/50-2D-3		100	2240		56	5,6		
F65/50-7D-1	7	100	2190	2215	106	10,6	10,7	2,47
F65/50-7D-2		100	2240		105	10,5		
F65/50-7D-3		100	2215		110	11,0		
F65/50-14D-1	14	100	2225	2222	131	13,1	13,3	1,89
F65/50-14D-2		100	2215		136	13,6		
F65/50-14D-3		100	2225		133	13,3		
F65/50-28D-1	28	100	2220	2207	174	17,4	16,8	3,28
F65/50-28D-2		100	2200		165	16,5		
F65/50-28D-3		100	2200		164	16,4		

Table A.9: Compressive strength results for mortar mix S65_50 (50% Portland cement & 50% GGBS; w/b = 0.65).

Specimen Reference	Age (days)	Cube Dim. (mm)	Saturated Density (kg/m^3)	Mean Saturated Density (kg/m^3)	Failure Load (kN)	Comp. Str. (MPa)	Mean Comp. Str. (MPa)	CoV (%)
S65/50-2D-1	2	100	2150	2147	48	4,8	4,8	3,20
S65/50-2D-2		100	2155		46	4,6		
S65/50-2D-3		100	2135		49	4,9		
S65/50-7D-1	7	100	2125	2148	125	12,5	12,8	2,25
S65/50-7D-2		100	2190		130	13,0		
S65/30-7D-3		100	2130		130	13,0		
S65/50-14D-1	14	100	2215	2165	197	19,7	19,4	1,58
S65/50-14D-2		100	2145		193	19,3		
S65/50-14D-3		100	2135		191	19,1		
S65/50-28D-1	28	100	2165	2185	263	26,3	26,0	3,94
S65/50-28D-2		100	2190		249	24,9		
S65/50-28D-3		100	2200		269	26,9		

Table A.10: Compressive strength results for mortar mix S65_70 (30% Portland cement & 70% GGBS; w/b = 0.65).

Specimen Reference	Age (days)	Cube Dim. (mm)	Saturated Density (kg/m^3)	Mean Saturated Density (kg/m^3)	Failure Load (kN)	Comp. Str. (MPa)	Mean Comp. Str. (MPa)	CoV (%)
S65/70-2D-1	2	100	2180	2163	18	1,8	1,8	0,00
S65/70-2D-2		100	2150		18	1,8		
S65/70-2D-3		100	2160		18	1,8		
S65/70-7D-1	7	100	2170	2178	98	9,8	9,5	3,23
S65/70-7D-2		100	2190		92	9,2		
S65/70-7D-3		100	2175		94	9,4		
S65/70-14D-1	14	100	2175	2175	153	15,3	15,3	5,55
S65/70-14D-2		100	2200		162	16,2		
S65/70-14D-3		100	2150		145	14,5		
S65/70-28D-1	28	100	2125	2155	194	19,4	19,3	4,20
S65/70-28D-2		100	2175		184	18,4		
S65/70-28D-3		100	2165		200	20,0		

A.2 Tensile strength results

Table A.11: 7-day tensile strength results for all mortar mixes.

Mix description	Notation	Spec. 1 (MPa)	Spec. 2 (MPa)	Spec. 3 (MPa)	Mean (MPa)	CoV (%)
100% CEM	C45	4,41	3,41	4,76	**4,19**	16,65
70% CEM/ 30% FA	F45_30	3,69	3,34	Failed	**3,52**	6,87
50% CEM/ 50% FA	F45_50	2,45	2,47	2,56	**2,49**	2,29
50% CEM/ 50% GGBS	S45_50	2,89	3,04	3,44	**3,12**	9,11
30% CEM/ 70% GGBS	S45_70	2,32	2,82	Failed	**2,57**	13,62
100% CEM	C65	2,87	2,82	3,07	**2,92**	4,57
70% CEM/ 30% FA	F65_30	2,18	2,42	1,88	**2,16**	12,47
50% CEM/ 50% FA	F65_50	1,35	1,47	Failed	**1,41**	6,31
50% CEM/ 50% GGBS	S65_50	2,00	1,80	1,96	**1,92**	5,59
30% CEM/ 70% GGBS	S65_70	1,57	0,77	Failed	**1,17**	48,27

Table A.12: 28-day tensile strength results for all mortar mixes.

Mix description	Notation	Spec. 1 (MPa)	Spec. 2 (MPa)	Spec. 3 (MPa)	Mean (MPa)	CoV (%)
100% CEM	C45	6,21	6,85	6,06	**6,37**	6,59
70% CEM/ 30% FA	F45_30	4,04	4,75	5,39	**4,73**	14,32
50% CEM/ 50% FA	F45_50	4,41	4,37	4,09	**4,29**	4,03
50% CEM/ 50% GGBS	S45_50	3,93	3,70	4,37	**4,00**	8,62
30% CEM/ 70% GGBS	S45_70	3,53	3,57	Failed	**3,55**	0,79
100% CEM	C65	5,34	5,24	4,75	**5,11**	6,18
70% CEM/ 30% FA	F65_30	3,47	3,56	3,64	**3,56**	2,41
50% CEM/ 50% FA	F65_50	2,62	3,01	3,01	**2,88**	7,74
50% CEM/ 50% GGBS	S65_50	3,43	3,34	3,33	**3,37**	1,54
30% CEM/ 70% GGBS	S65_70	3,00	2,80	Failed	**2,90**	31,02

A.3 Tensile relaxation results

Table A.13: 7-day tensile relaxation results for all mortar mixes.

Description	Notation	Spec. 1 (%)	Spec. 2 (%)	Mean (%)	CoV (%)
100% CEM	C45	21,1	20,8	20,9	0,98
70% CEM/ 30% FA	F45_30	22,5	24,3	23,4	5,44
50% CEM/ 50% FA	F45_50	32,6	31,6	32,1	2,16
50% CEM/ 50% GGBS	S45_50	18,5	20,2	19,3	6,37
30% CEM/ 70% GGBS	S45_70	26,1	24,2	25,2	5,42
100% CEM	C65	18,5	18,3	18,4	0,58
70% CEM/ 30% FA	F65_30	20,2	21,7	21,0	4,99
50% CEM/ 50% FA	F65_50	35,6	32,2	33,9	6,99

50% CEM/ 50% GGBS	S65_50	27,2	27,9	27,6	1,77
30% CEM/ 70% GGBS	S65_70	57,0	52,2	54,6	6,15

Table A.14: 28-day tensile relaxation results for all mortar mixes.

Mix description	**Notation**	**Spec. 1** (%)	**Spec. 2** (%)	**Mean** (%)	**CoV** (%)
100% CEM	C45	11,6	13,1	12,3	8,65
70% CEM/ 30% FA	F45_30	22,6	22,8	22,7	0,72
50% CEM/ 50% FA	F45_50	17,5	18,4	18,0	3,55
50% CEM/ 50% GGBS	S45_50	17,5	16,4	17,0	4,59
30% CEM/ 70% GGBS	S45_70	23,8	23,1	23,5	2,20
100% CEM	C65	10,9	9,5	10,2	9,71
70% CEM/ 30% FA	F65_30	17,7	16,2	16,9	6,06
50% CEM/ 50% FA	F65_50	23,4	25,2	24,3	5,33
50% CEM/ 50% GGBS	S65_50	25,4	23,1	24,2	6,65
30% CEM/ 70% GGBS	S65_70	44,5	41,1	42,8	5,65

A.4 Elastic modulus results

Table A.15: 7-day elastic modulus results for all mortar mixes.

Mix description	**Notation**	**Spec. 1** (GPa)	**Spec. 2** (GPa)	**Spec. 3** (GPa)	**Mean** (GPa)	**CoV** (%)
100% CEM	C45	25,8	26,7	25,4	**26,0**	2,6
70% CEM/ 30% FA	F45_30	19,7	21,3	20,1	**20,4**	4,1
50% CEM/ 50% FA	F45_50	13,1	15,5	13,6	**14,1**	9,0
50% CEM/ 50% GGBS	S45_50	17,0	20,2	17,4	**18,2**	9,6
30% CEM/ 70% GGBS	S45_70	11,7	13,2	8,4	**11,1**	22,1
100% CEM	C65	20,9	21,5	22,0	**21,5**	2,6
70% CEM/ 30% FA	F65_30	16,7	19,3	19,3	**18,4**	8,1
50% CEM/ 50% FA	F65_50	15,0	16,6	15,7	**15,8**	5,1
50% CEM/ 50% GGBS	S65_50	18,3	20,3	19,3	**19,3**	5,2
30% CEM/ 70% GGBS	S65_70	14,9	15,8	13,5	**14,7**	7,9

Table A.16: 28-day elastic modulus for all mortar mixes.

Mix description	**Notation**	**Spec. 1** (GPa)	**Spec. 2** (GPa)	**Spec. 3** (GPa)	**Mean** (GPa)	**CoV** (%)
100% CEM	C45	31,0	31,6	23,4	**28,7**	16,0
70% CEM/ 30% FA	F45_30	23,0	21,3	25,1	**23,1**	8,4
50% CEM/ 50% FA	F45_50	22,8	20,4	22,8	**22,0**	6,2
50% CEM/ 50% GGBS	S45_50	16,9	19,7	22,5	**19,7**	14,3
30% CEM/ 70% GGBS	S45_70	23,1	23,5	22,6	**23,1**	2,0
100% CEM	C65	23,3	23,8	23,8	**23,6**	1,2

70% CEM/ 30% FA	F65_30	20,5	19,9	21,6	**20,7**	4,2
50% CEM/ 50% FA	F65_50	19,5	18,7	18,1	**18,8**	3,7
50% CEM/ 50% GGBS	S65_50	21,1	21,7	21,1	**21,3**	1,6
30% CEM/ 70% GGBS	S65_70	20,6	20,6	19,9	**20,4**	2,0

A.5 Free shrinkage strain results

The free shrinkage results obtained from the free shrinkage tests described in Section 4.6.5 are provided below.

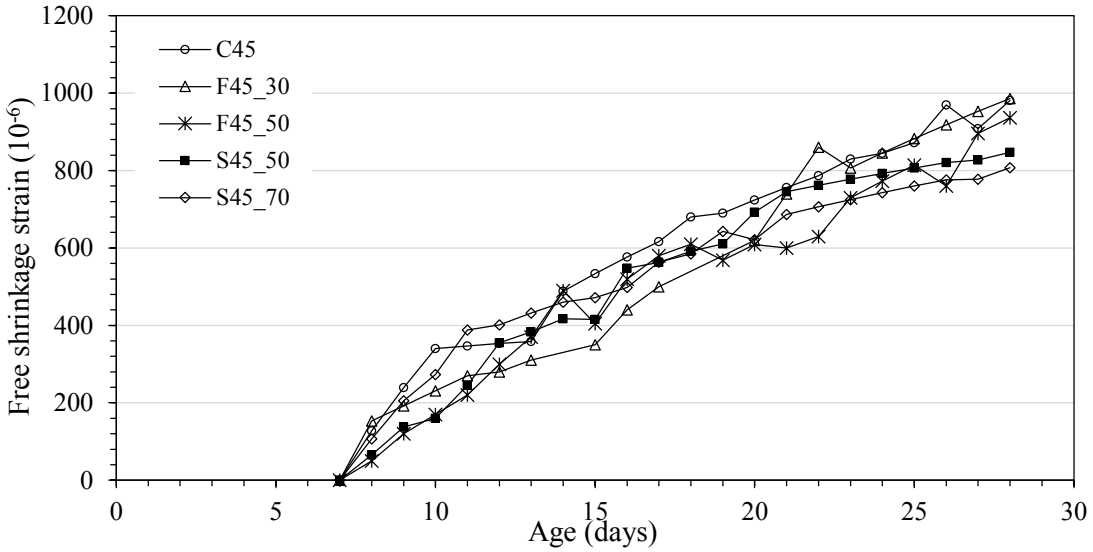

(d) All (w/b =0.45)

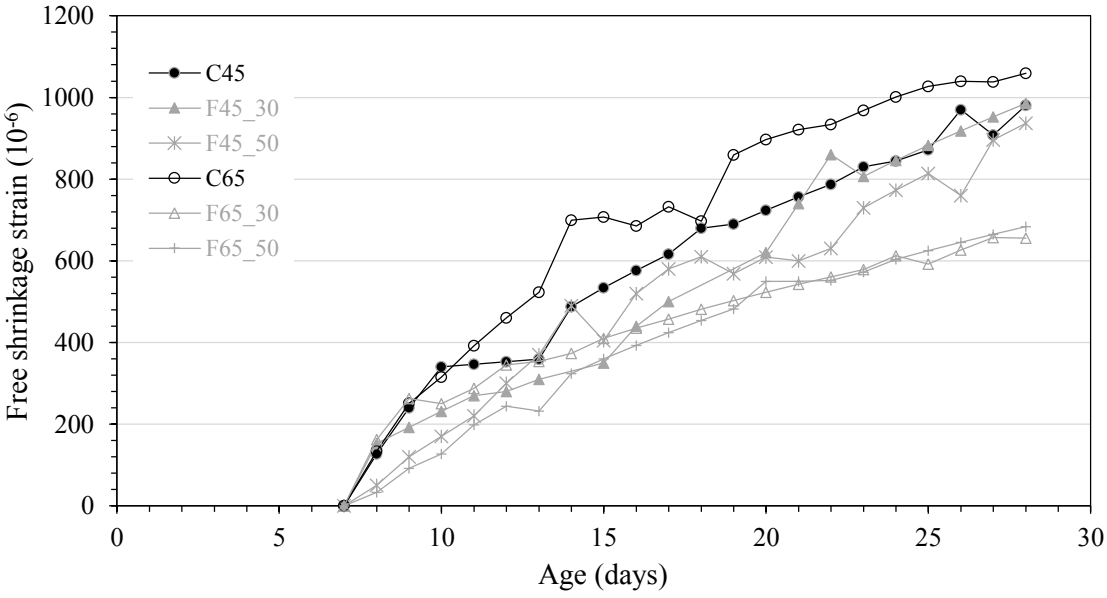

(e) Portland cement (comparison with fly ash mixes)

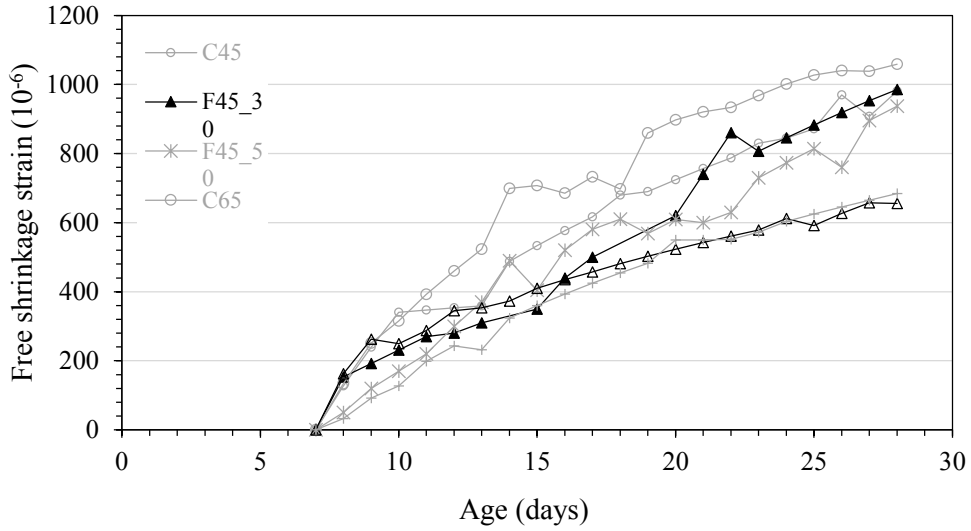

(f) 30% fly ash

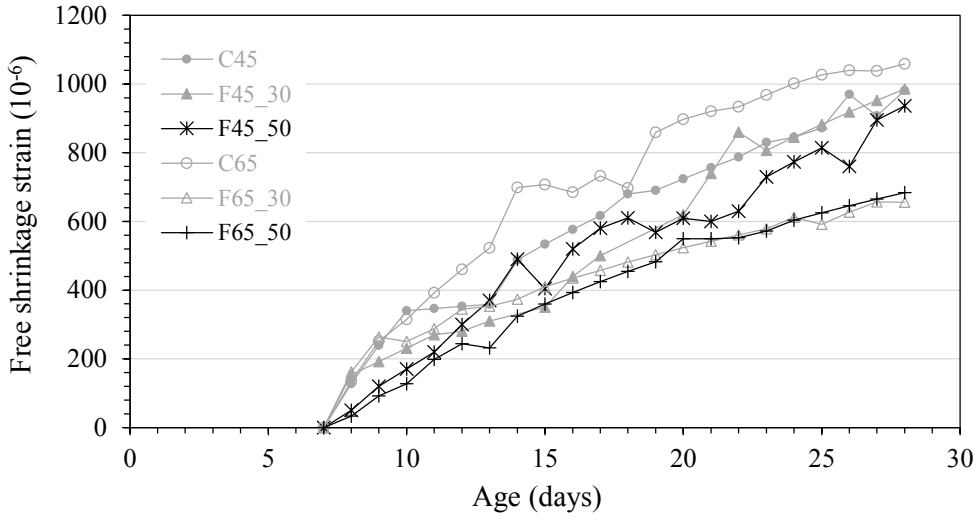

(g) 50% fly ash

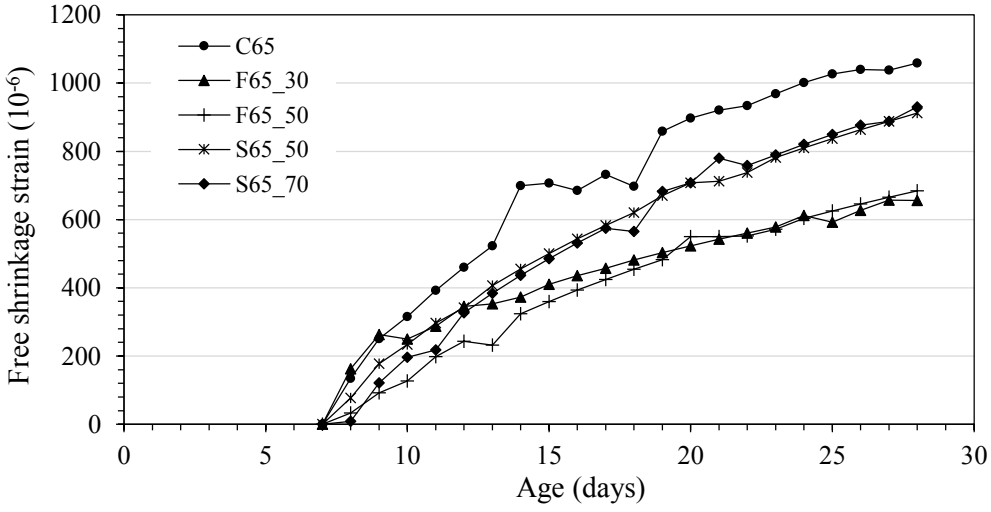

(h) All (w/b = 0.65)

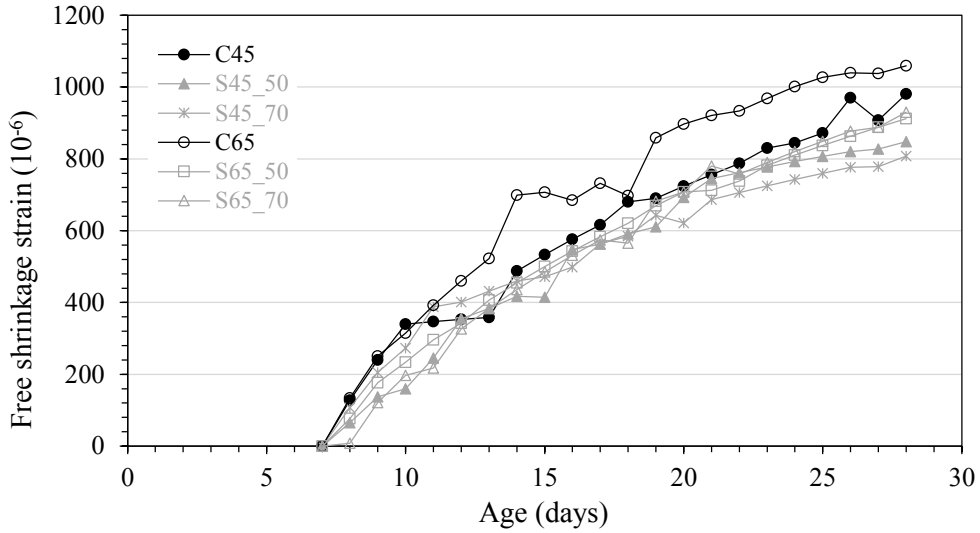

(i) Portland cement (comparison with GGBS mixes)

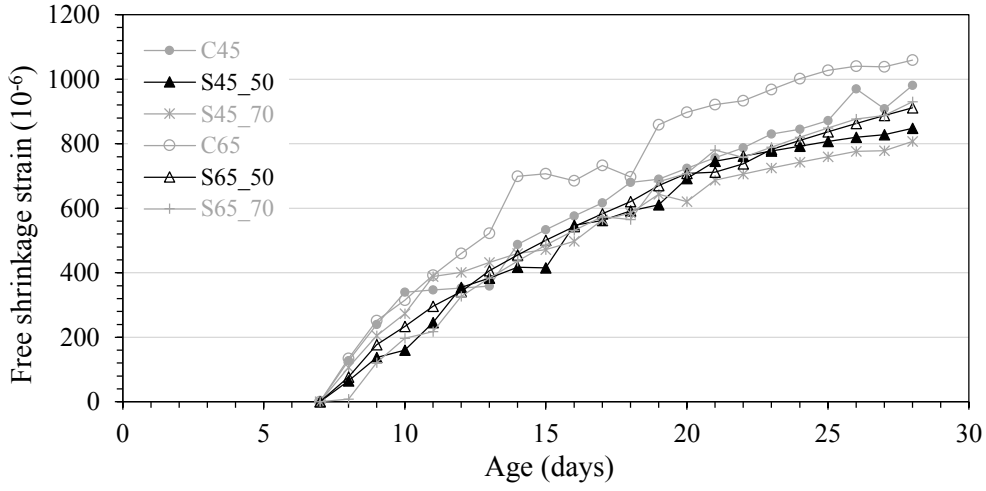

(j) 50% slag

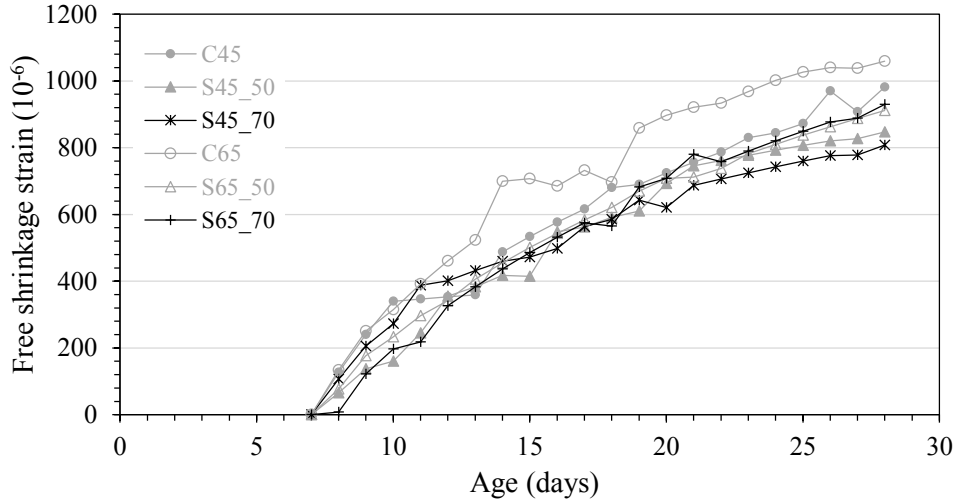

(k) 70% Slag

A.6 Ring test results

Table A.17: Age at cracking and net age at cracking results of ring test specimens cured for 7 days.

Notation	Age at cracking				Net age at cracking		
	Spec. 1 (days)	**Spec. 2** (days)	**Mean** (days)	**CoV** (%)	**Spec. 1** (days)	**Spec. 2** (days)	**Mean** (days)
C45	10	10	**10**	0	3	3	**3**
F45_30	11	12	**11,5**	6	4	5	**4,5**
F45_50	15	15	**15**	0	8	8	**8**
S45_50	9	9	**9**	0	2	2	**2**
S45_70	11	14	**12,5**	17	4	7	**5,5**
C65	12	14	**13**	11	5	7	**6**
F65_30	17	17	**17**	0	10	10	**10**
F65_50	17	17	**17**	0	10	10	**10**
S65_50	13	12	**12,5**	6	6	5	**5,5**
S65_70	19	21	**20**	7	12	14	**13**

Table A.18: Age at cracking results of ring test specimens not moist cured.

Mix Designation	**Spec. 1** (days)	**Spec. 2** (days)	**Mean** (days)	**CoV** (%)
F45_50	8	8	**8**	0
F65_50	11	13	**12**	12
S45_70	5	5	**5**	0
S65_70	6	6	**6**	0

Table A.19: Crack length and 3-day & 14-day crack width results of ring test specimens cured for 7 days.

Notation	Crack Length			3-Day Crack Width			14-Day Crack Width		
	Spec. 1 (mm)	**Spec. 2** (mm)	**Mean** (mm)	**Spec. 1** (mm)	**Spec. 2** (mm)	**Mean** (mm)	**Spec. 1** (mm)	**Spec. 2** (mm)	**Mean** (mm)
C45	185	173	**179**	1,8	1,6	**1,7**	2,3	2,1	**2,2**
F45_30	171	165	**168**	1,6	1,88	**1,74**	1,7	1,9	**1,8**
F45_50	202	182	**192**	0,5	0,1	**0,3**	0,96	0,42	**0,69**
S45_50	193	179	**186**	2,68	2,16	**2,42**	3,1	2,86	**2,98**
S45_70	191	180	**185,5**	1	1,84	**1,42**	1,3	2,2	**1,75**
C65	181	168	**174,5**	0,3	1,6	**0,95**	1,16	1,8	**1,48**
F65_30	176	192	**184**	0,2	0,1	**0,15**	0,5	0,2	**0,35**
F65_50	184	167	**175,5**	0,2	1,7	**0,95**	0,46	0,8	**0,63**
S65_50	176	202	**189**	1,5	0,2	**0,85**	1,9	0,4	**1,15**
S65_70	208	196	**202**	0,06	1	**0,53**	0,33	1,46	**0,895**

Table A.20: Crack length, and 3-day & 14-day crack area results of ring test specimens cured for 7 days.

Mix Designation	3-day Crack Area			14-day Crack Area		
	Spec. 1 (mm^2)	**Spec. 2** (mm^2)	**Mean** (mm^2)	**Spec. 1** (mm^2)	**Spec. 2** (mm^2)	**Mean** (mm^2)
C45	333	277	**305**	426	363	**394**
F45_30	274	310	**292**	291	314	**302**
F45_50	101	18	**60**	194	76	**135**
S45_50	517	387	**452**	598	512	**555**
S45_70	191	331	**261**	248	396	**322**
C65	54	269	**162**	210	302	**256**
F65_30	35	19	**27**	88	38	**63**
F65_50	37	284	**160**	85	134	**109**
S65_50	264	40	**152**	334	81	**208**
S65_70	12	196	**104**	69	286	**177**

Table A.21: Crack length, and 14-day crack width & area results of air cured ring test specimens.

Mix Designation	Crack Length			14-Day Crack Width			Crack area
	Spec. 1 (mm)	**Spec. 2** (mm)	**Mean** (mm)	**Spec. 1** (mm)	**Spec. 2** (mm)	**Mean** (mm)	**Mean** (mm^2)
F45_50	165	169	**167**	0,60	0,47	**0,54**	**89**
F65_50	163	165	**164**	0,10	0,10	**0,10**	**16**
S45_70	173	168	**170,5**	0,20	0,97	**0,59**	**100**
S65_70	167	165	**166**	0,23	0,23	**0,23**	**38**

APPENDIX B

B. Analytical modelling results

B.1 Regression analysis parameters

Table B.1: Regression coefficients

Notation	Tensile strength		Tensile relaxation		Elastic modulus		Free shrinkage	
	A (-)	**B** (-)	**C** (-)	**D** (-)	**E** (-)	**F** (-)	**G** (-)	**H** (-)
C45	1,060	2,837	-6,492	34,03	1,948	22,210	699.9	-1274.9
F45_30	0,873	1,822	-0,505	24,38	1,948	16,610	705.1	-1416.6
F45_50	1,298	-0,037	-10,170	51,89	5,699	30,190	648.6	-1300.7
S45_50	0,635	1,885	-1,659	22,53	1,082	16,094	656.7	-1304.6
S45_70	0,707	1,194	-1,226	27,59	8,656	-5,744	550.0	-1004.1
C65	1,580	-0,154	-5,915	29,91	1,515	15,552	765.4	-1435.9
F65_30	1,010	0,195	-2,958	26,76	1,659	15,172	411.0	-705.86
F65_50	1,060	-0,653	-6,925	47,38	2,164	11,589	519.71	-1047.9
S65_50	1,046	-0,115	-2,453	32,37	1,447	16,493	658.8	-1283.5
S65_70	0,209	0,763	-8,512	71,16	4,977	3,815	711.9	-1441.9

B.2 Material property data from regression analysis

Table B.2: Material property data for 100% Portland cement mortar mix, w/b 0.45.

Period (days)	**Tensile strength** $f_{t,i}$ (MPa)	**Mean tensile relaxation factor** Ψ (%)	**Mean elastic modulus** E_i (GPa)	**Change in free shrinkage strain** $\Delta\varepsilon_{FSS}$ ($\times 10^{-6}$)	**Induced tensile stress** $\sigma_{t,i}$ (MPa)	**Tensile strength-stress ratio** $f_{t,i}/\sigma_{t,i}$ (-)
0 - 7	3,1	25,9	24,6	0,0	0,0	0,00
7 - 8	4,3	21,0	26,1	118,1	1,5	2,94
8 - 9	4,5	20,1	26,4	78,9	2,5	1,83
9 - 10	4,7	19,4	26,6	70,6	3,4	1,39
10 - 11	4,8	18,8	26,8	63,8	4,2	1,15
11 - 12	5,0	18,2	27,0	58,3	5,0	1,00
12 - 13	5,1	17,6	27,1	53,6	5,7	0,90
13 - 14	5,2	17,1	27,3	49,6	6,4	0,82
14 - 15	5,3	16,7	27,4	46,2	7,0	0,76
15 - 16	5,4	16,2	27,5	43,2	7,6	0,72
16 - 17	5,5	15,8	27,7	40,6	8,2	0,68
17 - 18	5,6	15,5	27,8	38,3	8,7	0,65

18 - 19	5,7	15,1	27,9	36,2	9,2	0,62
19 - 20	5,8	14,7	28,0	34,4	9,7	0,60
20 - 21	5,9	14,4	28,1	32,7	10,2	0,58
21 - 22	6,0	14,1	28,2	31,2	10,6	0,56
22 - 23	6,0	13,8	28,3	29,8	11,1	0,54
23 - 24	6,1	13,5	28,4	28,5	11,5	0,53
24 - 25	6,2	13,3	28,4	27,3	11,9	0,52
25 - 26	6,2	13,0	28,5	26,3	12,3	0,51
26 - 27	6,3	12,8	28,6	25,3	12,7	0,50
27 - 28	6,3	12,5	28,7	24,4	13,0	0,49

Table B.3: Material property data for 30% fly ash content mortar mix, w/b 0.45.

Period (days)	**Tensile strength** $f_{t,i}$ (MPa)	**Mean tensile relaxation factor** Ψ (%)	**Mean elastic modulus** E_i (GPa)	**Change in free shrinkage strain** $\Delta\varepsilon_{FSS}$ ($\times 10^{-6}$)	**Induced tensile stress** $\sigma_{t,i}$ (MPa)	**Tensile strength-stress ratio** $f_{t,i}/\sigma_{t,i}$ (-)
0 - 7	2,9	23,8	19,0	0,0	0,0	0,00
7 - 8	3,6	23,4	20,5	49,5	0,5	7,66
8 - 9	3,7	23,3	20,8	83,0	1,3	2,92
9 - 10	3,8	23,2	21,0	74,3	2,0	1,91
10 - 11	3,9	23,2	21,2	67,2	2,6	1,47
11 - 12	4,0	23,1	21,4	61,3	3,2	1,22
12 - 13	4,0	23,1	21,5	56,4	3,8	1,06
13 - 14	4,1	23,1	21,7	52,2	4,3	0,95
14 - 15	4,2	23,0	21,8	48,6	4,8	0,86
15 - 16	4,2	23,0	21,9	45,5	5,3	0,80
16 - 17	4,3	23,0	22,1	42,7	5,7	0,75
17 - 18	4,3	22,9	22,2	40,3	6,1	0,71
18 - 19	4,4	22,9	22,3	38,1	6,5	0,67
19 - 20	4,4	22,9	22,4	36,2	6,9	0,64
20 - 21	4,5	22,9	22,5	34,4	7,3	0,61
21 - 22	4,5	22,8	22,6	32,8	7,6	0,59
22 - 23	4,5	22,8	22,7	31,3	7,9	0,57
23 - 24	4,6	22,8	22,8	30,0	8,2	0,56
24 - 25	4,6	22,8	22,8	28,8	8,5	0,54
25 - 26	4,6	22,7	22,9	27,7	8,8	0,53
26 - 27	4,7	22,7	23,0	26,6	9,1	0,51
27 - 28	4,7	22,7	23,1	25,6	9,4	0,50

Table B.4: Material property data for 50% fly ash content mortar mix, w/b 0.45.

Period (days)	Tensile strength $f_{t,i}$ (MPa)	Mean tensile relaxation factor Ψ (%)	Mean elastic modulus E_i (GPa)	Change in free shrinkage strain $\Delta\varepsilon_{FSS}$ ($\times 10^{-6}$)	Induced tensile stress $\sigma_{t,i}$ (MPa)	Tensile strength-stress ratio $f_{t,i}/\sigma_{t,i}$ (-)
0 - 7	1,6	39,2	10,2	0,0	0,0	0,00
7 - 8	2,6	31,4	14,5	48,0	0,3	9,00
8 - 9	2,7	30,1	15,2	76,4	0,8	3,54
9 - 10	2,9	29,0	15,8	68,3	1,2	2,34
10 - 11	3,0	28,0	16,4	61,8	1,7	1,80
11 - 12	3,1	27,1	16,9	56,4	2,1	1,50
12 - 13	3,2	26,2	17,4	51,9	2,5	1,30
13 - 14	3,3	25,4	17,9	48,1	2,9	1,16
14 - 15	3,4	24,7	18,3	44,7	3,2	1,06
15 - 16	3,5	24,0	18,6	41,9	3,6	0,98
16 - 17	3,6	23,4	19,0	39,3	3,9	0,91
17 - 18	3,7	22,8	19,3	37,1	4,3	0,86
18 - 19	3,8	22,2	19,6	35,1	4,6	0,82
19 - 20	3,8	21,7	19,9	33,3	4,9	0,78
20 - 21	3,9	21,2	20,2	31,6	5,2	0,75
21 - 22	3,9	20,7	20,5	30,2	5,5	0,72
22 - 23	4,0	20,2	20,8	28,8	5,8	0,69
23 - 24	4,1	19,8	21,0	27,6	6,1	0,67
24 - 25	4,1	19,4	21,2	26,5	6,3	0,65
25 - 26	4,2	19,0	21,5	25,4	6,6	0,63
26 - 27	4,2	18,6	21,7	24,5	6,9	0,61
27 - 28	4,3	18,2	21,9	23,6	7,1	0,60

Table B.5: Material property data for 50% slag content mortar mix, w/b 0.45.

Period (days)	Tensile strength $f_{t,i}$ (MPa)	Mean tensile relaxation factor Ψ (%)	Mean elastic modulus E_i (GPa)	Change in free shrinkage strain $\Delta\varepsilon_{FSS}$ ($\times 10^{-6}$)	Induced tensile stress $\sigma_{t,i}$ (MPa)	Tensile strength-stress ratio $f_{t,i}/\sigma_{t,i}$ (-)
0 - 7	2,7	19,3	15,8	0,0	0,0	0,00
7 - 8	3,2	19,1	18,4	60,9	0,5	5,80
8 - 9	3,2	18,9	18,9	77,3	1,3	2,58
9 - 10	3,3	18,7	19,3	69,2	1,9	1,74
10 - 11	3,4	18,5	19,6	62,6	2,5	1,35
11 - 12	3,4	18,4	20,0	57,1	3,1	1,12
12 - 13	3,5	18,3	20,2	52,6	3,6	0,97
13 - 14	3,5	18,1	20,5	48,7	4,1	0,87
14 - 15	3,6	18,0	20,8	45,3	4,5	0,79

15 - 16	3,6	17,9	21,0	42,4	5,0	0,73
16 - 17	3,7	17,8	21,2	39,8	5,4	0,68
17 - 18	3,7	17,7	21,4	37,5	5,8	0,64
18 - 19	3,7	17,6	21,6	35,5	6,2	0,61
19 - 20	3,8	17,6	21,8	33,7	6,5	0,58
20 - 21	3,8	17,5	22,0	32,0	6,9	0,55
21 - 22	3,8	17,4	22,2	30,5	7,2	0,53
22 - 23	3,9	17,3	22,3	29,2	7,5	0,51
23 - 24	3,9	17,3	22,5	27,9	7,9	0,49
24 - 25	3,9	17,2	22,6	26,8	8,2	0,48
25 - 26	3,9	17,1	22,8	25,8	8,4	0,47
26 - 27	4,0	17,1	22,9	24,8	8,7	0,45
27 - 28	4,0	17,0	23,0	23,9	9,0	0,44

Table B.6: Material property data for 70% slag content mortar mix, w/b 0.45.

Period (days)	**Tensile strength** $f_{t,i}$ (MPa)	**Mean tensile relaxation factor** Ψ (%)	**Mean elastic modulus** E_i (GPa)	**Change in free shrinkage strain** $\Delta\varepsilon_{FSS}$ ($\times 10^{-6}$)	**Induced tensile stress** $\sigma_{t,i}$ (MPa)	**Tensile strength-stress ratio** $f_{t,i}/\sigma_{t,i}$ (-)
0 - 7	2,1	25,2	5,1	0,0	0,0	0,00
7 - 8	2,6	25,0	11,7	139,6	0,7	3,57
8 - 9	2,7	24,9	12,8	64,8	1,1	2,44
9 - 10	2,8	24,8	13,7	57,9	1,5	1,90
10 - 11	2,9	24,6	14,6	52,4	1,8	1,58
11 - 12	2,9	24,5	15,4	47,9	2,1	1,36
12 - 13	3,0	24,4	16,1	44,0	2,5	1,21
13 - 14	3,0	24,4	16,8	40,8	2,8	1,09
14 - 15	3,1	24,3	17,4	37,9	3,1	1,00
15 - 16	3,1	24,2	18,0	35,5	3,4	0,93
16 - 17	3,2	24,1	18,5	33,3	3,7	0,87
17 - 18	3,2	24,0	19,0	31,4	3,9	0,82
18 - 19	3,3	24,0	19,5	29,7	4,2	0,78
19 - 20	3,3	23,9	20,0	28,2	4,4	0,74
20 - 21	3,3	23,9	20,4	26,8	4,7	0,71
21 - 22	3,4	23,8	20,8	25,6	4,9	0,68
22 - 23	3,4	23,7	21,2	24,4	5,2	0,66
23 - 24	3,4	23,7	21,6	23,4	5,4	0,63
24 - 25	3,5	23,6	21,9	22,5	5,6	0,61
25 - 26	3,5	23,6	22,3	21,6	5,9	0,60
26 - 27	3,5	23,5	22,6	20,8	6,1	0,58
27 - 28	3,5	23,5	22,9	20,0	6,3	0,56

Table B.7: Material property data for 100% Portland cement mortar mix, w/b 0.65.

Period (days)	**Tensile strength** $f_{t,i}$ (MPa)	**Mean tensile relaxation factor** Ψ (%)	**Mean elastic modulus** E_i (GPa)	**Change in free shrinkage strain** $\Delta\varepsilon_{FSS}$ ($\times 10^{-6}$)	**Induced tensile stress** $\sigma_{t,i}$ (MPa)	**Tensile strength-stress ratio** $f_{t,i}/\sigma_{t,i}$ (-)
0 - 7	1,8	22,5	17,4	0,0	0,0	0,00
7 - 8	3,0	18,0	18,6	155,8	1,4	2,12
8 - 9	3,2	17,3	18,8	90,2	2,3	1,42
9 - 10	3,4	16,6	19,0	80,6	3,0	1,12
10 - 11	3,6	16,0	19,1	73,0	3,7	0,95
11 - 12	3,7	15,5	19,3	66,6	4,4	0,84
12 - 13	3,8	15,0	19,4	61,3	5,0	0,77
13 - 14	4,0	14,5	19,5	56,7	5,6	0,71
14 - 15	4,1	14,1	19,6	52,8	6,1	0,67
15 - 16	4,2	13,7	19,7	49,4	6,6	0,63
16 - 17	4,3	13,3	19,8	46,4	7,1	0,60
17 - 18	4,4	13,0	19,9	43,8	7,5	0,58
18 - 19	4,5	12,7	20,0	41,4	8,0	0,56
19 - 20	4,5	12,3	20,1	39,3	8,4	0,54
20 - 21	4,6	12,0	20,1	37,3	8,8	0,53
21 - 22	4,7	11,8	20,2	35,6	9,2	0,51
22 - 23	4,8	11,5	20,3	34,0	9,5	0,50
23 - 24	4,8	11,2	20,3	32,6	9,9	0,49
24 - 25	4,9	11,0	20,4	31,2	10,2	0,48
25 - 26	5,0	10,8	20,5	30,0	10,5	0,47
26 - 27	5,0	10,5	20,5	28,9	10,9	0,46
27 - 28	5,1	10,3	20,6	27,8	11,2	0,46

Table B.8: Material property data for 30% fly ash content mortar mix, w/b 0.65.

Period (days)	**Tensile strength** $f_{t,i}$ (MPa)	**Mean tensile relaxation factor** Ψ (%)	**Mean elastic modulus** E_i (GPa)	**Change in free shrinkage strain** $\Delta\varepsilon_{FSS}$ ($\times 10^{-6}$)	**Induced tensile stress** $\sigma_{t,i}$ (MPa)	**Tensile strength-stress ratio** $f_{t,i}/\sigma_{t,i}$ (-)
0 - 7	1,5	23,0	17,3	0,0	0,0	0,00
7 - 8	2,2	20,8	18,5	148,7	1,3	1,70
8 - 9	2,4	20,4	18,7	48,4	1,7	1,35
9 - 10	2,5	20,1	18,9	43,3	2,1	1,16
10 - 11	2,6	19,8	19,1	39,2	2,5	1,03
11 - 12	2,7	19,5	19,2	35,8	2,8	0,94
12 - 13	2,7	19,3	19,4	32,9	3,1	0,88
13 - 14	2,8	19,1	19,5	30,5	3,4	0,83

14 - 15	2,9	18,8	19,6	28,4	3,7	0,78
15 - 16	3,0	18,6	19,7	26,5	3,9	0,75
16 - 17	3,0	18,5	19,8	24,9	4,2	0,72
17 - 18	3,1	18,3	19,9	23,5	4,4	0,70
18 - 19	3,1	18,1	20,0	22,2	4,6	0,68
19 - 20	3,2	18,0	20,1	21,1	4,8	0,66
20 - 21	3,2	17,8	20,2	20,1	5,0	0,64
21 - 22	3,3	17,7	20,3	19,1	5,2	0,63
22 - 23	3,3	17,5	20,3	18,3	5,4	0,62
23 - 24	3,4	17,4	20,4	17,5	5,6	0,60
24 - 25	3,4	17,3	20,5	16,8	5,8	0,59
25 - 26	3,5	17,2	20,5	16,1	5,9	0,58
26 - 27	3,5	17,1	20,6	15,5	6,1	0,58
27 - 28	3,5	17,0	20,7	14,9	6,2	0,57

Table B.9: Material property data for 50% fly ash content mortar mix, w/b 0.65.

Period (days)	**Tensile strength** $f_{t,i}$ (MPa)	**Mean tensile relaxation factor** Ψ (%)	**Mean elastic modulus** E_i (GPa)	**Change in free shrinkage strain** $\Delta\varepsilon_{FSS}$ ($\times 10^{-6}$)	**Induced tensile stress** $\sigma_{t,i}$ (MPa)	**Tensile strength-stress ratio** $f_{t,i}/\sigma_{t,i}$ (-)
0 - 7	0,7	38,7	14,3	0,0	0,0	0,00
7 - 8	1,5	33,4	15,9	32,8	0,2	7,09
8 - 9	1,6	32,5	16,2	61,2	0,6	2,64
9 - 10	1,7	31,7	16,5	54,8	1,0	1,77
10 - 11	1,8	31,0	16,7	49,5	1,3	1,39
11 - 12	1,9	30,4	16,9	45,2	1,6	1,18
12 - 13	2,0	29,8	17,1	41,6	1,9	1,04
13 - 14	2,1	29,3	17,2	38,5	2,2	0,95
14 - 15	2,2	28,8	17,4	35,9	2,5	0,88
15 - 16	2,3	28,3	17,5	33,5	2,7	0,82
16 - 17	2,3	27,9	17,7	31,5	3,0	0,78
17 - 18	2,4	27,5	17,8	29,7	3,2	0,74
18 - 19	2,4	27,1	17,9	28,1	3,4	0,71
19 - 20	2,5	26,7	18,0	26,7	3,6	0,69
20 - 21	2,5	26,4	18,1	25,4	3,8	0,66
21 - 22	2,6	26,0	18,2	24,2	4,0	0,64
22 - 23	2,6	25,7	18,3	23,1	4,2	0,63
23 - 24	2,7	25,4	18,4	22,1	4,4	0,61
24 - 25	2,7	25,1	18,5	21,2	4,6	0,60
25 - 26	2,8	24,9	18,6	20,4	4,8	0,58
26 - 27	2,8	24,6	18,7	19,6	4,9	0,57
27 - 28	2,9	24,3	18,8	18,9	5,1	0,56

Table B.10: Material property data for 50% slag content mortar mix, w/b 0.65.

Period (days)	**Tensile strength** $f_{t,i}$ (MPa)	**Mean tensile relaxation factor** Ψ (%)	**Mean elastic modulus** E_i (GPa)	**Change in free shrinkage strain** $\Delta\varepsilon_{FSS}$ ($\times 10^{-6}$)	**Induced tensile stress** $\sigma_{t,i}$ (MPa)	**Tensile strength-stress ratio** $f_{t,i}/\sigma_{t,i}$ (-)
0 - 7	1,2	29,3	18,3	0,0	0,0	0,00
7 - 8	2,0	27,4	19,4	86,4	0,7	2,73
8 - 9	2,1	27,1	19,6	77,6	1,4	1,52
9 - 10	2,2	26,9	19,8	69,4	2,0	1,12
10 - 11	2,3	26,6	19,9	62,8	2,5	0,92
11 - 12	2,4	26,4	20,0	57,3	3,1	0,80
12 - 13	2,5	26,2	20,1	52,7	3,5	0,72
13 - 14	2,6	26,0	20,3	48,8	4,0	0,66
14 - 15	2,7	25,8	20,4	45,5	4,4	0,61
15 - 16	2,8	25,6	20,5	42,5	4,8	0,58
16 - 17	2,8	25,5	20,6	39,9	5,1	0,55
17 - 18	2,9	25,4	20,6	37,7	5,5	0,53
18 - 19	2,9	25,2	20,7	35,6	5,8	0,51
19 - 20	3,0	25,1	20,8	33,8	6,1	0,49
20 - 21	3,0	25,0	20,9	32,1	6,4	0,47
21 - 22	3,1	24,8	20,9	30,6	6,7	0,46
22 - 23	3,1	24,7	21,0	29,3	7,0	0,45
23 - 24	3,2	24,6	21,1	28,0	7,3	0,44
24 - 25	3,2	24,5	21,1	26,9	7,5	0,43
25 - 26	3,3	24,4	21,2	25,8	7,8	0,42
26 - 27	3,3	24,3	21,2	24,9	8,0	0,41
27 - 28	3,4	24,2	21,3	24,0	8,2	0,41

Table B.11: Material property data for 70% slag content mortar mix, w/b 0.65.

Period (days)	**Tensile strength** $f_{t,i}$ (MPa)	**Mean tensile relaxation factor** Ψ (%)	**Mean elastic modulus** E_i (GPa)	**Change in free shrinkage strain** $\Delta\varepsilon_{FSS}$ ($\times 10^{-6}$)	**Induced tensile stress** $\sigma_{t,i}$ (MPa)	**Tensile strength-stress ratio** $f_{t,i}/\sigma_{t,i}$ (-)
0 - 7	0,9	60,5	10,0	0,0	0,0	0,00
7 - 8	1,6	54,0	13,8	38,6	0,1	11,10
8 - 9	1,8	52,9	14,5	83,9	0,5	3,58
9 - 10	1,9	52,0	15,0	75,0	0,8	2,29
10 - 11	2,0	51,1	15,5	67,9	1,1	1,74
11 - 12	2,0	50,4	16,0	61,9	1,4	1,44
12 - 13	2,1	49,7	16,4	57,0	1,7	1,25
13 - 14	2,2	49,0	16,8	52,8	2,0	1,12

14 - 15	2,3	48,4	17,1	49,1	2,2	1,02
15 - 16	2,3	47,8	17,5	45,9	2,5	0,94
16 - 17	2,4	47,3	17,8	43,2	2,7	0,88
17 - 18	2,4	46,8	18,1	40,7	3,0	0,83
18 - 19	2,5	46,3	18,3	38,5	3,2	0,79
19 - 20	2,6	45,9	18,6	36,5	3,4	0,75
20 - 21	2,6	45,5	18,8	34,7	3,6	0,72
21 - 22	2,6	45,0	19,1	33,1	3,8	0,69
22 - 23	2,7	44,7	19,3	31,6	4,0	0,67
23 - 24	2,7	44,3	19,5	30,3	4,2	0,65
24 - 25	2,8	43,9	19,7	29,1	4,4	0,63
25 - 26	2,8	43,6	19,9	27,9	4,6	0,61
26 - 27	2,8	43,3	20,1	26,9	4,8	0,59
27 - 28	2,9	43,0	20,3	25,9	5,0	0,58

EBE Faculty: Assessment of Ethics in Research Projects

Any person planning to undertake research in the Faculty of Engineering and the Built Environment at the University of Cape Town is required to complete this form before collecting or analysing data. When completed it should be submitted to the supervisor (where applicable) and from there to the Head of Department. If any of the questions below have been answered YES, and the applicant is NOT a fourth year student, the Head should forward this form for approval by the Faculty EIR committee: submit to Ms Zakiya Chikte (Zakiya.chikte@uct.ac.za); New EBE Building, Ph 021 650 5739). Students must include a copy of the completed form with the dissertation/thesis when it is submitted for examination.

Name of Principal Researcher/Student: Chizya Chibulu **Department:** Civil Engineering

If a Student: **Degree:** MSc. Civil Engineering **Supervisor:** A/Prof. Hans Beushausen

If a Research Contract indicate source of funding/sponsorship: CoMSIRU Scholarship

Research Project Title: The influence of fly ash and ground granulated blastfurnace slag on restrained shrinkage cracking of bonded overlays

Overview of ethics issues in your research project:

Question 1: Is there a possibility that your research could cause harm to a third party (i.e. a person not involved in your project)?		NO
Question 2: Is your research making use of human subjects as sources of data? If your answer is YES, please complete Addendum 2.		NO
Question 3: Does your research involve the participation of or provision of services to communities? If your answer is YES, please complete Addendum 3.		NO
Question 4: If your research is sponsored, is there any potential for conflicts of interest? If your answer is YES, please complete Addendum 4.		NO

If you have answered YES to any of the above questions, please append a copy of your research proposal, as well as any interview schedules or questionnaires (Addendum 1) and please complete further addenda as appropriate.

I hereby undertake to carry out my research in such a way that

- there is no apparent legal objection to the nature or the method of research; and
- the research will not compromise staff or students or the other responsibilities of the University;
- the stated objective will be achieved, and the findings will have a high degree of validity;
- limitations and alternative interpretations will be considered;
- the findings could be subject to peer review and publicly available; and
- I will comply with the conventions of copyright and avoid any practice that would constitute plagiarism.

Signed by:

	Full name and signature	Date
Principal Researcher/Student:	Chizya Chibulu	07 August 2015

This application is approved by:

Supervisor (if applicable):	A/Prof. Hans Beushausen	11 August 2015
HOD (or delegated nominee): Final authority for all assessments with NO to all questions and for all undergraduate research.	A/Prof. Marianne Vanderschuren	12 February 2016
Chair : Faculty EIR Committee For applicants other than undergraduate students who have answered YES to any of the above questions.	Not Applicable	Not Applicable